Effect of carbon nanotubes length on thermal and mechanical properties of carbon resin and carbon fibre reinforced polymer

Najihah Mohd Tamyis

The University of Sheffield

Faculty of Engineering

Department of Mechanical Engineering

Thesis submitted in partial fulfilment of the requirements for the degree of

Doctor of Philosophy

June 2018

Abstract

Over the last few decades carbon fibre reinforced polymer (CFRP) was used extensively because it offers attractive mechanical and thermal properties. Aircraft and some of high-end automobile constructions used CFRP, as it has an ability to be stuctured to aerodynamic efficient configurations. However, multi –layer laminates failure behavior is complex especially woven fabric composites. CFRPs' typical failure modes include matrix fracture, interface debonding between fibre and matrix and interlaminar delamination. One of the techniques to overcome such failure modes is by reinforcing the composites with nanoparticles. In this study, the objective is to develop a tougher resin by dispersing multiwalled carbon nanotubes (MWCNTs) into the resin which will improve the properties of CFRP composites. Two types of MWCNTs were used which lengths, a) MWCNT_long (length 10-30 μm) and b) MWCNT_short (length 0.5-2 μm).

There are two main parts in this thesis i.e., the investigation of thermal and mechanical properties of MWCNT_modified-epoxy and the investigation of mechanical properties of the MWCNT_filled-CFRP composite with an emphasis on interlaminar shear strength behaviour.

In the first part, an experiment was conducted to investigate the dispersion quality of MWCNTs as nanofillers in the resin systems. The effect of MWCNTs on compressive and flexural properties of epoxy polymers were studied. The epoxy resin used was Epikote 828 and dapsone (DDS) as the hardener. The thermal properties of MWCNT_modified-Epikote 828 as compared to Epikote828/DDS neat systems were also investigated. From

the results, the addition of MWCNT_short into Epikote 828 has significantly enhanced the compressive and flexural modulus.

The second investigation was done to study the effect of MWCNT on the interlaminar shear strength (ILSS) properties of Epikote828/CFRP composite by using . A number of plane weave carbon fibre (CF) laminates were fabricated using the hand-layup technique, wet resin impregnation and vacuum bagging techniques. The quality of laminate such as void content, fibre and MWCNTs volume fraction was examined. Short beam shear (SBS) test was performed on the plane weave laminates to test the quality of ILSS. It was found that the ILSS of MWCNT_short/Epikote828/CF CFRP composite was better than the neat Epikote828/DDS CFRP composites. The addition of 0.38% of MWCNT_short improved the ILSS of the CF/Epikote828 by 14 %.

Acknowledgements

Praises to Allah for giving me the strength to complete this thesis and, peace be upon the beloved Prophet Muhammad.

I would like to thank my supervisor, Professor Patrick Fairclough, for his encouragement and invaluable help and direction during this project.

I gratefully acknowledge both Majlis Amanah Rakyat (MARA) and Universiti Kuala Lumpur for the PhD scholarship.

I would like to thank all the members of the Composite System Innovation Centre (CSIC) University of Sheffield for their help. Particullarly to Ying and Pablo.

I grately acknowledge the Departments of Mechanical Engineering and the Department of Materials Scince and Engineering for providing me with the facilities for this project.

Finally, I would like to thank my beloved family, especially my husband Mizan, my kids Amirah, Ammar, Arina and A'isy for their patience and support, and to my mother and mother-in-law for their pray for my success.

Contents

List of Figures

List of Tables

1 Introduction

1.1 An over view

Reducing operating costs is an essential factor in the decision-making process in the airlines business. One of the major components of the operating costs is the fuel, therefore, a low fuel consumption is of great importance in this industry [1]. The impact of government regulations on airplane emissions and fuel efficiency is driving the change in the design of the modern aircrafts. Using new shapes and materials would have significant impact on reducing fuel consumption by improving the aerodynamics and using lightweight composite materials. This is not just cost effective, but it is also more environmentally friendly [2,3].

The increased use of composites in aerospace industry is driven by weight reduction and potential improvements in mechanical properties, such as fatigue behaviour. Traditional aircrafts, which are mostly made of metal and aluminium, have been replaced with aircrafts that have a higher proportion of composites. Nowadays, composites, such as Carbon Fibre Reinforced Polymer (CFRP), are accounting for 65% of the weight of an empty aircraft [4]. Aircrafts, such as Boeing 787 Dreamliner, Airbus A350, A350XWB and Bombardier's C-series, use composites for manufacturing of fuselage and wing components [4–6].

1.2 Problem Statement

Laminated CFRP materials have been used widely in many industries, such as automobile, aerospace and military. However, fastener holes and notches, which are

the source of stress concentration, and manufacturing defects, such as fibre discontinuity, can cause up to 50% reduction in the compressive strength of the CFRP composites laminate [7–9]. Thin panels used in aircraft structures are prone to buckle as a result of compressive load, which then can lead to delamination due to interlaminar shear stress (ILSS) [10]. ILSS is an important property in designing composite structures, which can be a limiting design factor in using CFRP composites. ILSS depends largely on the layer of the matrix between the composite laminate.

The compressive strength of woven CFRP composites is mainly affected by the micro-buckling failure occurs in the produced parts. This failure occurs as a result of the low shear strength of the polymer matrix or epoxy resin, as well as the imperfection of the fibre waviness during the manufacturing process [9–11]. Compressive property of CFRP is influenced greatly by the properties of the epoxy resin and the carbon fibre, as well as the interfacial properties between the resin and the fibre [11–13]. Therefore, different methods were used in order to improve mechanical properties, including the ILSS. For example, weaving fibres in the direction of thickness and using Z-pins to connect the laminate by stitching, weaving, braiding and knitting, which led to improve ILSS notably [14–19]. However, these methods are labour intensive and costly and require specific manufacturing processes [14,20]. Another promising method that can be used to increase the strength of the epoxy and improve the ILSS is by the addition of nanoparticles into a matrix resin. Therefore, producing CFRP with high strength and stiffness requires a strong interfacial bonding between the carbon fibre and the epoxy matrix. Ideally, tougher resin supported by carbon fibres is required in order to provide an efficient load transfer and lateral support. Given that fibre waviness is hardly

avoided, the recent research works are focused on the development of a tougher epoxy resin system by addition of nano materials.

There are extensive number of research on modifying epoxy resin with nano materials such as carbon nanotube (CNT) [21–25]. By dispersing CNTs into epoxy, excellent thermal properties and mechanical properties of CNTs, such as extremely high moduli and stiffness, can be transferred to carbon fibre by interfacial bonding [26–28]. This method can develop better resistance of carbon fibre towards micro-buckling and delay cracks initiation. The new CNT-modified epoxy will improve compressive strength, fracture toughness, in-plane shear and interlaminar shear stress, since these properties are epoxy dominated. However, there are some factors that can affect the potential of CNT-modified epoxy, including the degree of dispersion of CNT into the epoxy. Poor dispersion of CNT can reduce the overall properties of carbon fibre (CF) laminates.

1.3 Aims and Objectives

The aim of this project is to increase the strength and toughness of the epoxy resin used in the carbon fibre reinforced polymer (CFRP). The project is focused on the following research tasks:

i. Dispersing two types of multiwalled carbon nanotubes (MWCNT) in epikote 828 epoxy resin.

a) Investigating the degree of dispersion by TEM, SEM, XRD, Raman spectroscopy and FTIR.

b) Analysing the thermal and mechanical properties of the MWCNT modified epoxy resin and comparing them with pure resins.

ii. Fabrication of MWCNT modified-CFRP composites and:

a) Investigating the interlaminar shear properties of CFRP laminate with different epoxy resin systems.

2 Literature Review

2.1 Thermosets

Polymer materials are mainly divided into two categories; thermoplastics and thermosets. Thermoplastic polymers can be melted back into liquid and since the curing process is reversible, these polymers can be reformed and reused. This behaviour occurs due to the weak attraction of intermolecular forces, known as Van der Waals forces, between non-neighbouring segments of the same molecules or separate molecules [29]. On the other hand, thermoset polymers can cross-link during the curing process to form an irreversible chemical bond, therefore, these polymers do not melt when reheated but instead they degrade [30]. Covalent bonds are formed between polymer chains when the crosslinking occurs. Crosslinking requires di-functional or multi-functional resin and/or curing agent. The thermal and mechanical properties of the thermosetting systems depend on the matrix component, i.e. the resin. The curing agent, which is a highly reactive multi-functional group, creates an environment that will lead to crosslinking of the resin. Thermosets have higher specific modulus than metal, in other word, its resistance to deformation as a ratio of the material's density is better than metal. Thermoset is a good choice for applications where the weight is an issue. There are various type of thermosetting resins, such as phenolic resin and epoxy vinyl ester. Table 2.1 summarises various thermosetting resins with their precursors and field of applications which; as adapted from Handbook of thermoset resins by Debdatta Ratna [31].

Table 2.1: Various types of thermosetting resins and their field of application [31]

Resin	Precursor	Applications
Phenolic resin	Phenol and formaldehyde	Wood adhesive, moulding compounds, foundry binders, laminate mouldings, electrical laminates, ablative coating casting and fibre composites for household appliances, automotive, aircraft construction and accessories, electrical and lighting industries
Unsaturated polyester	Dicarboxylic acids, diols and reactive diluents e.g.,, styrene	Fibre composites for mechanical equipment surface coating, and building construction, electrical industries
Epoxy	Epichlorohydrin and bisphenols	Engineering adhesives, paints and surface coating, electrical laminates, fibre composites for automotive, marine construction and aerospace applications.
Vinyl ester	Epoxy resin and acrylic or methacrylic acid	Fibre composites for mechanical equipment and building construction, marine construction, electrical industries
Melamine	Melamine and formaldehyde	Coatings, moulding compounds, wood materials processing, friction linings, textile auxiliaries
Urea	Urea and formaldehyde	Moulding compounds, textile auxiliaries, wood materials, foundry binder, foams
Furan	Furfuryl alcohol	Refractory materials processing, fibre composites, moulding compounds, grinding wheels, acid-resistant cements
Bismaleimide	Bismaleic acid and amine	Fibre composites for aircraft, rockets, missiles and re-entry vehicles.

2.1.1 Epoxy-Amine systems

Epoxide resins are formed from the epoxide group shown in Figure 2.1. There are several factors that make epoxy resins different from other thermoset resins; the availability of the resins ranging from low viscous liquid to tack-free solid; use of a wide range of temperature by judicious selection of curing agents with good control of the crosslinking degree and low shrinkage [31,32]. Epoxy resins are widely used in surface coatings (because it possesses high chemical and corrosion resistance), structural adhesives, engineering composites and laminates in electrical and electronics industries [31–33]. Epoxide rings in the epoxy resins experience a large amount of ring strain and react freely in a ring opening in the growth reaction mechanism.

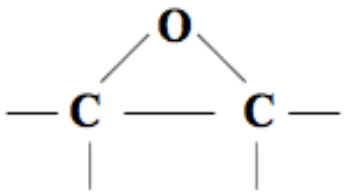

Figure 2.1: An epoxide group structure

There are several types of epoxy resin which are commercially used as matrices, such as Diglycidyl ether of bisphenol A (DGEBA), Diglycidyl ether of bisphenol F (DGEBAF), Triglycidy epoxide based on aminophenol (TGAP), Tetraglycidyl epoxide based on DDM (TGDDM). The structures of the epoxides are shown in Figure 2.2.

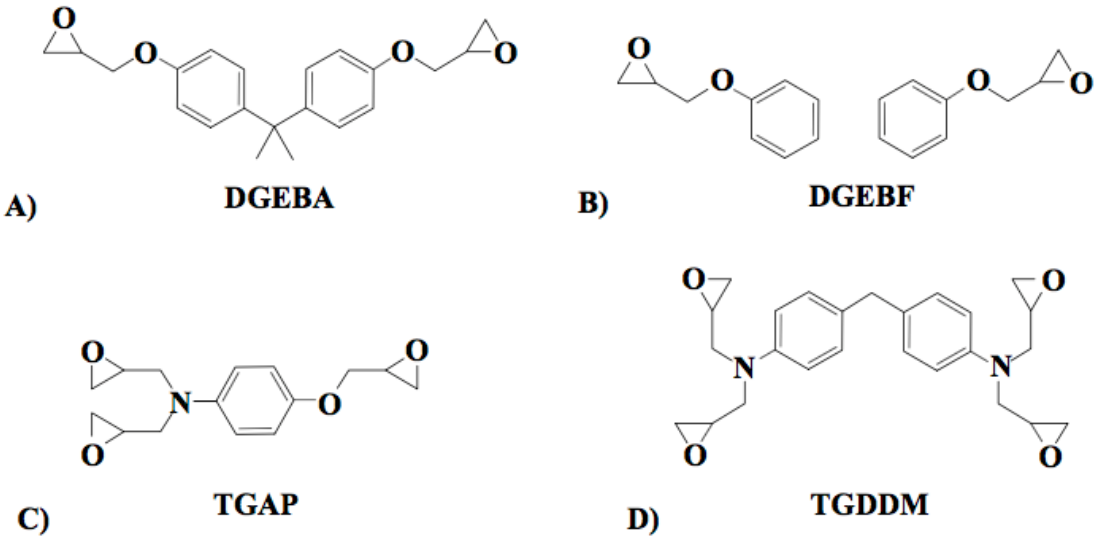

Figure 2.2: Structure of common epoxide resins

Curing agents or hardeners are used to develop and accelerate the growth of these resins and to ensure the crosslinks occur in a large number. Several types of curative agents are used to cure epoxies, such as amines, alcohols and thiols [32]. Ammines are commonly used to cure epoxy resins due to their high functionality per amine. Figure 2.3 shows the structure of curative amines; 4,4-diaminodiphenyl and 3,3-diaminodiphenyl sulfone. Amines can be grouped into three categories: aromatic, aliphatic and cycloaliphatic. Details of these amines are summarised in Table 2.2 which was adapted from Handbook of thermoset resin [31].

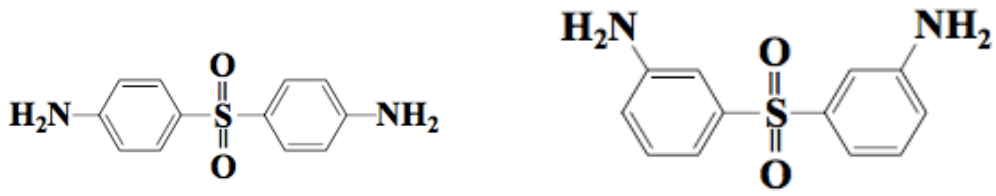

A) **B)**

Figure 2.3: Structure of amine A) 4,4-diaminodiphenyl and B) 3,3-diaminodiphenyl sulfone

Table 2.2: Comparison of different type of amine properties for epoxy curing [31]

Type of amine	Advantage	Limitation
Aromatic amine	Compared with aliphatic and cycloalipatic amine-cured network, aromatic amine has high Tg, better thermal properties and chemical resistance.	Curing requires high temperature, mostly solid, difficult to mix.
Aliphatic amine	Easy to mix, low viscosity, low cost, fast reacting, room temperature-curing.	Cured network can work only up to 80 °C, short pot life,high volatility and toxicity
Cycloalipatic amine	Long pot life, better thermal properties and toughness compared to aliphatic amine-cured network, curing at room temperatur.	Poor chemical resistance, poor solvent reisitance, high cost, can only work at a service temperature < 100 °C

Commonly, DGEBA is used commercially and has been the focus of a number of research pertaining to the resin's chemical and mechanical properties. X.Gong *et al* [34] investigated the decomposition behaviour and reaction mechanism of DGEBA

cured with 4-methyl tetrahydrophthalic anhydride (MeHHPA) with BDMA as an accelarator and DGEBA cured with dapsone (DDS) in near critical water. X.Gong *et al* found that DGEBA/MeHHPA/BDMA main chains were broken at the beginning of the decomposition due to the presence of ester groups. While, the DGEBA/DDS system was more difficult to decompose, due to the introduced benzene ring. X.Gong *et al* concluded that the decomposition mechanisms were different between the epoxy resin systems. For DGEBA uses MeHHPA/BDMA curing agent, the generated new ester bonds of curing reaction are thermally unstable which leads to relatively low decomposition temperature, as compared to the curing agent DDS. DDS contains rigid groups of benzene, which leads to an increase in the heat resistance and subsequently a relatively higher decomposition temperature [34]. Table 2.3 shows the results of crosslinking degree studied by X. Gong *et.al*. The degree of crosslinking of DGEBA/MeHHPA/BDMA and DGEBA/DDS were 6.5×10^{-4} mol cm^{-3} and 4.4×10^{-3} mol cm^{-3}, respectively. Therefore the DGEBA/DDS has higher decomposition temperature than the DGEBA/MeHHPA/BDMA.

Table 2.3: The crosslinking degree of DGEBA/MeHHPA/BDMA and DGEBA/DDS, results from X.Gong *et.al* [34]

Epoxy resin system	**DGEBA/MeHHPA/BDMA**	**DGEBA/DDS**
T_g (°C)	102.2	199.38
Storage modulus(MPa)(T_g+50°C)	1.629	21.41
The degree of crosslinking (mol cm^{-3})	6.5×10^{-4}	4.4×10^{-3}

2.2 Nano-filled CFRP composite

Aerospace industries are expanding the usage of CFRP/epoxy composite materials in the building of aircrafts [4,35]. High performance composites, such as CFRP, have a high mechanical strength, a light weight and a high temperature resistance. Thus, these characteristics led to the use of CFRP widely in aerospace, automobile, electronics and marine industries [36]. Compressive strength of CFRP composites is mainly influenced by the properties of the resin, the interface between fibre and matrix and also the fibre waviness [37–40]. The compressive failure of the Unidirectional CFRP laminate and woven CFRP laminate is usually occurred due to micro-buckling of the fibre and successive plastic kinking of the laminate [38,39,41]. Development of tougher and stiffer matrices can improve the properties of the CFRP composites. This will increase the resistance towards crack initiation, propagation and delaying the micro-buckling of CFRP laminates. Development of tougher matrices is essential in developing matrix–

dominated properties including, compressive strength, interlaminar shear stress, compression after impact and in-plane shear.

There are many studies suggesting that the enhancement of matrix properties can be achieved by the addition of nanomaterials. Common nanomaterial that are used to develop nano-modified epoxy matrix include nano-silica, carbon nanotube (CNT) and carbon nanofibre (CNF). Results from previous research revealed that the addition of nanomaterial to an epoxy will have positive effects on properties [42,43]:

i) Increases compressive and bending strength of CFRP laminates.
ii) Enhanced thermal stability and reduces thermal stress.
iii) Increases elastic modulus, which makes epoxy stiffer.
iv) Improves toughness due to pull-out toughening (resistance to crack propagation)

It is essential that the carbon nanotubes are well dispersed into the matrix before they can be used in the manufacturing of the structural components from the carbon fibre composites [44]. Generally, thermoplastic or thermosetting polymer matrix is used with carbon fibres to produce composites materials. The epoxy resin have become highly demanded matrices for the production of nanocomposites [44–47]. Epoxy matrix enhanced with CNT shows a significant improvement in the mechanical properties, thermal and electrical conductivity of the composite parts [48–51]. CFRP/CNT/epoxy composites provide a great potential in developing a wide range of applications in a vast number of industries including aerospace, automotive and marine [52]. Therefore, composites industry is now expanding and including nanocomposites materials in their

products. Thus, the process of nanocomposites production become critically important in composites industry.

2.3 Carbon nanotubes

Carbon nanotube (CNT) was invented by Sumio Iijima 1991 [53]. CNT is made of graphitic sheets that have been rolled up into cylindrical shape. The diameter of CNT is up to 100 nm with a length measured in micrometres [52,54]. There are three basic structures or chiralities (illustrated in Figure 2.4), which show how the graphene sheets are rolled, and these are:

1) armchair
2) zigzag
3) chiral

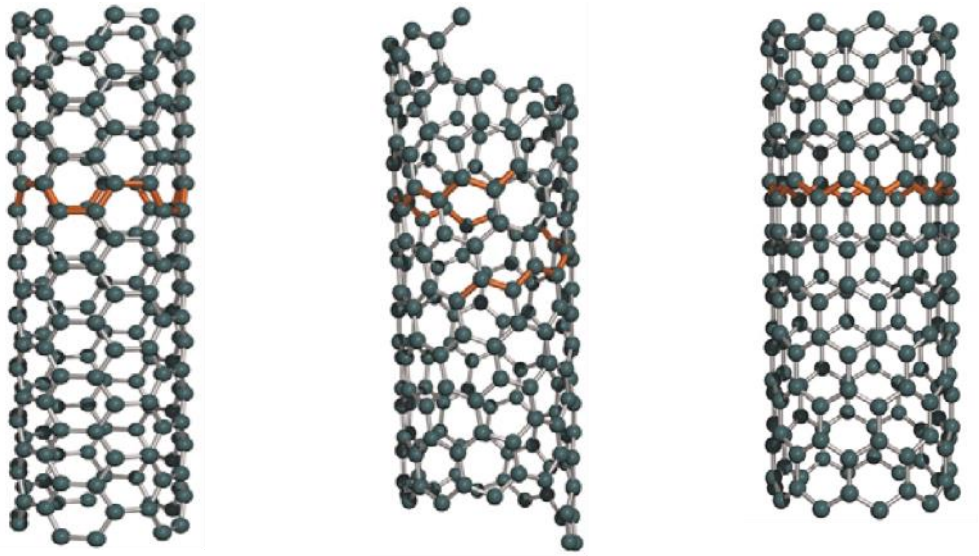

a **b** **c**

Figure 2.4: Nanotube chirality (a) armchair (b) chiral (c) zigzag [55]

CNT exhibit great mechanical, thermal and electrical properties. The tensile modulus and strength of the CNTs are between 250-1200 GPa and 10-200 GPa, respectively. Compared to the carbon fibres, the tensile modulus and strength are 500 GPa and less than 1GPa, respectively [44,56]. CNTs are widely known for their mechanical properties whereby its quality outweigh any existing materials [23,57]. CNT can be categorized into two basic types; single-walled carbon nanotube (SWCNT) and multi-walled carbon nanotube (MWCNT) as illustrated in Figure 2.5.

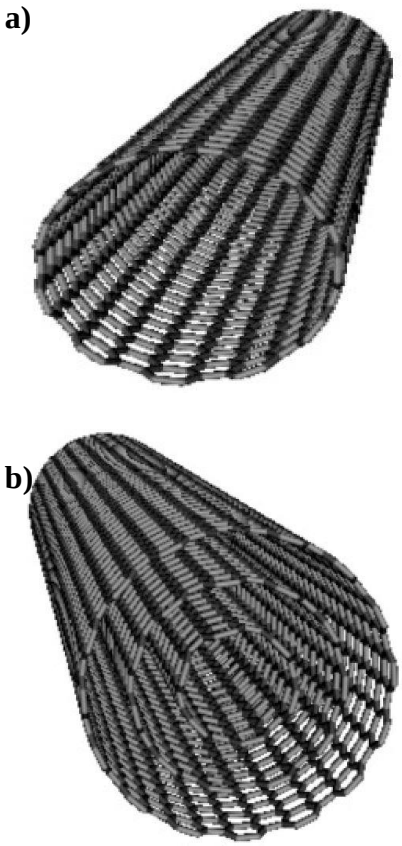

Figure 2.5: Structure of (a) SWCNT and (b) MWCNT

SWCNTs are defined by a single sheet of graphene which is rolled into cylinder forms with a diameter of 1 nm and length up to several centimeters [55]. SWCNTs can behave both as metallic and semiconducting depending on the chiral angle between carbon hexagons and the tubes [58]. The chiral, armchair and zigzag carbon nanotubes sometimes exhibit different properties. The zigzag and chiral CNTs show semiconducting behaviour, whereas armchair CNTs show metallic behaviour and are considered conducting materials [59]. SWCNTs are the most investigated types of CNTs [60–63]. Although SWCNTs have a simple structure, but they have outstanding electrical and mechanical properties. However, the production cost of the SWCNTs is

high and this restricts them from becoming commercialised materials, especially for composite industries.

MWCNTs are an array of two or more cylinders that are formed from graphene sheets which are separated from one another by 0.35nm [64] with a diameter ranges between 2 to 100nm and a length of tens of microns [65]. MWCNTs are more suitable for composite industries. Therefore, the attention of the nanocomposites research has been diverted from using SWCNTs to MWCNTs, in recent years [66].

Common production methods of CNTs [56,59]:-

1) arc discharge
2) laser ablation
3) catalysed decomposition
4) chemical vapour deposition (CVD)

CVD is considered to be a favourable method for producing high quantity of CNT (i.e. mass production). CVD requires a low processing cost, which is an important criteria for the industrial requirements [67]. Many researchers concluded that CNT acts as a reinforcing filler in a matrix which can enhance the mechanical and electrical properties of the new materials [51,68]. However, the content of CNTs used with the matrices is very small and it was observed that the glass transition temperature of the material decreases with the increase in the CNTs content [69].

2.3.1 Load transfer between CNTs and resin polymer

The interaction between CNT and polymer has been the interest of studies by nanomaterials researchers [70], [24], [21], [71], [72], [73], [74].

Wagner et. al. [70] investigated the tensile stresses of a single MWCNT fragmentation dispersed in thin polymeric films of a mixture of urethane/diacrylate oligomer EBECRYL 4858 with a thickness of approximately 200 μm. Wagner *et al.* found that the stress transfer is an order of magnitude higher than traditional filler of composites, such as carbon fibres. This finding was further supported by Cooper *et. al.* [75], who investigated the adhesion of CNTs (SWCNTs and MWCNTs) to epoxy resin (Araldite LY564, Ciba-Geigy, hardener HY560) by examining the interfacial shear strength. The technique they used involved the detaching of individual SWCNT bundles and MWCNTs from an epoxy matrix using a scanning probe microscope (SPM) tip. The interfacial shear strength was found to be varied from 35 MPa to 376 MPa. The bonding between CNTs and matrix material was also investigated by Gojny *et. al.* [24] by examining the mechanical properties (i.e. tensile and fracture properties) of the composites. These composites were reinforced with non-functionalised and amino-functionalised double-wall carbon nanotubes (DWCNT). Gojny *et al.* found that, with 0.1 wt% of DWCNT-NH_2 the Young's modulus increased from 3.29 GPa, for the neat resin, to 3.50 GPa.

However, poor interfacial interaction was also reported by many researchers. Ghaleb *et al.* [76] found that the addition of 0.05 vol% loading of MWCNTs decreases the tensile strength of unfilled epoxy from 53 MPa to 30 MPa (MWCNT/epoxy). However, a

slight increase was observed at 1 vol% of MWCNTs loadings. Schadler *et al.* [74] studied the load transfer in CNT/epoxy composites by monitoring the shift in Raman peak. They concluded that the load transfer between the CNT and epoxy is good in compression mode but showed poor characteristic in tension mode.

2.3.2 Dispersion of CNT

A good dispersion of CNT into the epoxy can improve the properties of CNT modified epoxy significantly. However, dispersion of CNT in a matrix is very challenging compared to the dispersion of other fillers, such as carbon fibres or spherical particles. This is due to the fact that commercialised CNTs are supplied in the form of entangled bundles, which in turn can contribute to the difficulty of the dispersion process [23]. The bundles of CNTs need to be separated in order to be uniformly dispersed and to maximise the surface contact area of the epoxy matrix.

CNTs are chemically stable and inert because of the strong carbon bonding that holds them together. Therefore they hardly can interact or bind with other atoms [23,59]. The Van Der Waals bonding between the CNTs and matrices is a major problem in achieving their full competency. Van der Waals bonding between the CNTs themselves create bundles of agglomerates, causing difficulty to process and disperse them into polymeric matrices [23,77]. Therefore, CNTs exhibit limited solubility and processability as a result of the Van der Waals interactions between individual carbon nanotube [77]. The presence of agglomerates, which is caused by poor dispersion, can initiate cracks and propagate easily and subsequently reduce the strength of composites [78,79]. Nanomaterials are used as reinforcement that enhance the mechanical

properties of the composites but the degree of this reinforcement depends highly on the state of nanomaterials dispersion.

Although CNTs possess excellent properties, such as high mechanical and thermal properties which allow them to be the ideal choice of filler in producing light weight polymer composite, their nature of being very prone to aggregating limits these properties [80]. The only interaction with the surrounding matrix is through the weak Van der Waals bonds, that hold the link between the CNT/matrix interface. Therefore, dispersion methods need to be developed to make full use of CNTs and produce improved properties. The quality of CNT particles dispersion into the host matrix will determine the potential of the bulk material [23,80]. Many methods are used to improve the dispersion of CNTs treatment, such as mechanical mixing and functionalisation of CNT.

2.3.3 Methods of dispersion of CNT

There are a number of techniques used for dispersing CNTs, including mechanical mixing, such as ultra sonication, high shear mixing and calendaring (also known as three-roll milling) [24,57].

Ultra sonication technique is widely used for CNTs dispersion with epoxy. Ajayan *et. al*. [81] used this technique to disperse multi-walled carbon nanotubes (MWCNTs) into an epoxy resin. After examining the sample under transmission electron microscope (TEM), no fractured nanotubes were found, indicating that the nanoparticles were strong enough to hold their structure during the mixing process. Nevertheless, a weak

interface bonding between the nanotubes and the matrix was observed. Good dispersion of MWCNTs, by using ultrasonic technique, was reported, however, the distribution of MWCNTs was relatively poor [82,83]. A homogeneous dispersion of MWCNTs in the epoxy resin can be achieved by ultra sonication method [84]. However, the aggregation of CNTs may form gradually once the stirring process stops. It was reported that sonication not only disaggregates CNTs bundles but also can segmented longer CNTs into shorter lengths [85–87]. Table 2.4 summarised the study of using sonication and the effect to the CNT's length.

Table 2.4: Previous study on dispersion using sonication and the effect to the CNT's length

Name of the author	Original length of the CNT	Length of the CNT after mixing,	Technique to analyse CNT length	The thickness of the TEM section	references
Asghar H. Korayem	5 -15 μm	a) 1.623 μm (after 15mins sonication) b) 1.063 μm (after 60 mins sonication)	TEM	Did not mentioned	[107]
Z. F. Li	1 mm	50 μm	SEM	-	[134]
Yan Yan Huang	Did not mentioned length, TEM images just comparing two different figures between 1h sonication and 10 h sonication	-	-	-	[88]
Fawad Inam	2 μm	1) 5mins sonication – 1689 nm, 2) 8 mins sonication – 1332 nm, 3) 11 mins sonication – 992 nm 4) 14 mins sonication – 502 nm	FE-SEM	-	[49]
Micheal Russ	50 μm	5 μm	Optical microscopy for the image and ImageJ was used to measured CNT length	-	[87]

High-shear mixing is used to separate nanotubes from agglomerates. In order to achieve fully dispersed MWCNTs in the epoxy resin, CNTs need to be high shear mixed for a long period of time (up to 24 hours in some cases)[88] . However, this could deteriorate the mechanical properties of the nanocomposites as a result of the fragmentation of the MWCNTs [66,88].

Three-roll milling is another technique used for CNTs dispersion in the epoxy without damaging or rupturing the CNTs [22]. Previous studies suggested that the dispersion of CNTs in epoxy resin is relatively a good approach to achieve homogenous dispersion [23,24,89]. In this process, the nanocomposite mixture paste is forced to pass through rotating cylinders with a specified gap between them, and the paste is uniformly sheared by these cylinders [89]. The minimum gap between the rollers is between 1-5μm. This can be an issue if the gap is much larger than CNTs individual diameter. To overcome this problem, the nanocomposite need to be viscous when the material is fed in to the system [23]. This technique can be used to produce high volume nanocomposite materials and it is cost effective. Therefore, it can be scalable from the laboratory to large-scale production [89].

The dispersion of CNTs into the matrix plays an important role to the performance of CNT/polymer nanocomposite and the interfacial interactions between the CNT and the polymer. Carbon atoms on the CNT walls are chemically stable due to the aromatic nature of their bond. Although CNTs can interact with the surrounding matrix through Van der Waals interactions, they are unable to provide efficient load transfer across the CNT/matrix interface [23]. Many research works have been focusing on achieving a maximum dispersion in polymeric matrices and efforts have been made to develop new methods to modify the surface properties of CNTs. Functionalisation of CNTs is one of these methods that showed a wide interest from many researches [61,90–93]. This method can enhance the ability of dispersion and stress transfer through the polymeric matrices interface [65].

Functionalisation is a process of improving dispersion and adhesion of CNTs particle to the polymer matrix. Functionalisation of carbon nanotubes can improve solubility and enhance the dispersion of CNTs in the matrix, as well as the interfacial adhesion between CNTs and the matrix [51,52,94]. Many approaches of functionalisation have been used, including covalent functionalisation [93,95–97], non-covalent functionalisation [98,99] ionic [doping] [63], ionic functionalisation [62] end defect-chemistry [100] and ionic liquid covalent functionalisation [96,97].

Covalent functionalisation is a method in which chemical components are bonded to CNTs surface by covalent bonds. This method requires reactive functional groups which can be formed by using acid treatment or by attaching reagents to the CNTs sidewalls [91]. The drawback of covalent functionalisation is that the conjugated graphitic chemical structures are disrupted during this process. The covalent sidewalls functionalisation is associated with the change of hybridization from Sp^2 to Sp^3. This will affect the mechanical strength and the electronic transport within CNTs conjugated system [54,61,66].

Non-covalent functionalization of CNTs has captured the interest of many researchers in composite materials [91]. The advantage of non-covalent functionalisation is that this method does not affect the electron bonding system and thus maintaining the stability of the CNT compounds or sidewalls. This would contribute to optimise the properties of the final structural of the material [51]. Non-covalent functionalisation involves the use of surfactants, bio-macromolecules and polymers [61,91]. Previous studies have shown that high volume of CNTs can effectively disperse in the polymer matrices without destructing the CNTs' conjugated system. However, the limitation of

using this type of functionalisation is that, the interfacial strength becomes relatively weak between nanotubes [61].

MWCNTs will be used since they offer more beneficial reinforcement in fibrous composite materials compared to the SWCNT. MWCNTs exhibit excellent properties, easier to process and also cheaper to produce [101,102]. Therefore, MWCNTs are suitable in producing nano-modified composite materials. Additionally, previous studies showed that the use of different lengths of CNTs can affect the mechanical properties of resin matrix [49]. Therefore, it has been decided to use two different lengths of MWCNTs in this project.

The combination of different techniques of MWCNTs dispersions, using ultra-sonication, high shear mixer and three-roll milling have been investigated. These techniques were used in a considerably short span of time to disperse MWCNTs, in order to avoid the degradation of the mechanical properties. The use of a combination of these three mechanical techniques would help to achieve a homogenous dispersion of MWCNTs in epoxy matrix system and also reducing the processing time.

3 Experimental details

3.1 Overview

This chapter outlines the materials and brief explanations on fabrication methods of and gives a brief description of the fabrication methods of (i) carbon nanotube filled epoxy nanocomposites and (ii) carbon nanotube filled carbon fibre reinforced polymer (CFRP) composites. It explains the procedures to characterise thermal, physical and mechanical properties of Epikote 828+DDS, MWCNT filled epoxy and CFRP. Epikote 828+DDS epoxy and MWCNT filled epoxy are characterised by using transmission electron microscopy (TEM), x-ray diffraction (XRD), infrared spectroscopy (IR), Raman spectroscopy, density measurement, thermogravity analysis (TGA), dynamic mechanical analysis (DMA), differential scanning calorimetry (DSC), flexural, tensile, compression and fracture toughness test. This chapter also described the measurement procedure of constituents contents. The characteristics of CFRP composites are tested by using interlaminar shear strength and determined by using a short beam shear test (SBS). Fractured test specimens were analysed using scanning electron microscopy (SEM) which correlate between mechanical and failure mode.

3.2 Materials

The resin system used in this experiment is Epikote 828 epoxy, a diglycidyl ether of bisphenol-A (DGEBA) Silmid Limited, cured with Amine hardner, 44'-Diaminodiphenyl sulfone (DDS) from Sigma Aldrich. This thermosetting resin is modified with multiwalled carbon nanotubes (MWCNTs). Two types of MWCNTs, which are different in length, are used. The properties of the materials are summarised

as shown in Table 3.1. The type of reinforcement element used in this study is plain carbon fibre from Sigma Aldrich.

Table 3.1: General properties of the resins and MWCNT given by the manufacturers

Properties of material used	Epikote 828	DDS	MWCNT *Purity: > 95%	
			Type1	Type2
Appearance	Clear liquid	Off white powder	Black powder	Black powder
Density	1.16g/ml	0.25 -0.35 g/cm^3	2.1 g/cm^3	2.1 g/cm^3
Viscosity (at 25^{0}C)	13 pa.s	N/A	N/A	N/A
Epoxy 828 manufacturer equivalent weight	184-190 g/eq	N/A	N/A	N/A
Amine hydrogen equivalent weight		62 g/eq	N/A	N/A
Length	N/A	N/A	10-30μm	0.5-2 μm
Outside diameter	N/A	N/A	10-20nm	10-20nm
Inside diameter	N/A	N/A	5-10nm	5-10nm
Bulk density	N/A	N/A	~0.04-0.05g/cm^3	~0.17g/cm^3
Manufacturer/Supplier	Silmid Limited	Sigma Aldrich	Nanostructand and Amorphous Materials Inc.	Nanostructand and Amorphous Materials Inc

3.2.1 Epikote 828 epoxy resin

Epikote 828 is an epoxy resin made from bisphenol A and epichlorohydrin is supplied by Sigma Aldrich. The average viscosity as presented in Table 3.1 is low, making it suitable for various fabrication techniques such as adhesives and matrices of composite. In this study Epikote 828 is used as matrix of composites. To cure and cross-linked Epikote 828, DDS (Diamino diphenyl sulfone) from Amine family from Sigma Aldrich was chosed as a curing agent or hardener. The combination of these two elements will determine intermolecular cross-linking and produce a hard thermosetting system.

3.2.2 Multiwalled carbon nanotube (MWCNT)

The MWCNTs with trade name (carbon nanotubes, 1236YJS with the length of 0.5-2μm and carbon nanotubes, 1205YJ length of 10-30 μm) presented in Figure 3.1 were procured from Nanostructured and Amorphous Materials, Inc. USA. The MWCNTs for both types have the same diameter in the range of 10-20 nm for outside diameter and 5-10 nm for inside diameter respectively and with purity of 95%. Manufacturing method was by catalytic chemical vapor deposition (CVD).

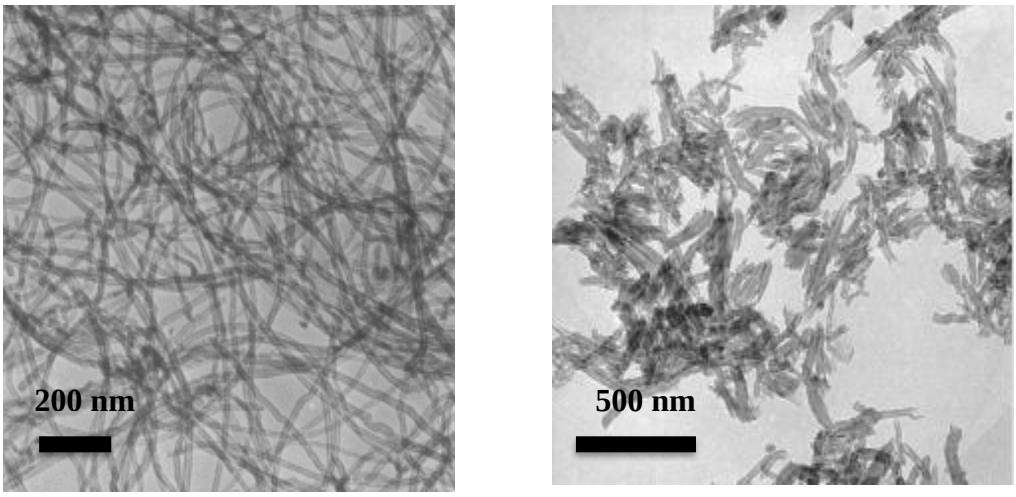

(a) (b)

Figure 3.1: TEM images of as-received a) MWCNT (length 10-30 μm) and b) MWCNT (length 0.5-2 μm) from manufacturer [103]

3.2.3 Carbon Fibres

Plain weave carbon fibre from Easycomposite is used in this study for making the carbon fiber reinforced polymer (CFRP).

3.3 Developement of MWCNTs / Epikote 828 composites resin

Two nanofilled resin systems were developed from two types of MWCNTs mixed with Epikote 828 epoxy, i.e., MWCNT_short/828 and MWCNT_long/828. The two types of MWCNTs are different in length (type 1, length of 0.5-2 μm and type 2, length of 10-

30 μm) were dispersed in combination of three methods: i) soniction probe ii) high shear mixer iii) three-roll mills.

3.3.1 Epikote 828 resin polymer

Epoxy resin consisting of 100 parts of Epikote 828, a diglycidyl ether of bisphonel A (DGEBA), cured with 30 per hundred of resin (phr) DDS, a hardener consisting of 4,4'-Diaminodiphenylsulfone are used for the polymer matrix in this study. The mixture is stirred with over head stirrer in a heated oil bath of 140°C for 10-15 minutes, then it was degassed in a vacuum oven at 120°C for another 10-15 minutes. After the degassing process, the resin is used in different ways, namely: cured in silicone mould for mechanical testing sample and in corporated as a matrix to carbon fibre fabric (plain weave (1x1)).

Before manufacturing the mechanical testing samples, the silicon rubber moulds were degassed overnight in the vacuum oven at 25^{o}C to 30^{o}C. The purpose of degassing is to prevent air from trapping in the silicone moulds which can create voids in the samples. Various shapes of silicon rubber moulds were prepared including dogbone, rectangular plate and cylindrical to produce test samples. The silicone moulds were produced by mixing a high-performance silicon rubber RTV 3325 with a catalyst 6H in the ratio 100:5 in a paper cup. The mixture was stirred until it was completely mixed and then was poured on the positive which is made from aluminium and taped in a container. The mixture was cured at room temperature for 24 hours.

After degassing the Epikote 828/DDS resin, it was poured into the silicone rubber mould, which has been preheated in the oven to 100^{o}C, and curing it in the conventional oven. The curing cycle is illustrated as shown in Figure 3.2. MWCNTs-filled Epikote 828 resin for both types of MWCNTs were cured following the same process used for curing the Epikote 828+DDS resin and the same curing cycle Figure 3.2.

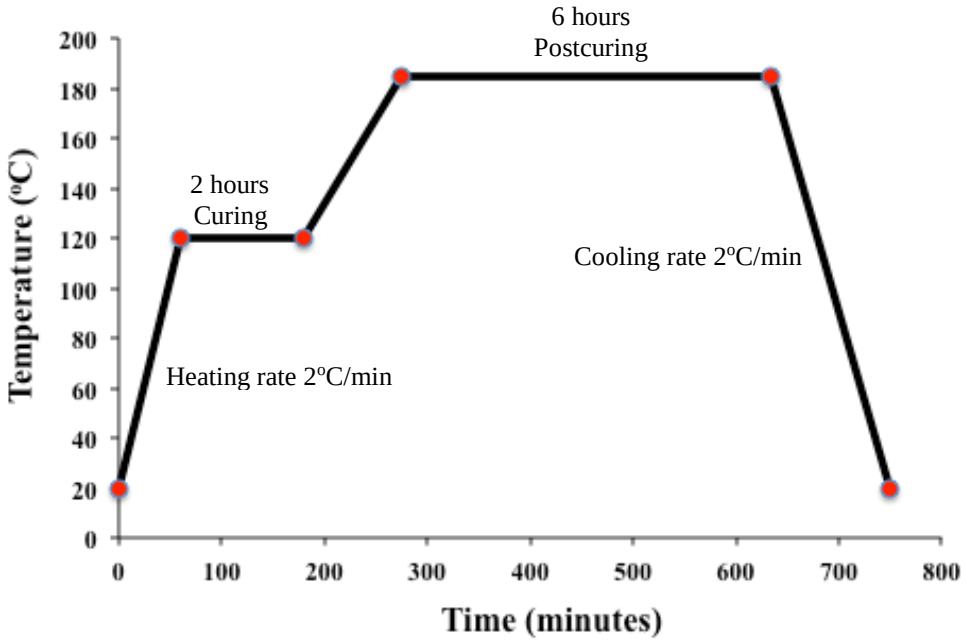

Figure 3.2: Curing cycle for Epikote 828 resin system.

3.3.2 MWCNTs-filled Epikote 828

Two batches of MWCNTs composites were developed using MWCNT_long (length 10-30 μm) and MWCNT_short (length 0.5-2μm) and were labelled as MWCNT_long/828 and MWCNT_short/828, respectively. Figure 3.3 shows a schematic illustrating the procedure used for the fabrication of MWCNTs/828 nanocomposites.

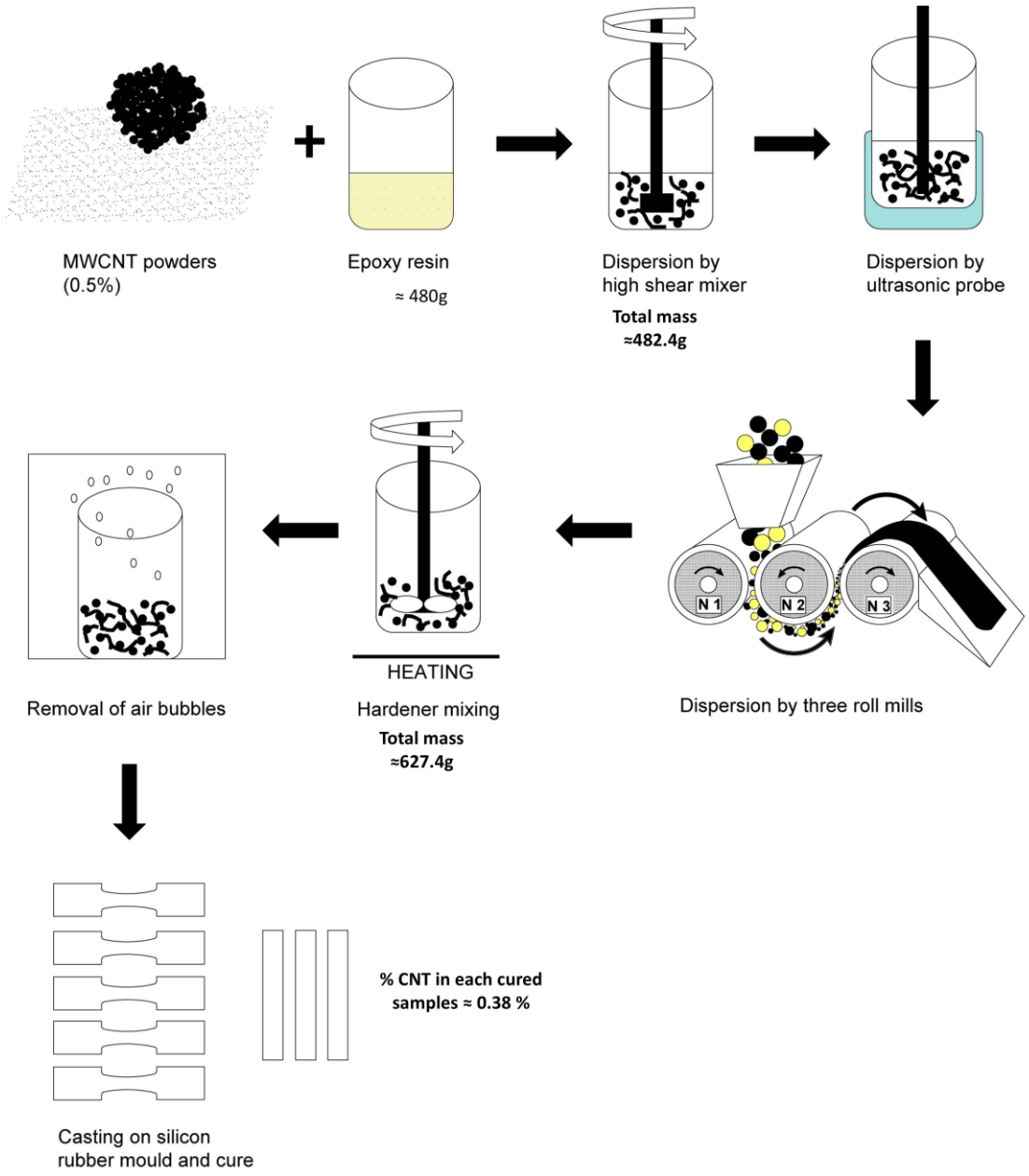

Figure 3.3: A schematic illustration of the fabrication of MWCNT/828 nanocomposites.

3.3.2.1 Dispersion of MWCNTs/Epikote 828

Dispersion of MWCNTs is a crucial stage in the composite manufacturing process that requires an efficient and effective method for MWCNTs dispersion to limit the fragmentation and the damage to the MWCNTs. Nano-modified epoxy containing damaged MWCNTs can negatively affect the mechanical and thermal properties and also the electrical conductivities [104]. The dispersion of MWCNTs was obtained by mixing 100 weight percent of Epikote 828 with 0.5 weight percent of MWCNTs. The mixture was mixed by using a Silverson L2R high shear mixer for 10 minutes. Stages of mixing are illustrated in Figure 3.4.

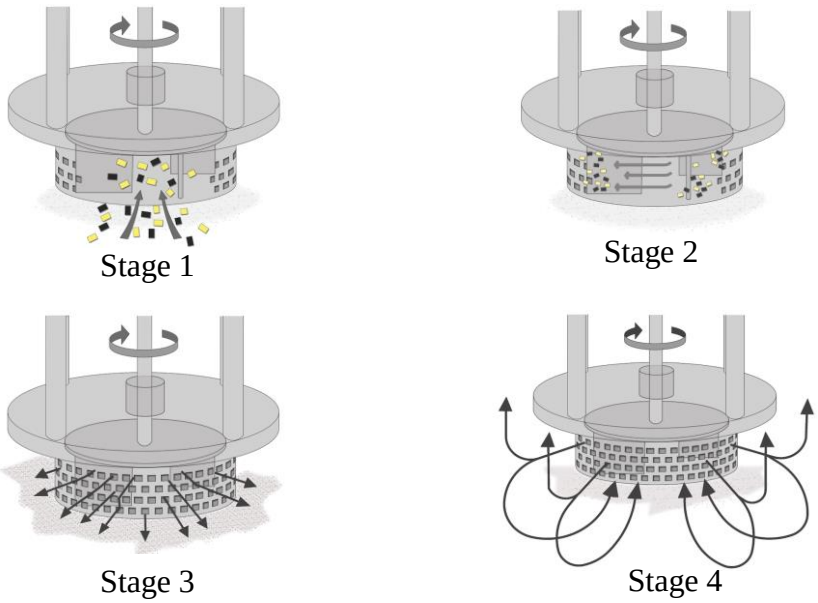

Figure 3.4: Silverson shear mixer include four stage mixing process [105].

In the first stage, the nanomodified epoxy mixture was sucked up from the bottom of the beaker into the workhead. The rotary blade and the inner wall of the stator created centrifugal forces and mixed the MWCNTs/Epikote 828 epoxy mixture. Under high

hydraulic shear forces, the nano-modified epoxy mixture is forced out from the workhead. The workhead/screen used in this study is square hole high shear screen as shown in Figure 3.5, and works as stator with four blade rotor. The head type was used because it works to initially breakdown large agglomerates of MWCNTs into multi-agglomeration [105,106].

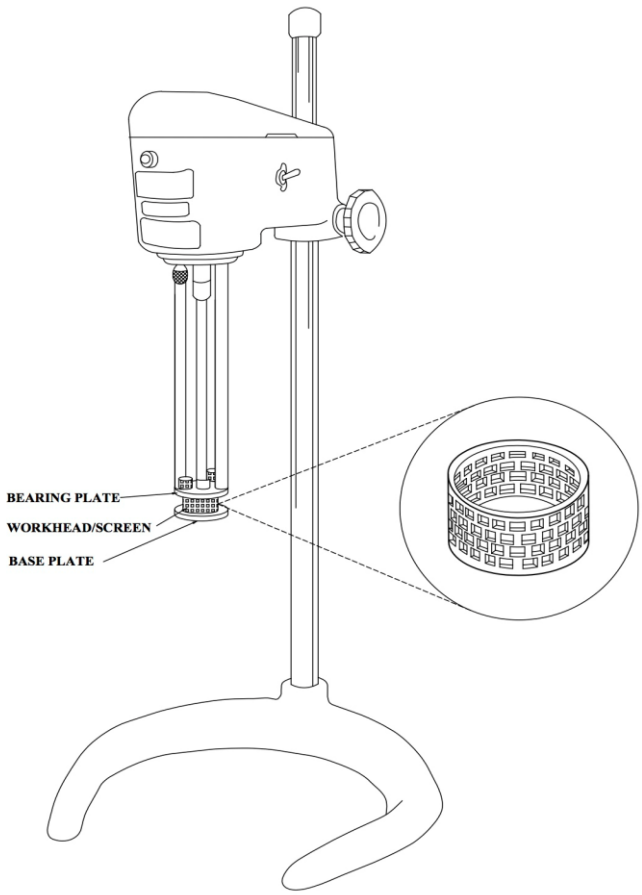

Figure 3.5: Work head/screen or also known as stator, which was used for Silverson high shear mixing is from type Square Hole disintegration screen

After mixing with the high shear mixer to breakdown the large agglomerates, the MWCNT/Epikote 828 mixture was then mixed further with ultrasonic probe. Previous research works indicated that the ultra-sonication treatment can break up multi-

agglomerates into smaller parts [104]. The MWCNTs/epikote828 mixture was sonicated by using Hielscher UP 200s (200 watts, 24 kHz). Sonotrode S7 was used with a tip diameter of 22 mm. The immersion of the sonotrode depth is 3.5 cm from the MWCNTs/Epikote828 mixture surface in a standard 400 mL of the MWCNTs/Epikote 828 mixture. During the dispersion of MWCNTs in Epikote 828, the beaker, which contains the mixture, was immersed into water and a 15s On/OFF cycle was used to reduce the heat produced by the sonicator. The time duration for a batch of 400 ml of the MWCNTs/Epikote 828 mixture was 15 minutes. The time duration of mixing by high shear mixer was used base on the study shows in Table 3.2.

Previous studies suggested that longer sonication time can significantly shorten the CNTs length, which will then reduce the aspect ratio (length/diameter) of CNTs [107]. High aspect ratio of CNTs are required to enhance the mechanical properties of the reinforced composites [52,107]. Both mixing methods were carried out at the laboratory of the Department of Mechanical Engineering, University of Newcastle.

Table 3.2: Comparison of different dispersion methods by Y.Wang et al. [104]. The sample used in this study are dry s-MWNTs for shearing method and for ultrasonication the r-MWNTs are dispersed in deionised water containing a little ionic dispersant of sodium dodecyl sulfate (SDS).

Method	Scale	Mechanism	Main treatment condition	Sample code
Shearing	10 -100 μm	Breaking up the multi-agglomerates	24 000 r/min, 5 min	s-MWNTs
Ball milling	10 – 100 μm	Breaking up the multi-agglomerates	Porcelin ball (20 mm,11g), 3.5 h	m-MWNTs
Ultrasonication	1 – 300 μm	Dispersing of the single-agglomerates	59 kHz, 80 W, 10h	r-u-MWNTs m-u-MWNTs
Concentrated H_2SO_4 / HNO_3	None-scale (individual nanotubes	Dispersing the MWNTs by shortening their length and adding carboxylic groups	3:1 concentrated H_2SO_4 / HNO_3	r-s-MWNTs r-b-MWNTs a-b-MWNTs

The final step of dispersion MWCNTs in the Epikote 828 involved mixing the mixture by calendaring process using Exakt 80E three-roll milling machine. This process was carried out at the laboratories of the University of Bradford. The diameter of the rollers was 80 mm with a length of 200 mm. The diameter for all the rollers was 80 mm with the length of 200 mm. The rotational speeds of all the rollers can be adjusted but the ratio of the angular velocity of roller were fixed ($\omega_{1(\text{feed roll})}$: $\omega_{2\ (\text{center roll})}$: $\omega_{3(\text{apron roll})}$ = 1: 3 : 9) [71,108,109]. The feed roll and the apron roll rotate in the same direction while the center roll rotate in the opposite direction as, illustrated in Figure 3.6.

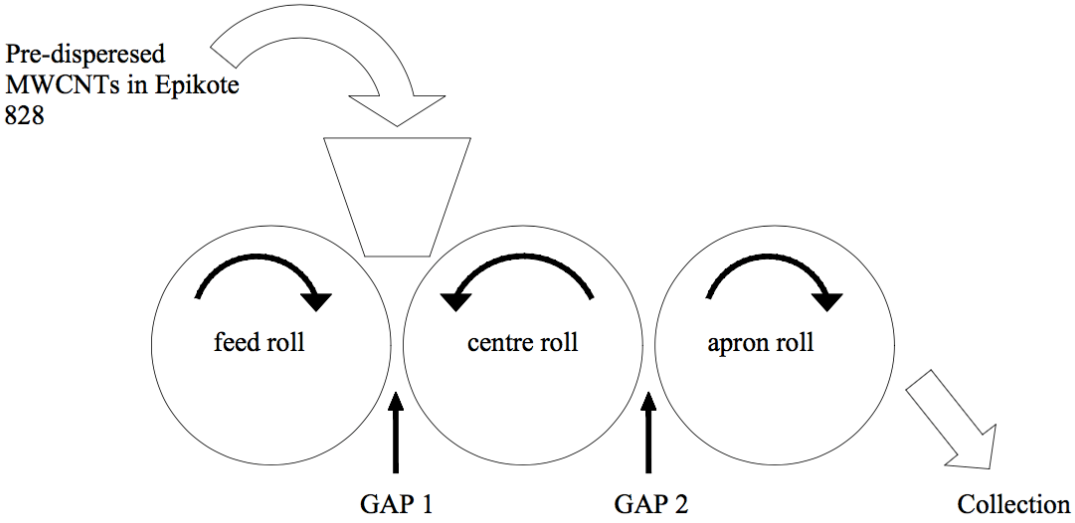

Figure 3.6: Position of gap 1, gap 2 and the direction of rollers.

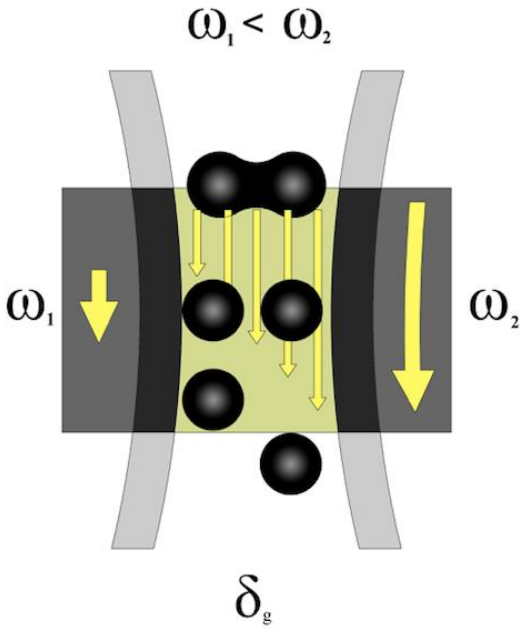

Figure 3.7: High shear mixing area between feed and centre rollers.

The differences in the angular velocity generate a shear strain that induces shear stress in the viscouse mixture of MWCNTs / Epikote 828. Figure 3.7 highlights the intense shear mixing area, the small gap between rollers, δ_g, and the difference angular velocity of the adjacent rollers, $\omega_1 > \omega_2$, that produced the high shear rate. The shear strain rate at the first gap (1) and second gap (2) can be expressed by the following equations [109]:

$$\dot{t} = \frac{r(w_2 - w_1)}{d_g} = \frac{2}{9}\frac{rw_3}{d_g} \qquad (1)$$

$$\dot{t} = \frac{r(w_3 - w_2)}{d_g} = \frac{2}{3}\frac{rw_3}{d_g} \qquad (2)$$

where: r = roll radius, d_g = gap distance and w= angular velocity.

Equations (1) and (2) show that the second gap gives more shear-strain due to the increase in shear stress. This can be achieved by reducing the gap between rollers or by increasing the speed of the rollers. Reducing the gap between the rollers is the easiest option as the gap setting can be monitored by an electronic control system and adjusted accurately. In this study, the method of dispersion using three-roll mills was carried out using the configuration given in Table 3.3.

Agglomeration of MWCNTs occurs during the mixing process with Epikote 828 resin. Thus, it is necessary to start with a bigger gap in the first pass, and 1/3rd of that in the second pass due to the gear ratio. The gaps are reduced step by step for every pass and

the rollers will gradually become cleaner as the gaps get smaller. In Table 3.3, the 4th pass, force is adjusted to suit the viscosity until the 2nd gap indicated 0 microns on the display screen. This step is necessary in order to obtain a finer dispersion that increases the mechanical strength of the epoxy. One of the concerns when using the 3 roll mills, is that the minimum gap between the rollers is between 1-5μm, which is larger than the diameter of individual MWCNTs. Pre-dispersion of MWCNTs in Epikote 828 resin, using a high shear mixer and an ultrasonic probe, can create a viscous paste which is suitable to run with three-roll mills and gives better dispersion. As the viscosity of the mixture is good for dispersion using 3 roll mills, the design of the number of passes can be decreased, thus reducing the time of dispersion. The temperature of rollers was maintained at 20 °C to 25 °C to avoid heating, which can decrease the shear effect.

Table 3.3: Configuration of the gaps between rollers of the three roll-mills and speed at every passes. Speeds are of the apron roller, measured in rpm.

Roller by pass	**Gap 1/Gap 2 (μm)**	**Speed (rpm)**
1st pass	106/40	200
2nd pass	60/20	300
3rd pass	15/5	300
4th pass	5/Force mode – 0 gap	300

3.4 Fabrication of carbon fibre reinforced (CFRP) composites laminates

3.4.1 Resin impregnation

Hand lay-up technique was used for resin impregnation of 16 layers of plain carbon fibre. The plain carbon fibre is cut into 250 mm x 350 mm in dimension. The setup for impregnation of resin is presented as shown in Figure 3.8. The hotplate temperature was set to 80 °C to decrease the viscosity of the resin. The viscosity of the resins was very high, particularly the MWCNT/828 modified resin system. Plastic applicator was used to consolidate the resin into the carbon fibre. The resin was placed in the beaker and was soaked into the oil bath at 80 °C along the process. This process needs to be carried out as quickly as possible to prevent the crosslinking of the resin from occurring.

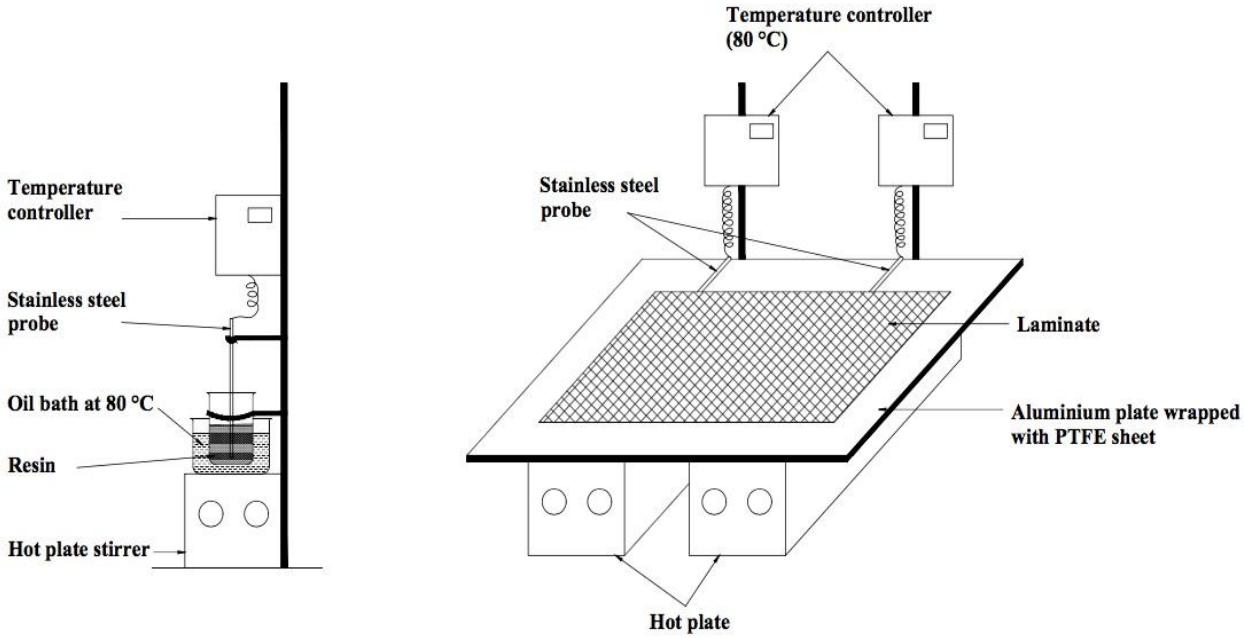

Figure 3.8: Setup for CFRP lay-up

3.4.2 Curing procedure

Vacuum bagging was used by stacking all the necessary components for this process as shown in Figure 3.9. The layup was cured in an oven using curing schedule shown in Figure 3.2. The curing program comprised of a 2 hours curing period at 120 °C and 6 hours post curing period at 185 °C. Dwell period was separated by a 2 °C/min ramp rise and the same ramp rate was used for cooling to room temperature.

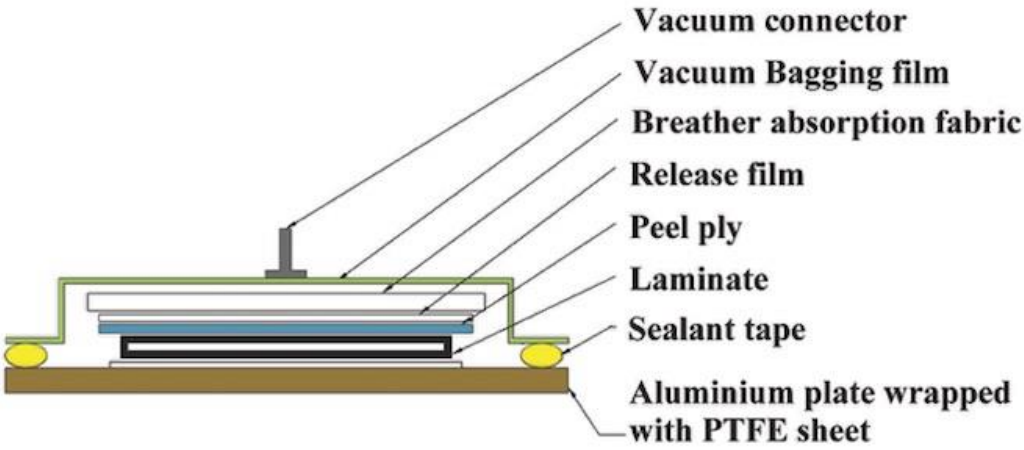

Figure 3.9: Schemmatic diagram of vacuum bagging that uses atmospheric pressure to hold laminated components.

3.5 Thermal analysis

Thermal analysis was conducted by using differential scanning calorimeter (DSC), dynamic mechanical analysis (DMA) and thermogravimetric analysis (TGA). DSC was used to analyse the curing behaviour and glass transition (Tg) of the neat Epikote 828 resin and the MWCNTs/Epikote 828 composite. According to previous studies, measuring Tg using DMA gives better information and resolution for highly crosslinked and filled polymers [110]. In this study, the TGA is also been used to obtain the samples weight fractions.

3.5.1 Differential Scanning Calorimeter (DSC)

A Pyris Diamond DSC was used to determine the samples glass transition (T_g). The DSC apparatus consists of a measurement chamber with two pans and connected to

computer. The two pans are placed separately, in self-contained calorimeters as shown in Figure 3.10. One of these pans is a sample pan and the other pan is a reference pan, which is always left empty.

The technique DSC works by measuring the differences between the heat flow rate of a sample and a reference pan as a function of temperature. The sample is exposed to a controlled temperature using a predefined protocol[111,112]. When the sample temperature is increased or decreased, energy is applied or removed from the calorimeter and the system is maintained at "null state".

According to ISO 11357-2:2013 standard, the glass transition temperature of polymer is the reversible transition in amorphous materials from a hard and relatively brittle state into a molten or rubber-like state [113]. T_g is determined by the DSC curve of heat flow versus temperature.

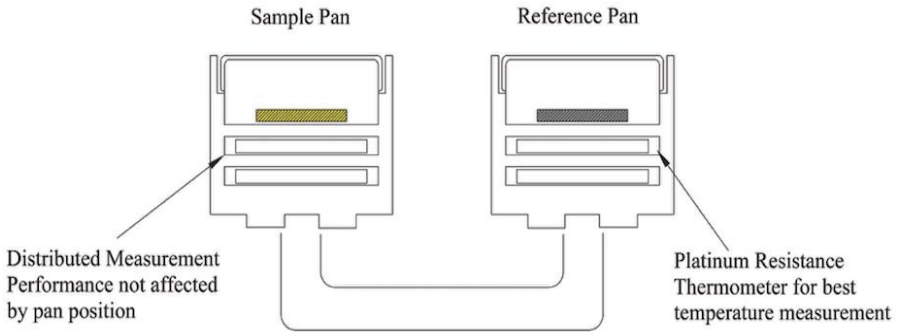

Figure 3.10: Diagram of Pyris Diamond DSC calorimeter cell containing reference and sample pan [114].

The weight of the cured samples of the Epikote828+DDS and MWCNTs/Epikote828 resin system was between 7-12 mg. The specimen was placed in the sample pan and

heated according to the oven curing cycle, as shown in Figure 3.11. The determination of T_g was performed according to the British standard BS ISO 11357-2:2013. The samples were heated from 25°C to 250°C at heating rate of 10°C/min. All samples were purged with Argon gas which was supplied at 40.0ml/min.

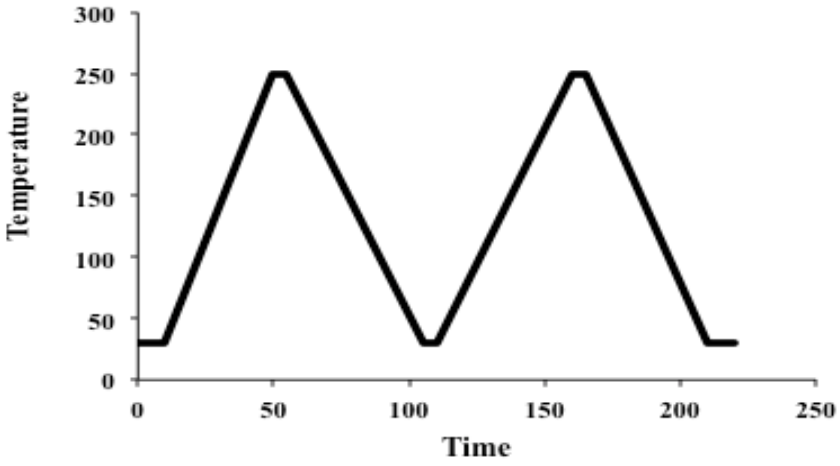

Figure 3.11: DSC program for Epikote828+DDS, MWCNT_long/Epikote828, MWCNT_short/Epikote828 resin system

3.5.2 Dynamic mechanical analysis (DMA)

Perkin Elmer DMA 8000 was used to determine the glass transition temperature (T_g) of the resin based polymers. Rectangular bar samples of approximately 40mm x 10mm x 3mm were tested by using a dual cantilever bending deformation mode. The temperature was scanned from 25 °C to 250 °C with a ramp rate of 3 °C/min. A single oscillating frequency of 1 Hz was used throughout the measurement with a displacement of 0.05mm. DMA works by applying sinusoidal stress to the sample. The

sinusoidal stress was created by using the oscillatory force supplied by DMA which eventually generates a sinusoidal strain [115].

3.6 Density and volume fraction measurement

The density and volumetric measurement of neat Epikote 828 and MWCNT/828 were conducted by using Micromeritics AccuPyc II 1340 pycnometer and GeoPyc 1360 pycnometer.

3.6.1 Accupyc II 1340

The AccuPyc II 1340 uses gas displacement method to determine the density and volume of the samples. The inert gas used in this method was a helium gas. The volume of the displaced helium gas was measured at a constant chamber temperature of 25.72 ^{0}C with a number of purges of 20 at an equilibrium rate of 0.005 psig/min and 20 cycles. Volatiles were automatically purged from the samples and the analysis was repeated until it reaches a consistent result [116].

3.6.2 Geopyc 1360

A non-hazardous quasi-fluid, known as Dry Flo^{TM}, is used in a dry flow powder technique, using GeoPyc 1360 to determine the envelope density of the samples. The sample was placed in a precision cylinder in a bed of Dry Flo^{TM}, which has a high degree of flow-ability. The powder is then slowly and steadily compressed by a plunger with a consolidation force of 38 N and a conversion factor of 0.2907. The calculation

of voids in the samples were then obtained from the data collected from the AccuPyc and GeoPyc as described in the following equations:-

$$\rho_A = \frac{m_s}{v_s}$$

$$\rho_G = \frac{m_s}{V_v + V_s}$$

$$\frac{\rho_A}{\rho_G} = \frac{\frac{m_s}{v_s}}{\frac{m_s}{v_s + v_v}}$$

and,

$$\frac{v_s + v_v}{v_s} > 1, \text{ so, } \frac{\rho_G}{\rho_A} = \frac{v_s}{v_s + v_v} = Æ$$

$$\backslash \ \%void = 1 - \varnothing = \left(1 - \frac{\rho_G}{\rho_A}\right)$$

where,

ρ_A : density of sample from Accupyc measurement

ρ_G : is density of sample from Geopyc measurement

m_s : is mass of sample

v_s : is volume of sample

3.6.3 Thermogravimetry analysis (TGA)

The values of the fiber volume fraction, resin content and nanoparticles content are vital as they have a significant impact on the failure of the composite materials [117]. In this

project, TGA was used to obtain the weight fraction of the constituent in the MWCNT/828 composites and CFRP composites. Table 3.4, summarizes past studies of researchers using TGA to determine the volume fraction from composites using epoxy and nanomaterial.

Table 3.4: A summary of past studies using TGA to determine the volume fraction from composites containing of epoxy and nanomaterial

Type of filler	Epoxy type	TGA temperature range and ambient gas	TGA type	References
MWCNT (purity>95%), d=30 to 50 nm, l=3 to 10um from Carbon Nanotechnologies, Inc.	Epon 862 (bisphenol F epoxy)	270 ºC – 800 ºC in nitrogen gas, heat rate 10 ºC/min	TA Instru-ments TGA2950	[118]
CNTF (CVD synthesized, produced in lab)	Araldite LY 1564(bisphenol A epoxy)	Room temp – 700 ºC, oxidative atmosphere(air), flow rate 60 mL/min.	TA instruments Q500	[119]
EpMWCNT	Epon 828 resin	50 ºC to 800 ºC, nitrogen gas, heat rate 10 ºC/min	TA Instruments Q50	[120]
MWCNT (purity>95%), d=30 to 50 nm, l=3 to 10um from Carbon Nanotechnologies, Inc.	Epon 862 (bisphenol F epoxy)	Room temp – 600 ºC in nitrogen gas, heat rate 10 ºC/min	TA Instru-ments TGA2950	[121]
MWCNT from Bayer Material About 6–8 mg of sample	Epoxy resin (DGEBA)	room temp. – 800 ºC in nitrogen gas heat rate 20 ºC/min	TA instruments TGA Q500	[66]

3.6.3.1 Production of TGA sample and method of heating.

The sample used for TGA analysis was a mixture of 100 parts of neat Epikote828 and 30 parts of 4’4’DDS as a curing agent. The same ratio was mixed with MWCNT_short/828 and MWCNT_long/828. A mechanical stirrer was used to mix the mixture in a 140^0C oil bath for 10 to 15 minutes. The mixture was then degassed in

vacuum oven in a temperature of 110-120 ^{0}C for another 10 to 15 minutes. The mixture was then poured on a glass plate to make a splat. The glass plate was glazed with Frekote^{TM} three times to avoid damaging the samples and the glass plate. The splat was further dried in a vacuum oven for 2 hours at 30^{o}C to eliminate any moisture in the samples.

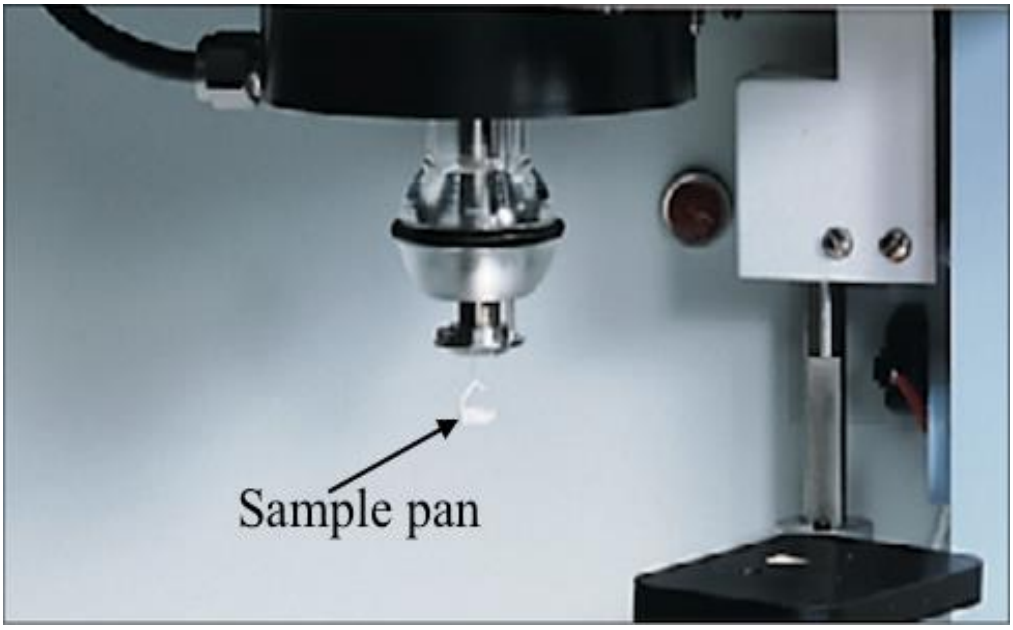

Figure 3.12: Pyris 1 TGA [122]

TGA records the mass changes in the sample as it is heated at a controlled temperature rate using a microbalance. Figure 3.12 shows Pyris 1 TGA that has been used in this study which the sample pan is "hangdown" below the balance and controlled by Pyris Software. In this study, the sample was heated in an inert nitrogen gas atmosphere, air atmosphere and a combination of both, with a temperature range of 28 ^{0}C to 800 ^{0}C. The weight of the Epikote 828+DDS and nanomodified Epikote 828 samples was measured between 8 mg to 12 mg. Three different methods of heating profile were used

to determine the thermal behaviour of the Epikote 828 and also the constant residual weight. The methods of achieving the desired temperature are shown in Figure 3.13, Figure 3.14 and Figure 3.15. The TGA analysis was run using Perkin Elmer Pyris 1 TGA and according to the ASTM Standard E1131 [123].

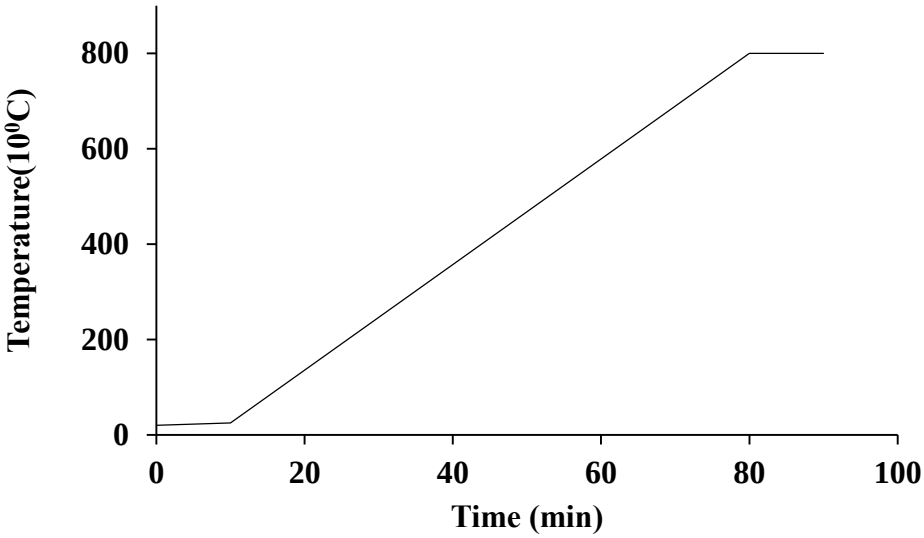

Figure 3.13: TGA heating method develop in nitrogen atmosphere. The temperature is increased from 20 ºC to 800 ºC at a rate of 10 ºC/min

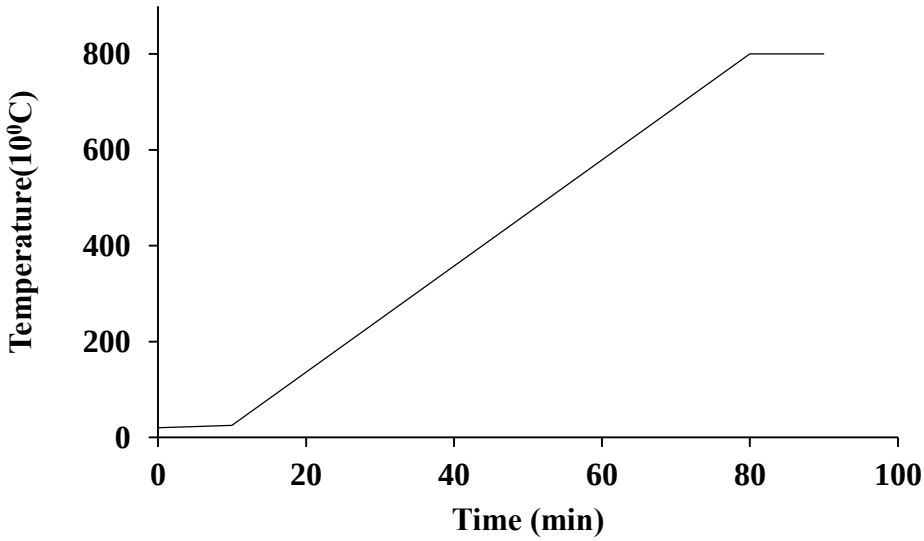

Figure 3.14: TGA heating method develop in an air atmosphere. The temperature is increased from 20 ºC to 800 ºC at a rate of 10 ºC/min

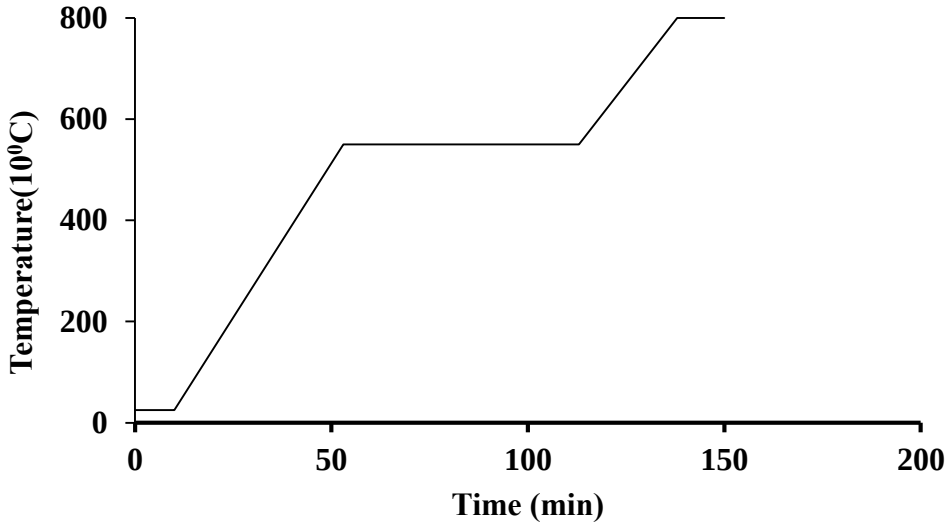

Figure 3.15: TGA heating method is first heated in nitrogen from 20 ^{o}C to 550 ^{o}C and kept for an hour, then increased to 800 ^{o}C at a rate of 10 ^{o}C/min

3.6.3.2 Data determination on constituent of volume fraction

The TGA is used to obtain the weight fraction of the constituents in the composite samples in order to determin the carbon fibre and nanoparticles volume fractions using basic equations from ASTM Standard D3171-99 [124]. The equations are as follows:

(i) The carbon fibre volume fraction :

$$V_{cf} = \left(\frac{m_{cf}}{m_i}\right) \times \left(\frac{r_i}{r_{cf}}\right) \times 100$$

where m_{cf} = mass of the fibre, m_i = initial mass of the composite sample, ρ_{cf} = density of the carbon fibre and ρ_i = density of the composite sample.

(ii) The MWCNTs volume fraction :

$$V_{mwcnt} = \left(\frac{m_{mwcnt}}{m_i} \right) \times \left(\frac{r_i}{r_{mwcnt}} \right) \times 100$$

where m_{mwcnt} = mass of the MWCNTs, , ρ_{mwcnt} = density of the MWCNTs.

3.7 Physical analysis of dispersion

3.7.1 Transmission electron mcroscopy (TEM)

TEM was used to study the degree of dispersion of MWCNTs in Epikote 828. The sample was prepared by curing nanomodified resin in a trapezium shape as shown in Figure 3.16. The cured trapezium shaped resins were cut using Ultracut E, Ultramicrotome, and the thickness of the sections was checked by comparing the interference colours with a predefined colour reference chart. This chart shows a colour spectrum with the corresponding section thickness. The TEM samples with a thickness of about 80 nm, are examined by using FEI Tecnai G^2 Transmission Electron Microscope, with accelerating voltage of 80 kV. Gatan MS600CW digital camera and Gatan digital micrograph are used to collect and capture images of the samples.

Figure 3.16: Cured resin in trapezium shape for TEM analysis

3.7.2 X-ray diffraction (XRD)

The microstructure of the neat Epikote 828 and MWCNTs/828, for short and long MWCNTs, was examined using Siemens D5000 X-ray diffraction. The XRD was equipped with Cu-tube as an anode. Each scan was recorded with 2θ scanning range from 10° to 80°. with a step size of 0.02 at a rate of 0.048 s^{-1}. The operating voltage was 45kV and the current was 40mA.

3.8 Mechanical properties

3.8.1 Compression test

Cylindrical shaped samples were prepared according to the ASTM standard D695-02 [125] and [126], for the uniaxial compression test. The samples were made with a height of 10mm and a diameter of 10mm (1:1 dimension ratio) as shown in Figure 3.17. The cylindrical shape prevents buckling and premature failure in the samples compared to the samples with sharp corners. The casted samples were machined on a lathe machine and then polished. The dimensions were measured using a micrometre with an accuracy of 0.01 mm. The samples were carefully cured and polished to avoid bubbles, scratches or chips at the edge of the samples which may lead to premature failures. After the curing process, all the samples were dried in a vacuum oven before placing them in a vacuum desiccator. At least six samples were tested for each resin system.

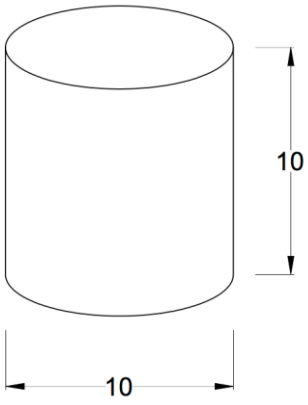

Figure 3.17: Samples of cylindrical shape with dimensions.

Static uniaxial compression test is carried out using British standard BS EN ISO 604:2003 [127] and ASTM standard D695-96 [125]. The cylindrical samples were examined by using Zwick Roel universal testing machine with a 50 kN load cell and two different crosshead speeds of 1 mm/min and 3 mm/min were used. The samples ends were smeared with a petroleum jelly to minimise the friction between the surfaces of the compression bars and the sample loaded to avoid barrelling effect, which may occur on the edges of the samples. A technique, suggested by [128] is employed to calculate the actual displacement of samples. The compliance correction of the testing machine load displacement is measured without any specimen between the compression bars.

The true measurement data was calculated by subtracting the non-sample displacement from the total displacement, which was recorded by the actuator. From these measurement, the compressive properties were obtained using the following equations:

(i) Engineering compressive stress, σ_e, is compressive load, F, divided by initial surface area, A, of the test sample.

$$s_e\left(MPa\right) = \frac{F}{A}$$

(ii) Engineering compressive strain, ε_e, is a decrement in the length of the test sample, divided by the original length of, L_o, of the test samples

$$\varepsilon_e = \frac{\Delta L}{L_\circ}$$

(iii) Compressive stress at yield, σ_y.

(iv) Compressive strain at yield, ε_y.

(vi) Compressive strength, σ_u.

3.8.2 Flexural test

Rectangular samples of cured resins with 70 mm length, 4 mm thickness and 10 mm width were used for three-point bending test. The flexural test was carried out according to the British Standard BS EN ISO 178: 2010 [131]. At least 6 specimens are tested for each system. Six samples were tested for each system. The actual width and thickness of the samples were measured at four different points using a digital electronic Vernier

calliper and the average values were taken and used for the three-point bending test. The samples are placed symmetrically on two spans. The distance between the two spans was 60 mm. A TA500 Texturimeter (Lloyd instruments) with 10kN load cell was used with a crosshead speed of 1 mm/min. The corresponding deflection of the samples is recorded by the displacement of the crosshead of the machine. The compliance correction of the testing machine load displacement was measured by placing a metal block bar between the three-point bending fixtures. The true measurement data was calculated by subtracting the metal block sample displacement from the total displacement recorded by the actuator. The data analysis of the samples from the flexural test are as follows:

(i) Flexural test, σ, is expressed in mega pascal.

$$s\left(MPa\right)=\frac{3FL}{2bh^2}$$

where:

F = the applied force expressed in (N)

L = the span seperation, (60 mm)

b = the width in (mm)

h = the thickness in (mm)

(ii) Flexural strain, ε,

$$e=\frac{6sh}{L^2}$$

where:

s = the deflection in (mm)

h = the thickness in (mm)

(iii) Flexural stress - strain ($\sigma - \varepsilon$) response.

(iv) Flexural modulus is detremined by using a linear regression procedure on the part of the flexural stress-strain curve between $\varepsilon_1 = 0.005$ and $\varepsilon_2 = 0.0025$

3.9 Interlaminar shear stress of CFRP laminates

A delamination between the layers of laminates occurs when transverse shear load applied to the laminates exceed interlaminar shear strength (ILSS). ILSS of a laminate composites is measured directly by generated a pure shear stress pattern between the laminar to induce an interlaminar shear failure. There are several methods were designed to load the specimen and fails in interlaminar shear stress. The methods have been developed to characterise ILSS such as short beam shear (SBS), tensile stretching, compression, curved-double-cantilever-beam and compression shear test [14,132]. In this study SBS was chosen as a method to measure ILSS. Compared to the other methods, SBS is the simplest method and most commonly used in measuring the interlaminar shear failure. According to classical beam theory, three point bending as shown in Figure 3.18 was the cause to the transverse shear failure. The SBS test was measured according to ASTM D 2344 [133] and the average dimensions for the samples were about 30 mm x 8 mm x 4.5 mm. The sample was placed on two cylindrical rod and a force was applied by forcing a cylindrical head moving down at the centre of the samples. The first failure was recorded as the transverse load was increasing, and this data will be used to determine the apparent interlaminar shear strength of the composite.

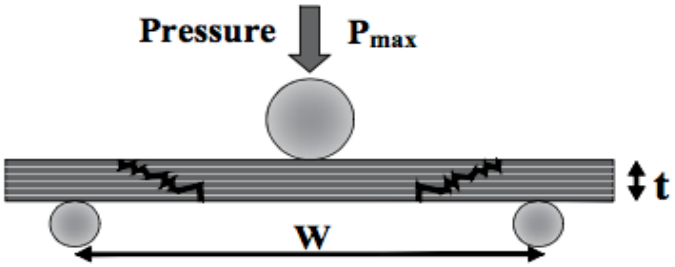

Figure 3.18: Schematic diagram of short beam shear (SBS)

The apparent interlaminar shear strength or short beam strength was determined using the formula [133] which is adopted based on Bernoulli-Eular beam theory,

$$F_{sbs} = 0.75 \times \frac{P_{max}}{w \times t}$$

Where P_{max} is the maximum load and w and t is the width and the thickness of the samples.

4 Analysis of the degree of dispersion

Three combined methods were used for dispersing MWCNTs in Epikote 828, which were discussed in chapter 3. The MWCNTs were mixed with the resin using a high shear mixer and then the mixture was mixed further using a sonication probe and finally the consolidation of the MWCNT nano-modified mixture was achieved by using a three-roll mills.

This chapter is focusing on the results of the characterisation methods used to evaluate the quality of dispersion. The characterisation methods include TEM analysis, XRD analysis, Raman spectroscopy analysis and FTIR analysis. These techniques were used to examine the degree of dispersion of MWCNTs in the Epikote 828 (MWCNTs/828) and also to observe the structure of the MWCNTs after the dispersion process.

4.1 TEM analysis

Two types of nano-filled resin systems were analysed; MWCNT_long/828 and MWCNT_short/828 with a MWCNTs length of 10-30μm and 0.5-2μm, respectively. TEM micrographs are as shown in Figure 4.1, Figure 4.2, Figure 4.3 and Figure 4.4 The images revealed that the MWCNT_long and MWCNT_short are well dispersed in Epikote 828 epoxy at 0.38 wt% loading. Comparing the two nanomodified resins, the MWCNT_long spread more evenly in the Epikote 828. Figure 4.1 shows that most of the MWCNTs were fragmented into shorter lengths and are evenly spread. The average length of the MWCNTs appeared to be shorter than 500 nm (Figure 4.1). Determining

the true length by TEM is difficult as the sections are 80nm thick (see section 3.7.1) and therfore the MWCNT will be cut in the process of sectioning for TEM. Figure 4.5 shows a single strand of MWCNT_long after dispersion process with the length of 1.4 μm. Although MWCNT_short appears dispersed but they were close to each other, into higher density areas. In MWCNT_short, some agglomerated zones were visible within the nanomodified resin as shown in Figure 4.7.

According to Korayem [107], the length of CNTs does not have significant effect to the quality of dispersion in solution. In their research, they used four types of MWCNTs with three different diameters and two different lengths. These were L1020; the diameter of 10 – 20 nm and length of 5-15 μm, S1020; the diameter of 10 – 20 nm and length of 1 – 2 μm, L2040; the diameter of 20 – 40 nm and length of 5-15 μm, L4060; the diameter of 40 – 60 nm and length of 5 – 15 μm. They suggested that the diameter of CNTs can affect the quality of dispersion. Using a larger diameter would improve the ability of CNTs to be dispersed. A smaller diameter of CNTs will have larger surface area which will lead to poor dispersion quality. On the other hand, Li *et al*. [134], suggested that both the length and diameter of MWCNTs do not affect the degree of dispersion. They studied the characterisation of MWCNTs dispersion by measuring UV-vis absorption by the suspension been dispersed with MWCNTs in the range of wavelength from 350 to 750 nm. Three types of MWCNTs were used in their study with the average diameter and length of 5 to 50 nm and 15 nm – 1mm respectively. Both studies showed that the dispersion of MWCNTs gave different results according to the types of CNTs, methods of dispersion and the materials to be dispersed into (the dispersant). In both studies, the ultra-sonication method was used for the dispersion. They observed that the length of the MWCNTs were fragmented into shorter lengths.

Huang *et. al*. [88] concluded that for a complete separation of CNTs, the tubes need to be broken during the process. This can be achieved by sonicated the CNTs. However, a high shear mixer was used to separate the big aggregates to smaller aggregates as shown in Figure 4.6 (a) and Figure 4.6 (b). Therefore, using a combination of both dispersion methods is important. In this research, a three-roll mill method was used to consolidate MWCNT_long and MWCNT_short in Epikote 828 resin and resulted in a good end of dispersion.

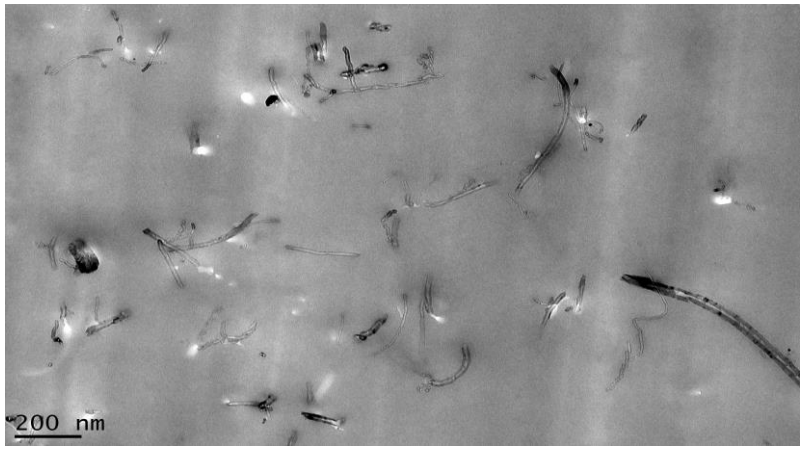

Figure 4.1: TEM images showing achieved dispersion of MWCNT_long / Epikote 828. The scale bar is 200 nm

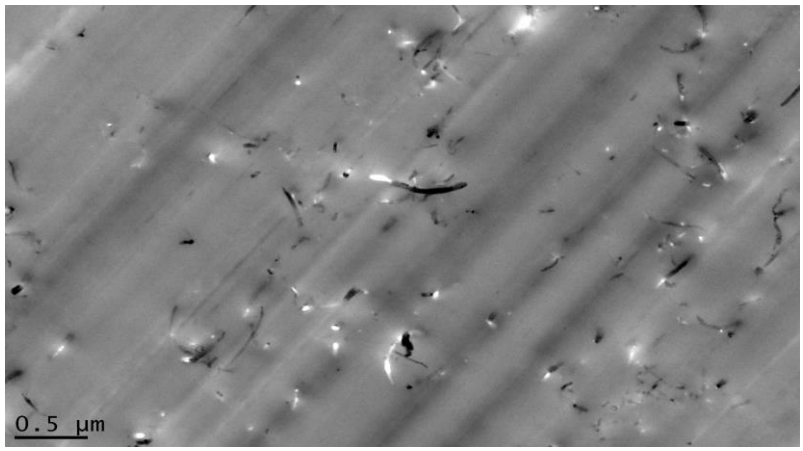

Figure 4.2: TEM images showing achieved dispersion of MWCNT_long / Epikote 828. The scale bar is 0.5 µm

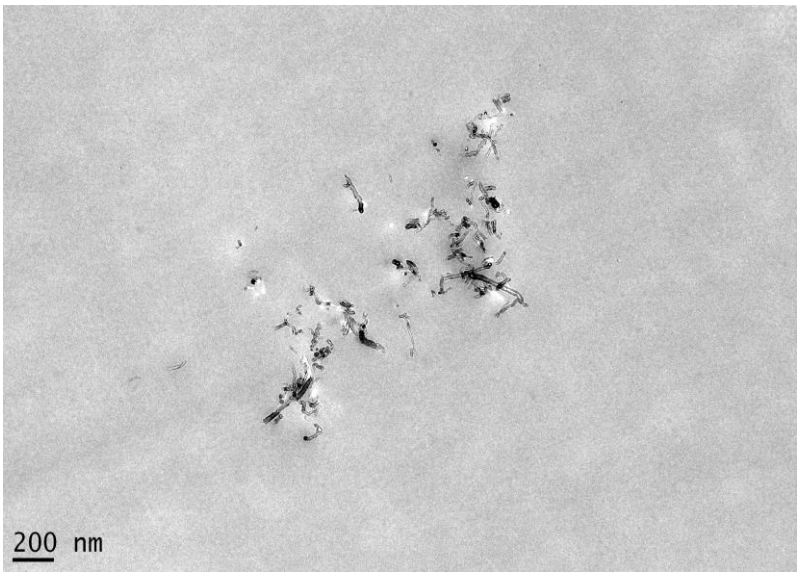

Figure 4.3: TEM images showing achieved dispersion of MWCNT_short / Epikote 828 at 200 nm scale bar

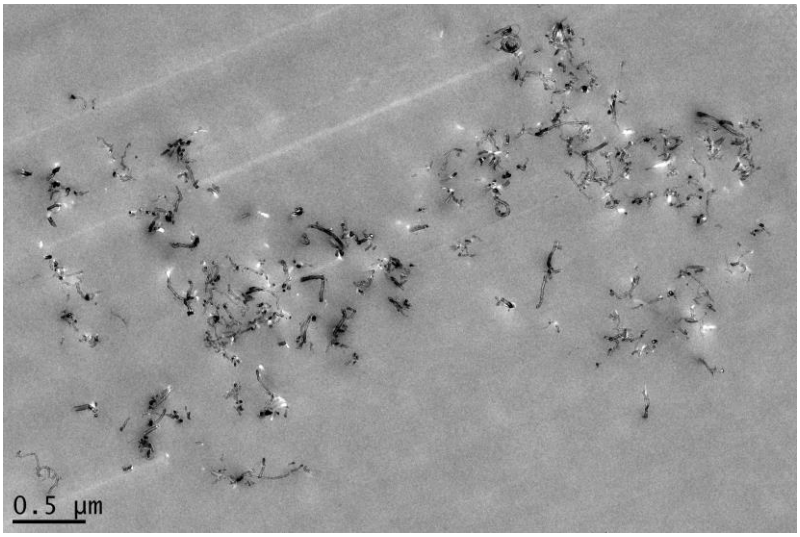

Figure 4.4: TE images showing achieved dispersion of MWCNT_short / Epikote 828. The scale bar is 0.5 µm.

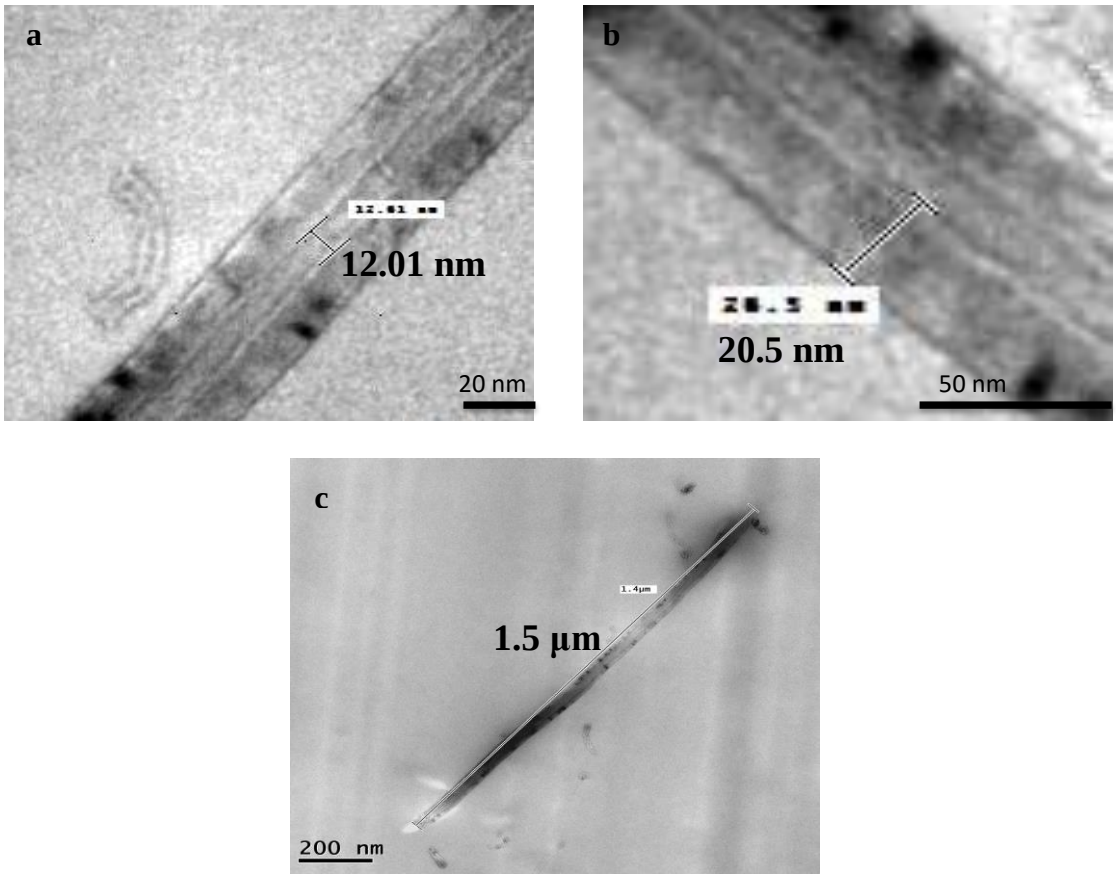

Figure 4.5: Dimension of MWCNT_long after a complete dispersion using the combination of the three methods used.

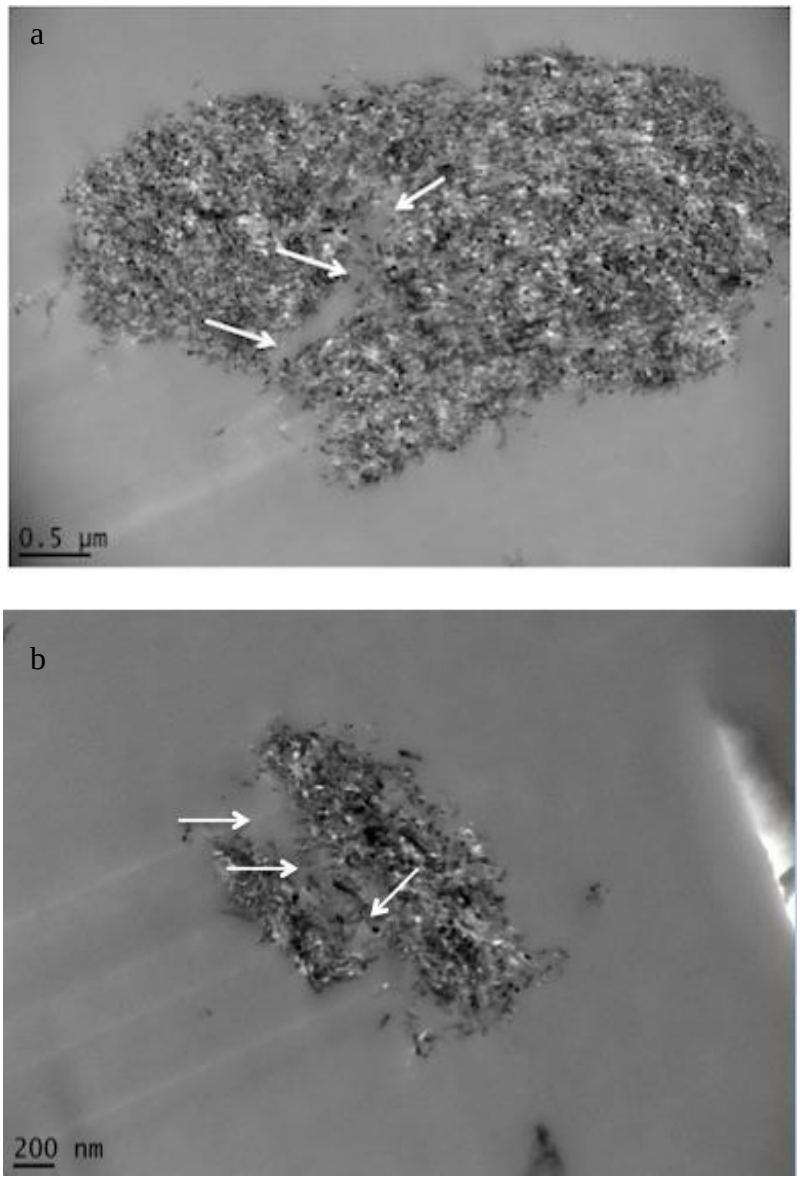

Figure 4.6: Arrows show the path in the process to break the large agglomeration into smaller agglomerations

Previous studies concluded that ultrasonication treatment can significantly shorten the CNT length [49,76,87,88,104,107,135]. Korayem *et. al*. analysed 200 CNTs in TEM images and found that there were about 30% reduction in length after 15 min sonication and 52% of reduction after 60 min sonication. The reduction in the CNTs length was also studied by Inam *et. al* [49]. They used a sample of MWCNTs with 2 µm length

and after sonication time of 5, 8, 11 and 14 minutes, the length of the MWCNTs was reduced to 1689 nm, 1332 nm, 992 nm and 502 nm, respectively. At least 5000 CNTs were analysed and measured using software Image-Pro Plus. The study concluded that the reduction of CNTs length is propotional to the increament of sonication time. Figure 4.1 and Figure 4.2 shows a good agreement with all the prevoius research mentioned above. The MWCNT_long were fragmented into a shorter length and dispersed evenly in Epikote 828. Previous studies reported that the three-roll mill dispersion can lead to a significant reduction in the agglomeration size and the consolidation of the CNTs in the matrix with a small reduction in the length of CNTs [24,89,136]. Shear mixing, described by Y.Huang *et. al.* [88], is able to effectively separate MWCNTs without causing damage. Coleman *et al.* [65] reported an improvement in dispersion by using a high shear mixer and suggested that the dispersion was increased as the total mixing energy was increased and the average nanotube length was reduced with the decrease in the mixing energy.

Further observation shown in Figure 4.3 and Figure 4.4, revealed that the separation between MWCNT_short is slightly higher as compared to the MWCNT_long. Huang *et. al.* [135] indicated that when the CNTs are exposed to sonication, after a while, they reach a constant length and the length distribution becomes narrower than the initial population of CNTs filament. The filament gradually becomes shorter mostly by the mechanical shearing process resulting from the fluid flow, rather than by thermal or chemical effects of sonication. An equation based on shear-induced scission was modelled by estimating the stress that is exerted on a filament caused by transmitted viscous forces (shear forces) from the solvent. This equation estimates a steady-state and limiting length, L_{lim}, with no further reduction in length at a given sonication power.

Considering a filament length *L*, and diameter *d*, tensile strength σ^* of, the estimated L_{lim} will be [135]:

$$L_{lim} \approx 7 \times 10^{-4} \, d \, \sqrt{\sigma^*} \quad \text{(in SI units)} \qquad (4.1)$$

Using equation 4.1, the L_{lim} for MWCNT's length, was investigated. An estimation of σ^* was taken from other references [135,137–140]. σ^* was assumed ~ 4 GPa [135,140] for CVD MWCNT. The value of L_{lim} was calculated using equation 4.1 for MWCNT_long and MWCNT_short and for both type MWCNT it found to be between 0.4 μm – 1.3 μm. This result is in a good aggrement with the results shown in Figure 4.1, Figure 4.2, Figure 4.3, Figure 4.4 and Figure 4.5 (c) where the lengths of MWCNTs are between the range of calculated L_{lim}. Figure 4.7 and Figure 4.8, show that the average length of the MWCNTs around the agglomeration was less than 0.5 μm.

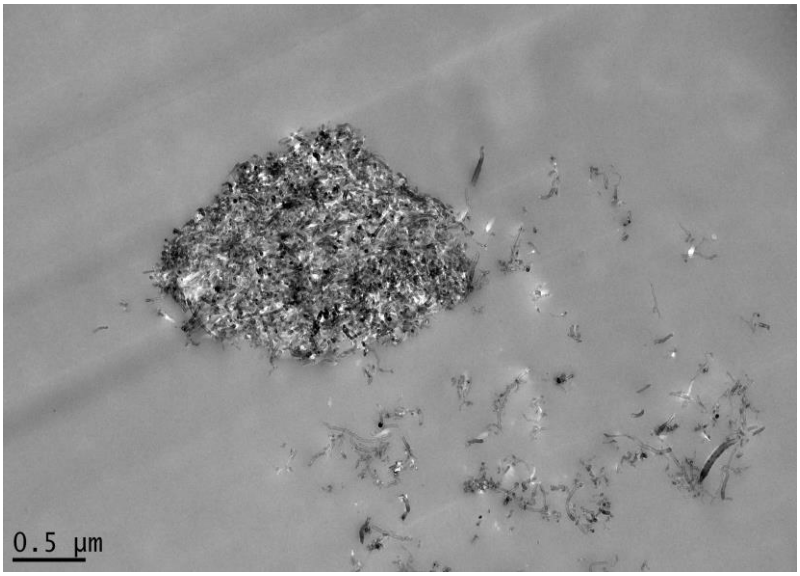

Figure 4.7: Agglomeration appeared at scale bar 0.5 µm for MWCNT_short/828 after complete mixing using the combination of the three methods

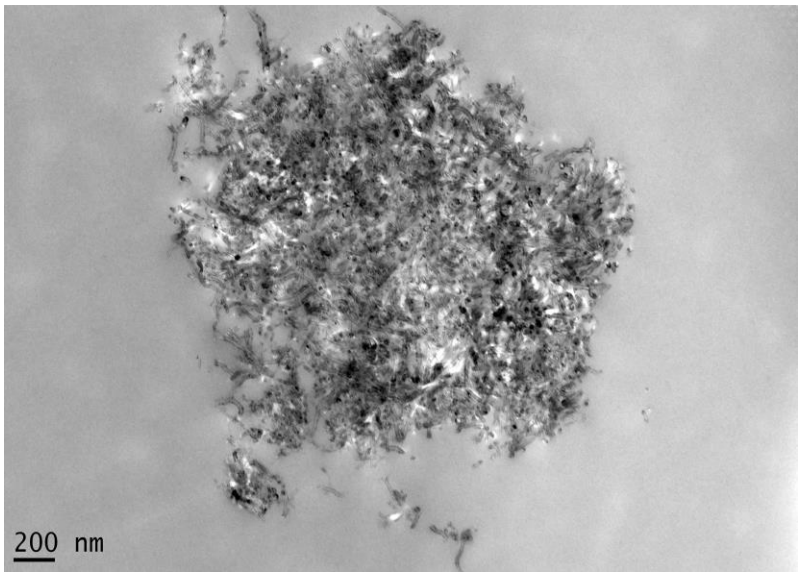

Figure 4.8: Agglomeration for MWCNT_short/828 after a complete mixing by combining the three methods.

A number of MWCNT_short with a length of 0.5 µm – 2 µm were very close to the value of the predicted L_{lim}. It seems that the sonicated treatment could not further crack

the small agglomerations into single MWCNTS. Nevertheless, according to Huang *et. al.*, this equation is only applicable for low viscosity solvents, because at higher viscosities, the probability for cavitation is much lower, but it shows qualitative picture in tube breakage.

4.2 Scanning electron microscope (SEM) analysis

Flexural fractured surfaces of the Epikote 828+DDS epoxy resin and MWCNTs/Epikote 828 epoxy resin system were examined using SEM. Epikote 828 +DDS epoxy resin exhibits a relatively smooth flexural fracture surface as shown in Figure 4.9. This demonstrate a typical fractography of brittle fracture behaviour which is a sign of the low fracture toughness of Epikote 828+DDS epoxy resin. From Figure 4.9, it can be observed that the distance between two cleavage steps is about 100 μm – 200 μm and the cleavage plane between them is flat and plain.

In comparison to the Figure 4.10 and Figure 4.11 of MWCNT_short/828 and MWCNT_long/828 epoxy resin respectively, the surface fracture are rougher. The addition of MWCNTs in epoxy resin clearly increased roughness of the surface failure [121,141] which was likely indicated the reason why nanocomposites show further improve fracture toughness. Figure 4.10 and Figure 4.11 also shows that the size and the distance of the cleavage plane decreased as compared to the Epikote 828+DDS which was the result of a ductile deformation [142], unlike the Epikote 828+DDS epoxy resin that has brittle fracture. Figure 4.12 shows the difference in between the area that contains MWCNTs and does not contain any MWCNTs. The area which contain

MWCNTs form a network of cleavage compare to the area which does not contain MWCNTs it seems plain and featureless.

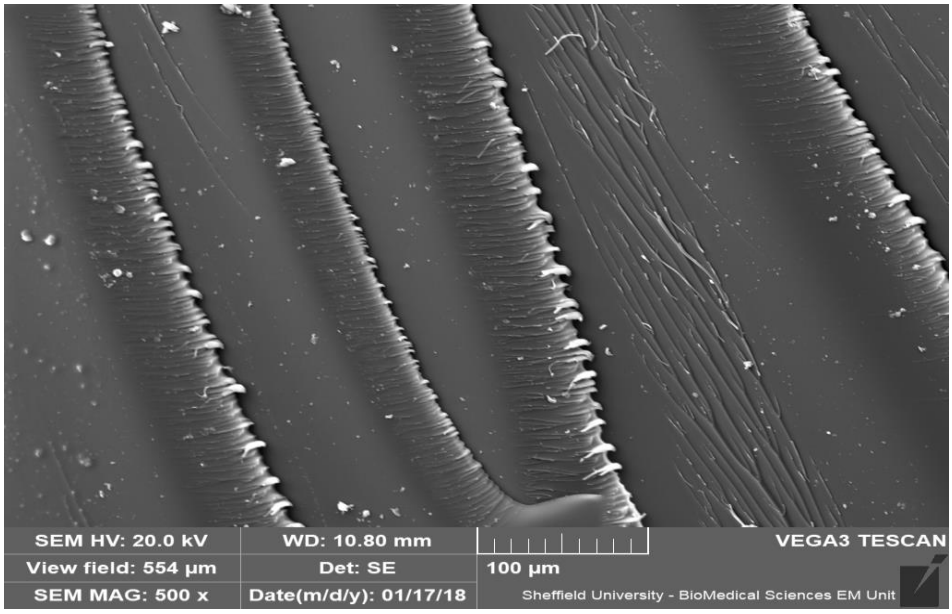

Figure 4.9: Epikote 828+DDS flexural fractured surface

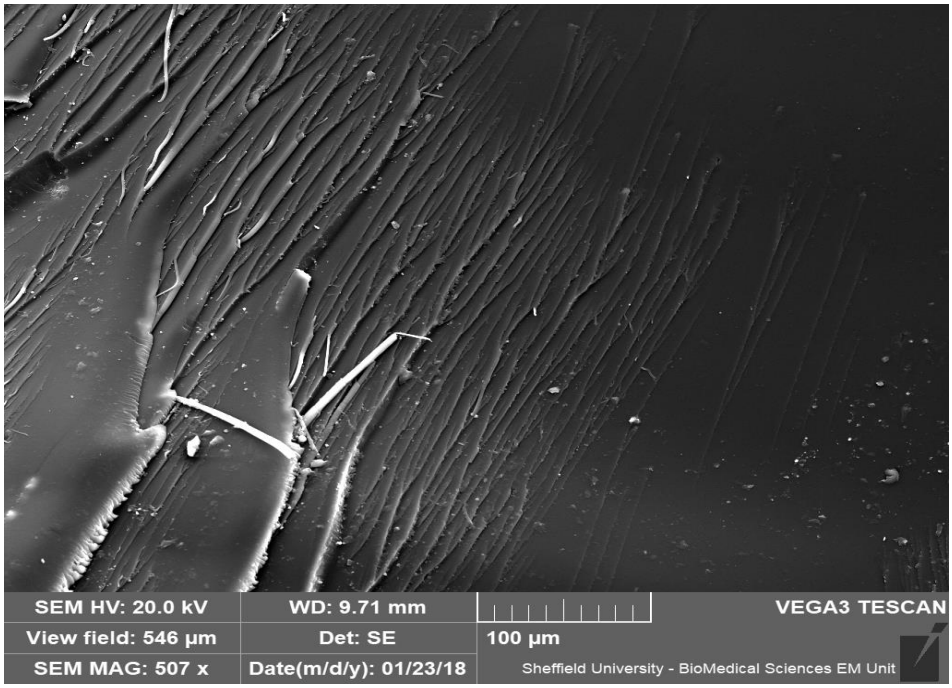

Figure 4.10: MWCNT_short/828 flexural fractured surface

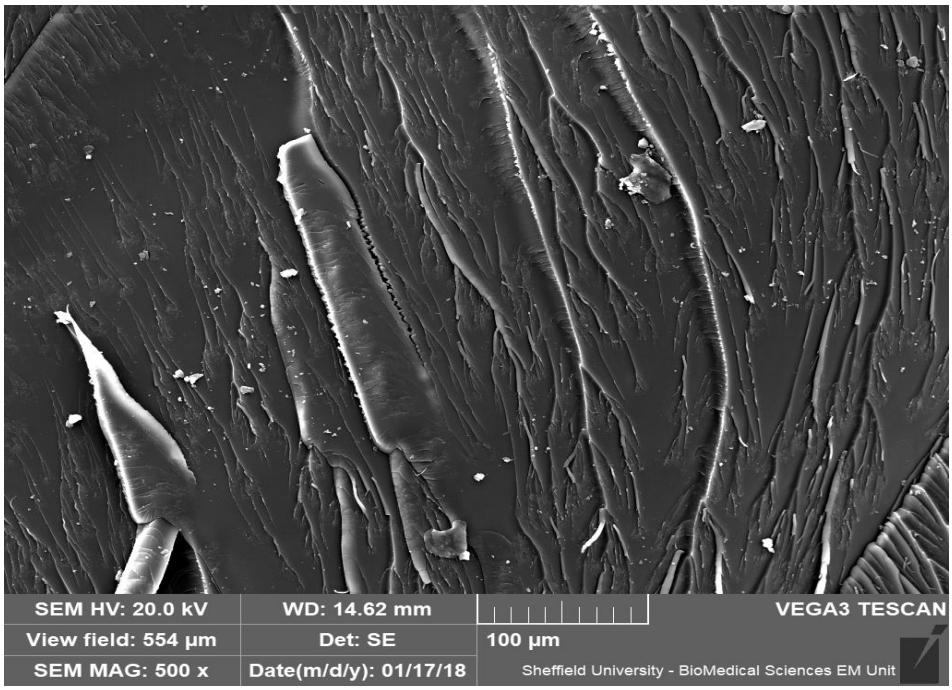

Figure 4.11: MWCNT_long/828 flexural fractured surface

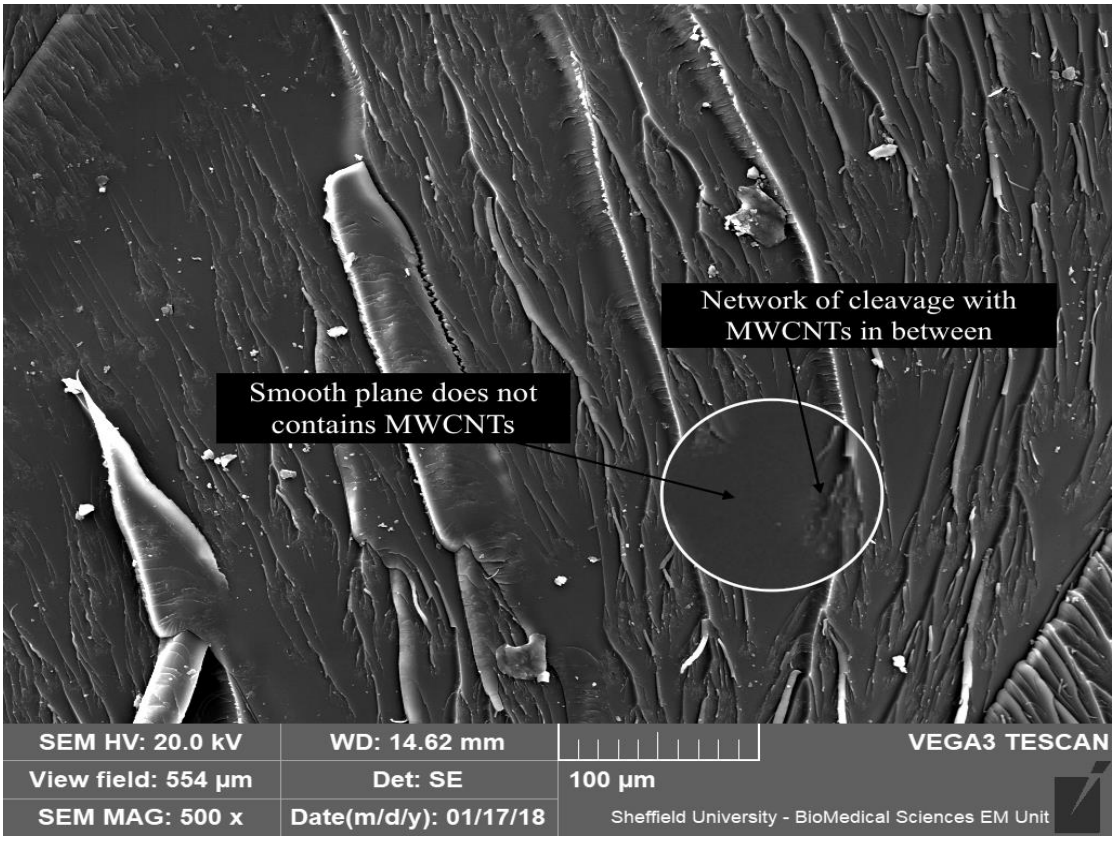

Figure 4.12: Magnification of MWCNT_long/828 flexural fractured surface that distinguished between the area that consist MWCNT and featureless area

4.3 XRD

The XRD results of Epikote 828+DDS, MWCNT_powder, MWCNT_short/828, MWCNT_long/828 are shown in Figure 4.13.

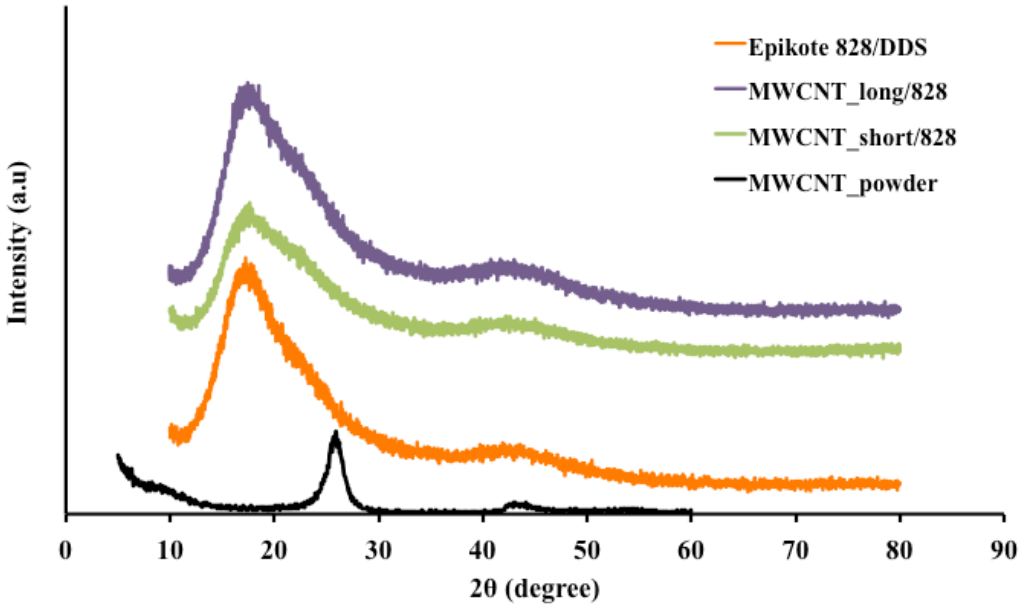

Figure 4.13: XRD patterns

The narrow peak of MWCNT powder at $2\theta \approx 25.6°$ was caused by the interlayer spacing of graphite layers (002). The weak peak located at 42.9° for MWCNT powder ascribed to the indication of graphite-like structure (100) [143,144]. For neat Epikote 828 sample, the broad peak centered at $2\theta \approx 16.4°$ and $2\theta \approx 41.06°$ indicate the amorphus structure of the epoxy due to the scattering from cross linked network of Epikote 828

with hardener [145,146]. However, the graphite-like peak (002) could not be seen in MWCNTs/828 composites because MWCNTs loading is only 0.38 wt%.

4.4 Raman

Raman spectra results were analysed to study the degree of structural defects in the MWCNTs after dispersion process. Raman spectroscopy provides beneficial information about the crystalline and amorphous of materials from the carbon structure [147] and CNTs structural changes during the dispersion [148] . The main characteristics of MWCNT in the Raman spectrum are the G-band, which represents the crystalline graphitic and tangent vibrational of sp^2 carbon (1500 – 1600 cm^{-1}) and D-band which indicates for defects in disordered carbon (~1350 cm^{-1}) [72,149,150].

In Figure 4.14, the Raman spectra MWCNT_long/828 shows peaks at 1577 cm^{-1} (G-band), 1340 cm^{-1} (D-band) and MWCNT_short/828 Raman spectra shows peaks at 1616 cm^{-1} (G-band) and 1325 cm^{-1} (D-band). The quality of dispersed MWCNT, was measured by analysing the integrated intensity ratio, R, the ratio of D-band to the G-band (I_D/I_G) [72,151]. The samples with low I_D/I_G shows that carbon atoms with sp^2 bonded have few defects or high purity and high I_D/I_G indicates that the samples contain large quantities of defects or impurities.

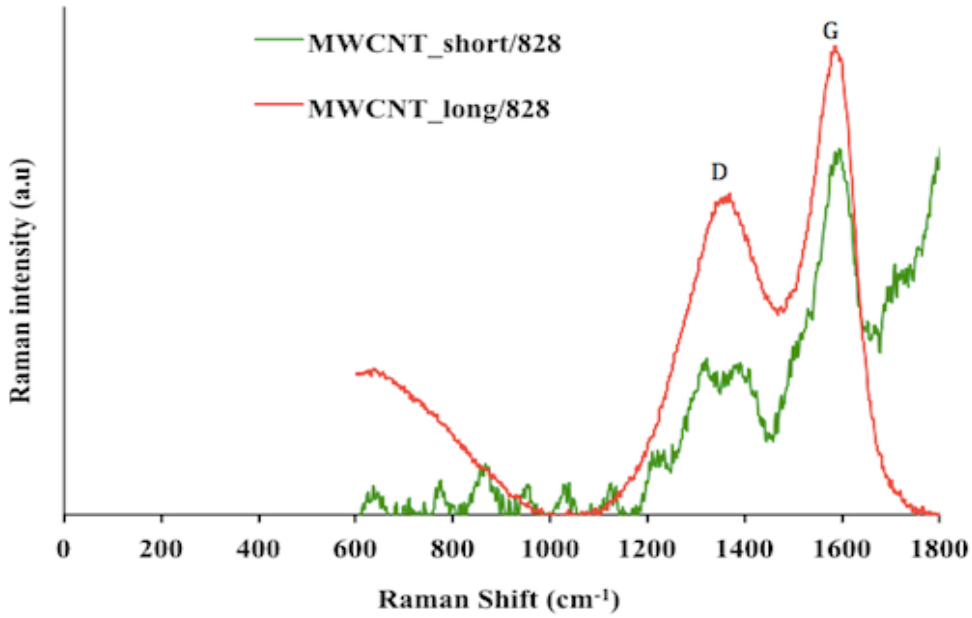

Figure 4.14: Raman spectra of MWCNT_long/828 and MWCNT_short/828

Table 4.1: A summary of results from Raman spectra

	Raman shift (cm^{-1})		**Intensity**		**R**
Samples	X_D	X_G	I_D	I_G	I_D/I_G
MWCNT_long	1340	1577	427	627	0.68
MWCNT_short	1325	1616	200	501	0.39

From Table 4.1, the intensity ratio (I_D/I_G) of the MWCNT_long and MWCNT_short after dispersion were calculated as 0.68 and 0.39 respectively. The result shows that the MWCNT_long has a higher value of I_D/I_G. This value is consistant with TEM micrograph, which shows that most of MWCNT_long were fragmanted into shorter length. According to F. Tuinstra and J.L. Koenig [152] , the increament of (I_D/I_G) ratio value was proportional with the incresed of the amount of ‘unorganized’ carbon and/or

decrease in the mean crystal size [153] and if $I_D/I_G > 2$ shows that a serious damaged form of carbon [152,154].

4.5 Fourier Transformed Infrared Spectroscopy (FTIR)

FTIR uses an infrared spectrum and interact to the vibration of frequencies which is created between the bonds of the atoms [155]. The fingerprint of a sampple is represent in terms of absorption peaks. FTIR spectra were recorded using a Bruker Alpha with (single bounce Diamond) Platinum-ATR accessory. Spectra were obtained at 4 cm^{-1} resolution and averages of at least 16 scans in the standard wave number ranging from 400–4000 cm^{-1} at room temperature (23 °C).

4.5.1.1 FTIR analysis

The chemical structure of Epikote 828+DDS, MWCNT_long/828 and MWCNT_short/828 nanocomposites were studied by FTIR to determine the type of the chemical bonds and the functional groups on the surface of the nanocomposites. Figure 4.15 shows, the FTIR spectra of the uncure Epikote 828+DDS, MWCNT_long/828 and MWCNT_short/828 and Figure 4.16 shows FTIR spectra for all the cured samples. FTIR spectroscopy was used to characterise the nature of the epoxy using Table 4.2. It is observed that the absorption bands of Epikote 828+DDS, MWCNT_long/828 and MWCNT_short/828 were quite similar, indicating that neither MWCNT_long nor MWCNT_short appeared to change the chemical structure of the epoxy [156]. The uncured epoxy was examined under the FTIR for the epoxide group, which can be

indicated by the presence of a major band at 913 cm^{-1}, as shown in Figure 4.17. This band is related to C-C bond contraction while both C-O bonds are stretching [157]. As can be seen in Figure 4.18, this peak has disappeared for all the cured samples. The absence of the peak after the curing process is an evidance of a high degree of cure in the MWCNTs/828 nanomodified composites and in the neat Epikote 828. [157–159].

Table 4.2: Characteristic bands of epoxy [160–162]

Band (cm^{-1})	Assignment
3470	O-H stretching
3057	Stretching of C-H of the oxirane ring
2965-2871	StretchingC-H of CH2 and CH aromatic and aliphatic
1625	Stretching C=C of aromatic rings
1505	Stretching C-C of aromatic
1030	Stretching C-O-C of ethers
913	Epoxy ring mode: Stretching C-O of oxirane group, while C-C bond contracts
825	Stretching C-O-C of oxirane group
770	Rocking CH2

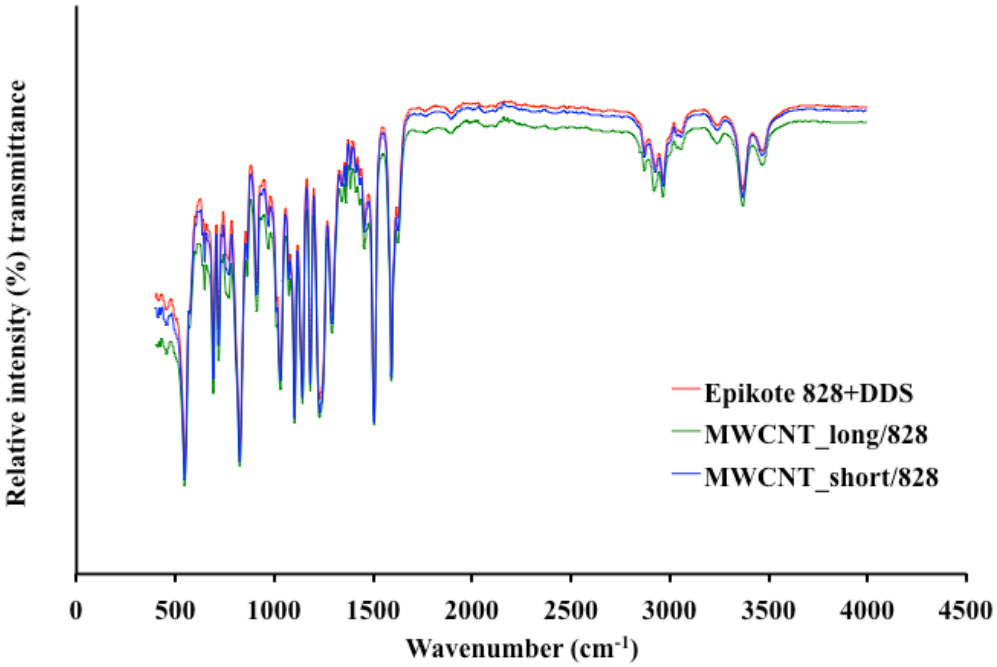

Figure 4.15: Structure of uncure Epikote 828+DDS, MWCNT_short/828 and MWCNT_long/828

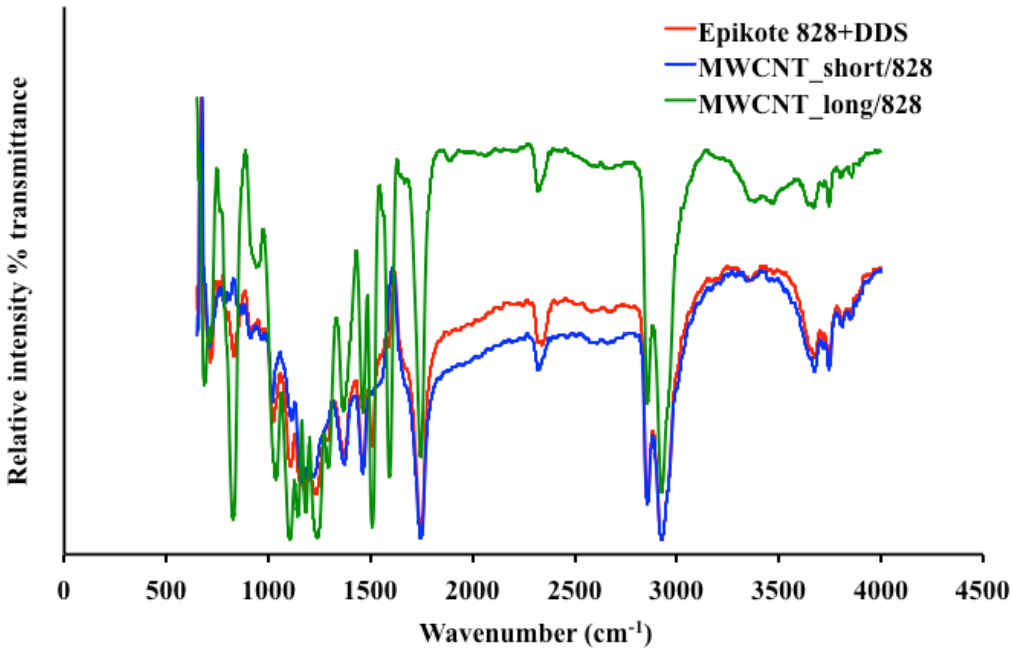

Figure 4.16: Structure of cured Epikote 828+DDS, MWCNT_short/828 and MWCNT_long/828

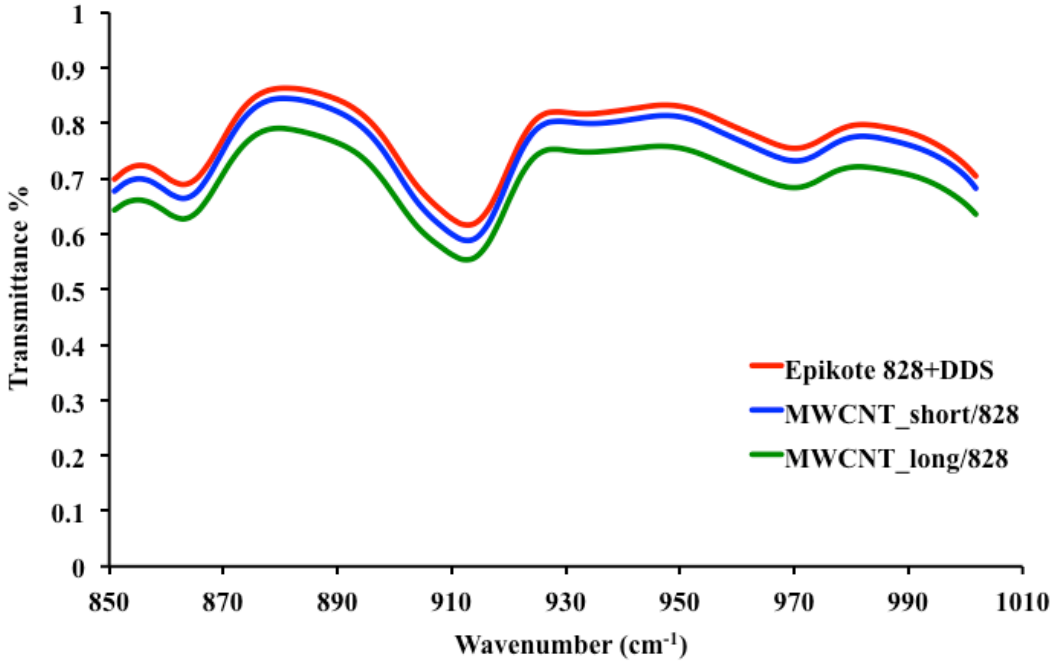

Figure 4.17: FTIR spectra illustrating band of 913 cm^{-1} for all uncure samples

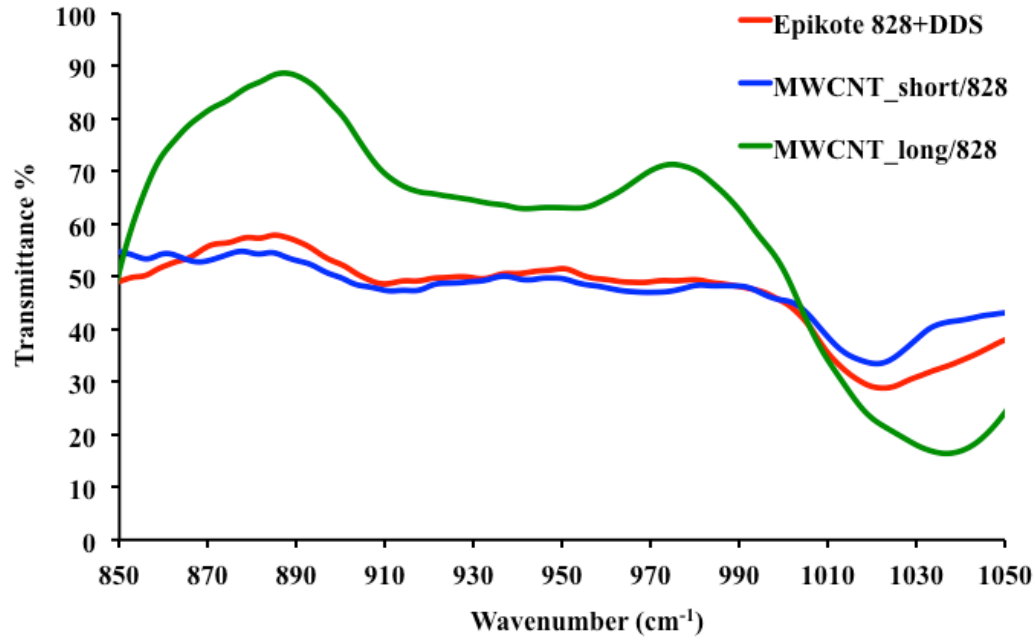

Figure 4.18: FTIR spectra illustrating disappearance of 913 cm^{-1} band for all cured samples

5 Thermal analysis

5.1 TGA analysis for neat Epikote 828

TGA was used to study the weight change of samples in order to measure the constituent volume fraction of nanocomposites and CFRP composites as outlined in Section 3.6.3.2. This analysis is important for the evaluation of MWCNTs nanofiller and carbon fibre contents. However, in this study, the MWCNTs weight fraction cannot be obtained due to the limitation of the TGA temperature (800 °C), the small mass of added MWCNT and the creation of carbon char from the resin. The thermal degradation of neat Epikote 828 (neat Epikote 828 was defined as Epikote 828 + DDS and was not mix with any MWCNT as mentioned in section 3.1) was initially studied by heating in nitrogen and air, as shown in Figure 5.1 and Figure 5.2. The maximum degradation occurred at 432.14 °C when the samples were heated in a nitrogen atmosphere which was about 5 °C higher than heating in an air atmophere, which is 428.88 °C. The degradation temperature of Epikote 828+DDS started at 330 °C as shown in Figure 5.1. The decomposition temperature was observed when the Epikote 828+DDS samples were heated in air. The weight loss increased gradually from 360 °C to around 550 °C - 560 °C; with total mass loss of 77.21% as shown in Figure 5.2. At 550 °C – 560 °C, a mixture of epoxy and residue can be observed. Thus, the epoxy forms a char and does not fully decompose. A higher amount of resin char residue was formed when the resin was heated in air (see Figure 5.2), compared to that of the nitrogen (see Figure 5.1). These data have an important implication in aiding in the selection of the optimum isothermal temperature for constant residual weight of Epikote 828. Due to time limitations, it was decided that one optimum temperature to be studied. Considering the study by Jumahat et. al. [163] and the result obtained in Figure 5.2, a temperature of

550 °C was used as the optimum isothermal temperature in this study. By heating the samples in nitrogen from room temperature to 550 °C and keep the temperature constant at 550 °C for one hour, a constant residual weight of the resin can be achieved, and therefore the actual amount of resin residue can be collected.

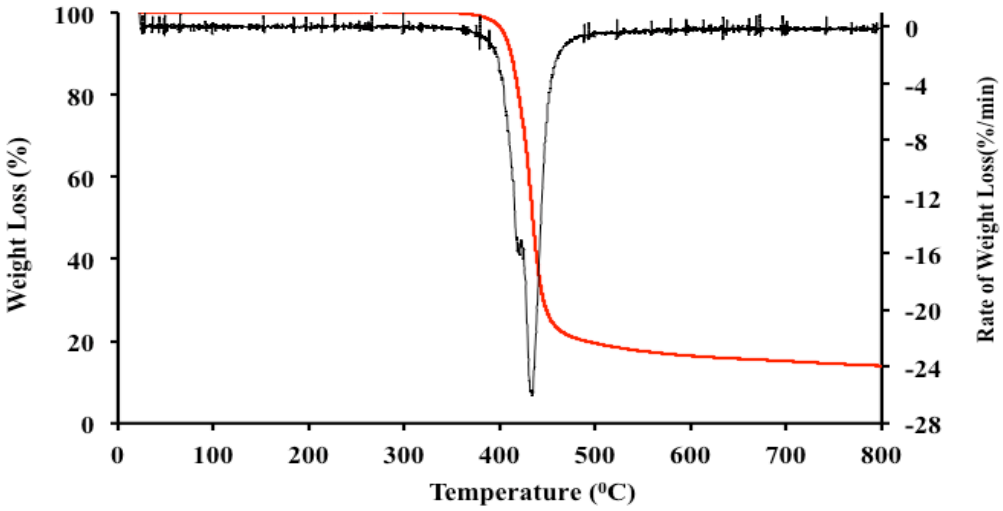

Figure 5.1: Neat Epikote 828 heated in nitrogen from 20 ºC to 800 ºC

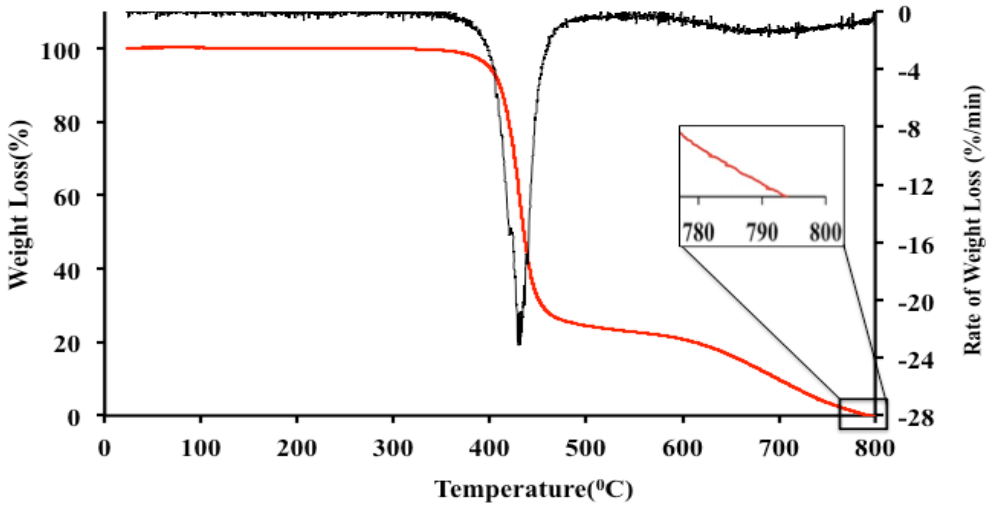

Figure 5.2: Neat Epikote 828 in air from 20 ºC to 800 ºC. Note the final mass is now 0 % from an initial 22.78 % at 550 ºC

Figure 5.3 shows the heating method used in nitrogen and air atmospheres. The temperature of 550 °C was chosen as an optimum isothermal temperature to burn off the Epikote 828+DDS. The TGA profile can be divided into three stages namely stage A, B and C. Stage A indicates the initial weight loss of 0.1% to 0.2% , which is due to the loss of moisture. Stage B shows the decomposition of the Epikote 828+DDS in nitrogen. The weight gradually decreases from 360 °C to 550 °C with total weight loss of 82.14% as summarised in Table 5.1. The temperature was held at 550 °C for one hour before the purge gas was switched to air. In stage C the residue of Epikote 828+DDS was heated until 800 °C. There was some residue with a weight of 1.2 % still visible, even though the temperature had reached 800 °C. This amount residual char varied in subsequent measurements

This study shows that a higher temperature is needed when decomposing Epikote 828/DDS resin system in nitrogen, thus the optimum isothermal temperature should be slightly higher than 550 °C. Again, because of the time limit, the result obtained from using optimum isothermal temperature of 550 °C was the best available option. Also, the resin residue left (about 0.62 wt%) was considered to be within the acceptable range. A maximum degradation temperature of 429.85 °C when heated in nitrogen and 660.16 °C when heated in air, respectively. These temperatures were obtained from the peak (see Figure 5.3 (i) and (ii)) of the rate of weight loss versus temperature curve. The amount of resin residue collected from the method shown in Figure 5.3 was compared to the amount of resin residue collected when heating the sample in nitrogen atmosphere (Figure 5.1). This is to confirm the weight fraction of the epoxy resin. A constant residual weight was collected by both methods, which was about 18 wt% at a temperature between 650 °C to 800 °C. Table 5.1 shows the detail from the TGA results.

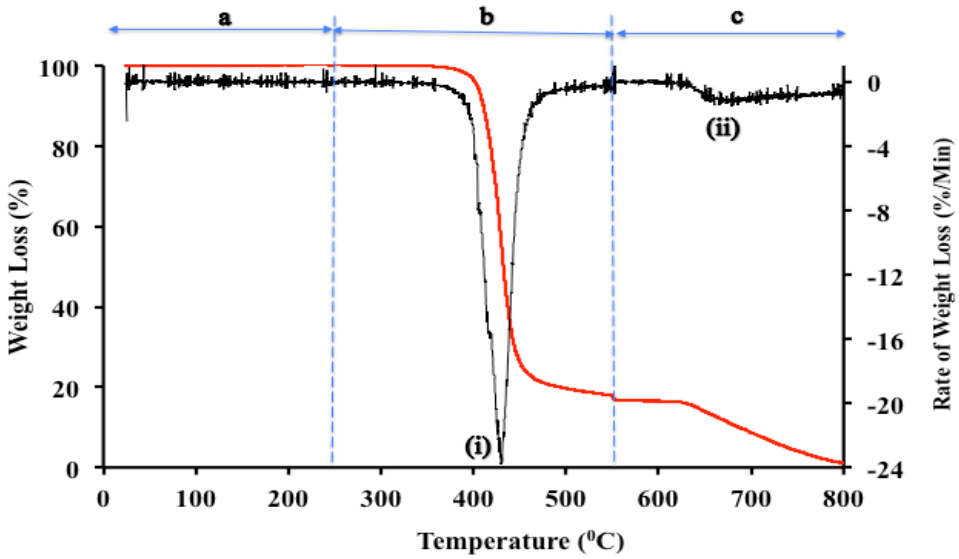

Figure 5.3: TGA result generated by heating Epikote 828+DDS showing degradation of polymer pattern. The heating method applies heating from 25 ^{0}C to 550 ^{0}C in N_2 and heated at 550 ^{0}C for 1 hour, then switched to air until 800^{0}C. The isothermal temperature is at 550 ^{0}C for constant residual weight of Epikote828

Table 5.1: Degradation temperature and weight fraction of Epikote 828+DDS

Heating methods	Weight fraction (wt-%)		Maximum degredation temperature (^{0}C)	
	Epoxy resin	**Carbon residue**	**Epoxy resin**	**Carbon residue**
Heating from 20 ºC to 800 ºC in air	**77.21**	**22.79**	**428.88**	**678.34**
Heating from 20 ºC to 800 ºC in nitrogen	**80.03 ± 3.42**	**17.58± 0.61**	**433.37 ± 0.78**	**-**
Heating from 20 ºC to 550 ºC in nitrogen; then held isothermally for 1 hour at 550 ºC. The purge gas was switched to air after 1 hour to 800 ºC	**82.14**	**17.86**	**429.85**	**660.16**

5.2 TGA analysis for MWCNT modified Epikote828

TGA was used to study the effect of MWCNT on thermal degredation behaviour of Epikote 828+DDS. The initial objective was to determine the volume fraction of MWCNT, but this was unachievable due to the equipment limitation and epoxy char formation. Figure 5.4 and Figure 5.5 show the percentage of weight loss and the rate of weight loss as a function of temperature. All the samples started to decompose at 330 °C. Figure 5.4, has a similar thermal decomposition behaviour to that of the Epikote 828+DDS. This would be expected for the 0.38% MWCNT added. The results show that the addition of MWCNTs to the resin matrix does not influence the onset temperature (330 °C in both cases) but it does decrease the weight loss at a given temperature. Figure 5.4 shows that, at 455 °C the loss weight are (76 %, 71 % and 70 %) for Epikote 828+DDS, Epikote 828 + 0.38 % MWCNT_short and Epikote 828 + 0.38 % MWCNT_long respectively. Similar results were observed for the samples heated in air.

Table 5.2 summarised the TGA results for Epikote 828+DDS and MWCNT modified Epikote 828. The decrease in weight loss percentage with temperature suggest that there was an improvement in the interfacial interaction between the resin matrix and the MWCNTs in the nano-modified composites [142,164]. This behaviour occurred as a result of the higher energy requirement to overcome the strong interfacial bonding between the MWCNTs and the resin system in the nano-modified composites samples.

A number of authors in previous studies, point out that the thermal conductivity of the MWCNTs is high (about 3000 $Wm^{-1}K^{-1}$[165] compared with epoxy resins about 0.15-0.3 $Wm^{-1}K^{-1}$ [166–168]), and therefore the dissipation of the heat in the nano-modified

resin is faster than that of the neat epoxy resin [164,169,170]. However, this is a false argument. The TGA operates as a heater that controls a temperature. So while the MWCNT may conduct heat better, the sample, even with a poor thermal conductivity will rapid reach thermal equilibrium, due to its small size. Thus the effect of thermal conductivity, can at best, show a effect that relies on kinetics, for example the temperature where degradation beings. There is no effective path for heat to be dissipated in the TGA, the gas stream is at the set temperature and so is the sample. As heat flows from hot to cold, there is no heat flow in an isothermal system. Thus thermal conductivity is not relevant to this discussion.

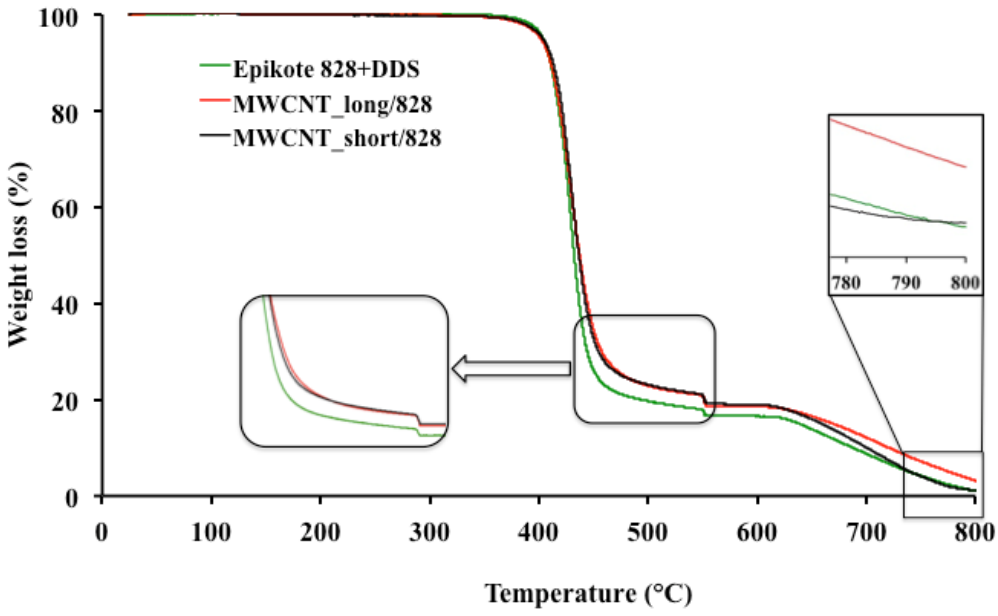

Figure 5.4: TG curves when heated in nitrogen from 25 °C, isothermal at 550 °C for 1 hour, then heated to 800 °C in air

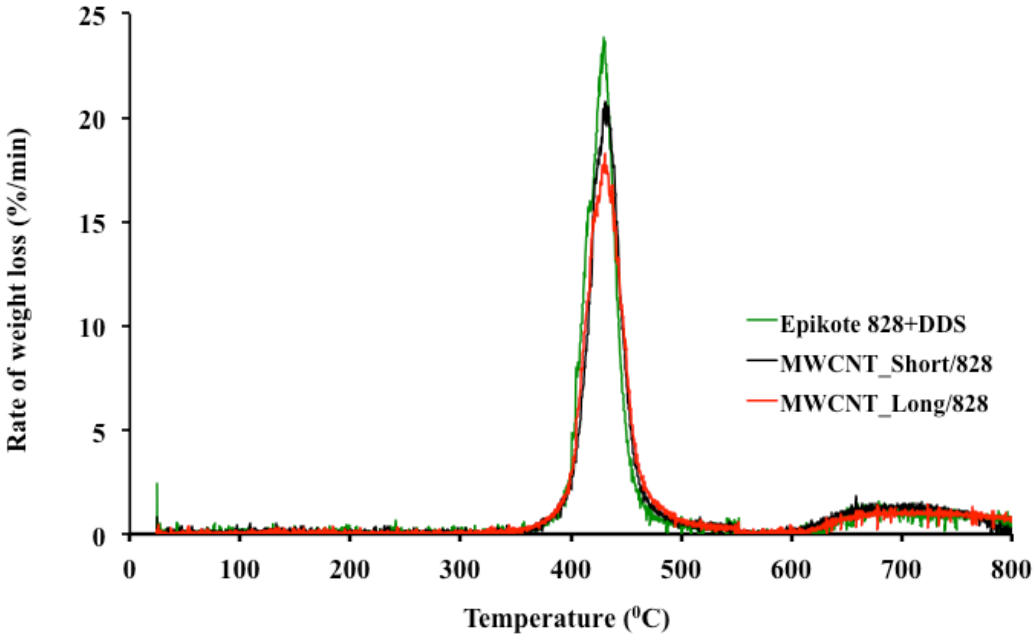

Figure 5.5: Derivative weight curves when heated in nitrogen from 25 °C, isothermal at 550 °C for 1 hour, then heated to 800 °C in air

Figure 5.6 and Figure 5.7 show the decomposition mechanism of the samples heated in air. Epikote 828+DDS shows no residue after 790 °C, however there were some residues left from MWCNT_long/828 and MWCNT_short/828 as in Figure 5.6. SEM micrograph of the residue taken from MWCNTs/828 heated in air are shown in Figure 5.8(a) and Figure 5.8(b). Figure 5.8(a) clearly shows that the MWCNT were homogenously dispersed in the resin with no bubbles, while Figure 5.8(b) shows the traces of bubbles in between the MWCNTs. This is possibly due to the fact that under a high temperature, the strong interaction between MWCNTs and the resin could retard the diffusion of small molecules of the resin matrix and resulting in the improvement of thermal stability of the nanomodified composites [51,171]. Additionally the bubbles appeared between the MWCNTs promote carbonisation and the increase in carbon content would increase the amount of residues [172,173].

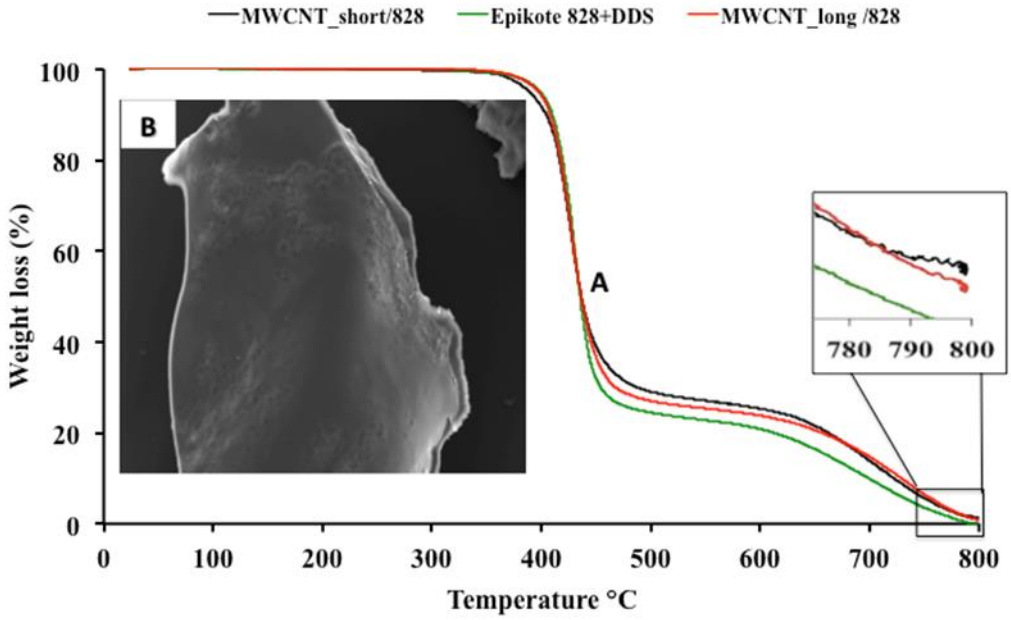

Figure 5.6: (A) TG curves when heated in air from 25 °C, isothermal at 550 °C for 1 hour, then further heated in air to 800 °C, (B) Micrograph from SEM shows some residue left for MWCNT_long/828 sample and MWCNT_short/828 sample

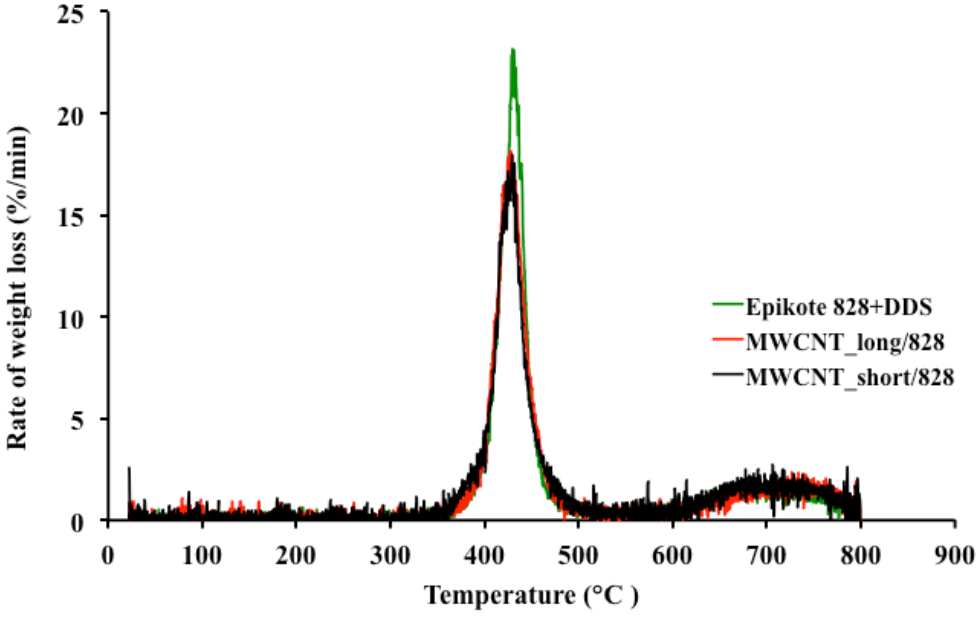

Figure 5.7: Derivative weight curves when heated in air

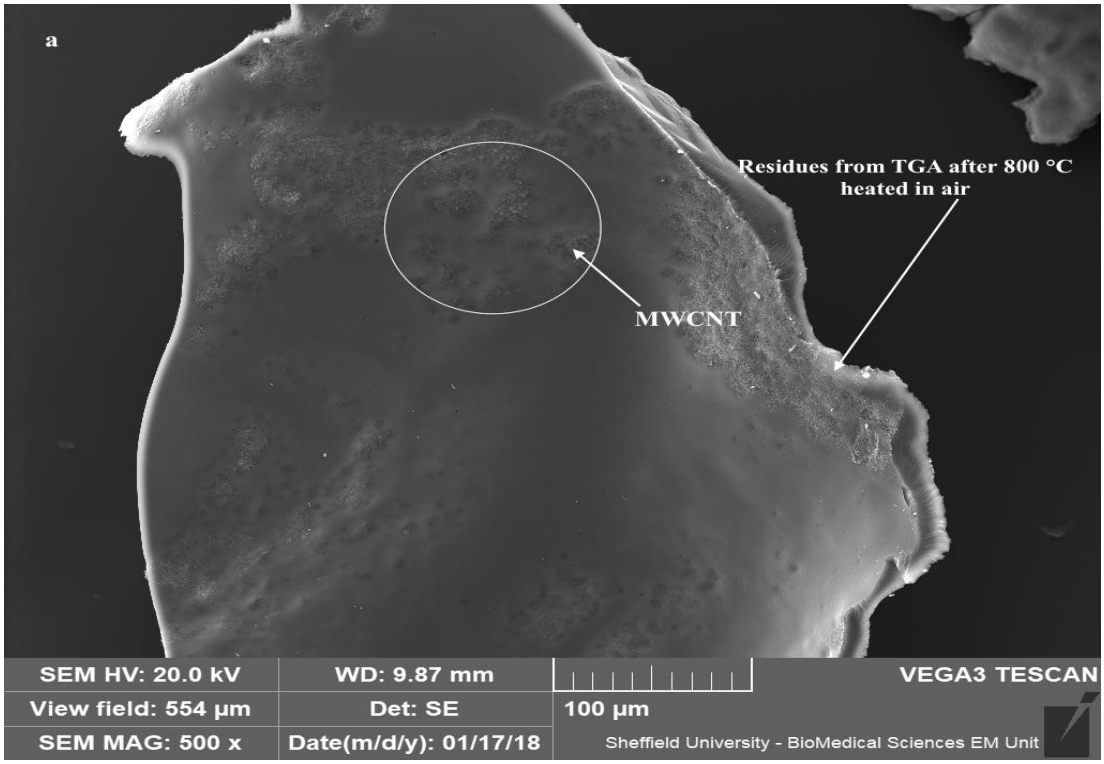

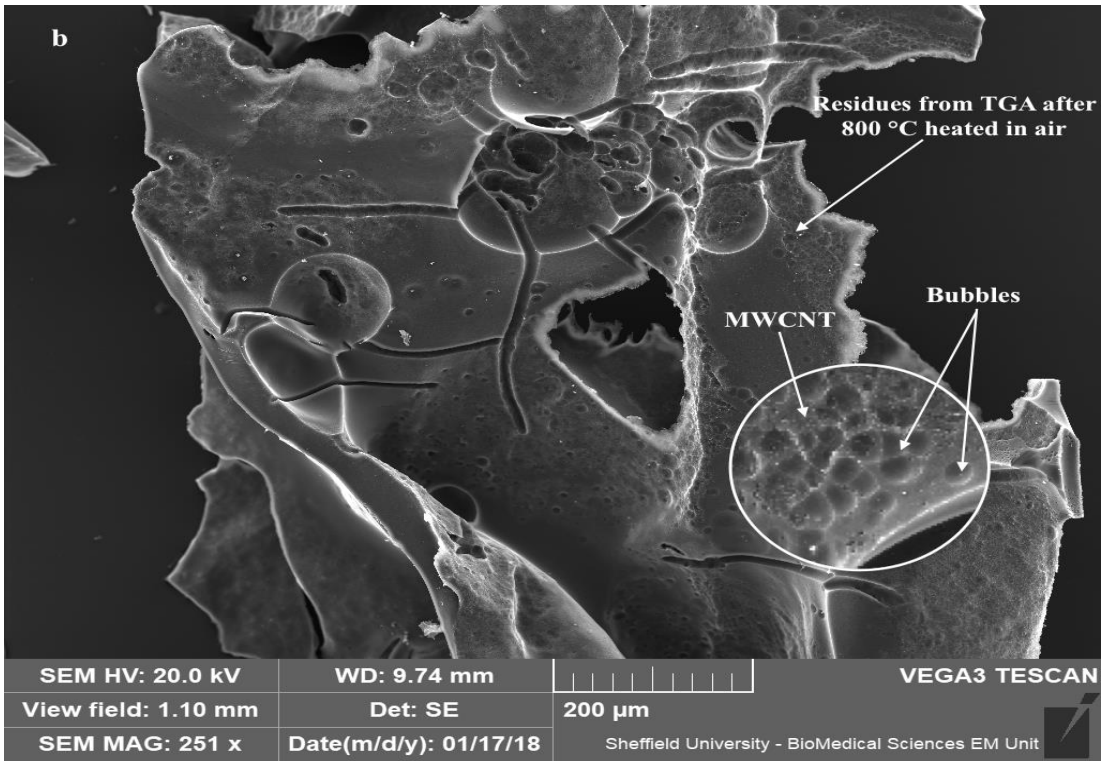

Figure 5.8: Micrograph (a) and (b) from SEM shows residues left after 800 °C when heated in air

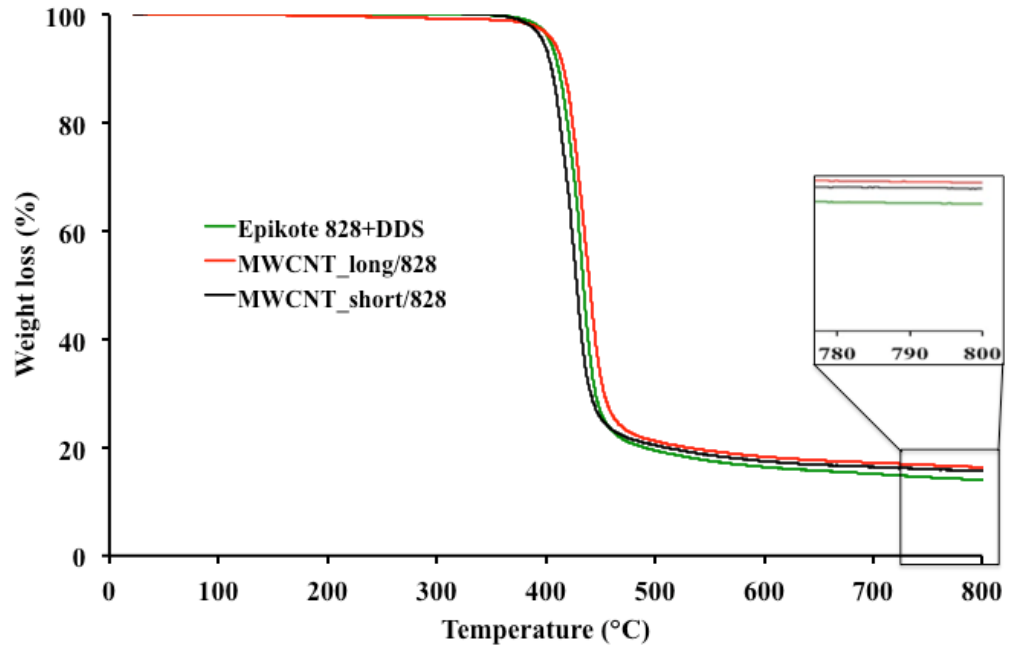

Figure 5.9: TG curves when heated in nitrogen

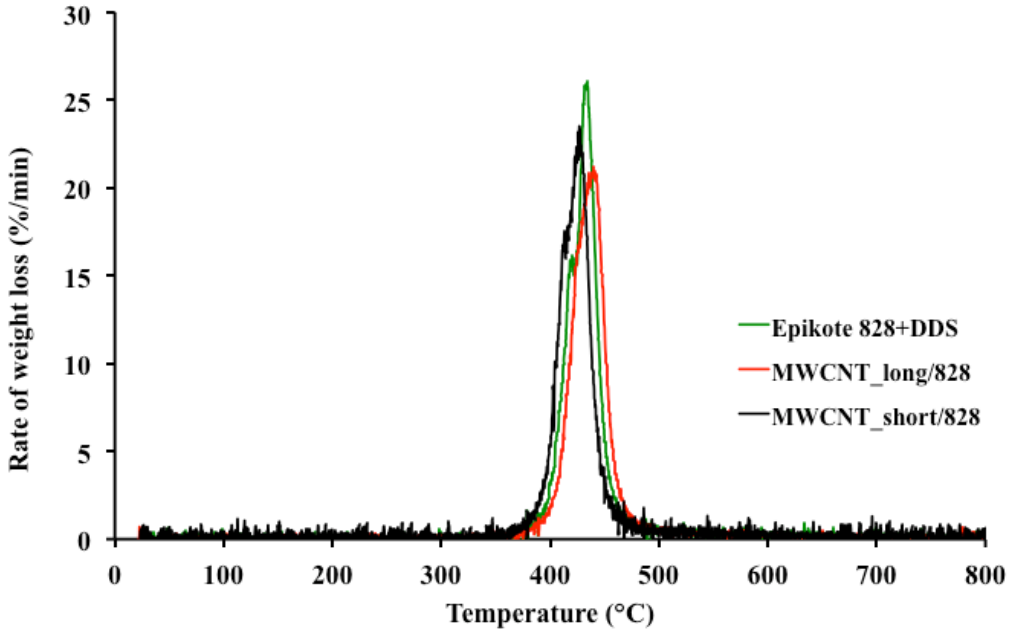

Figure 5.10: Derivative weight curves when heated in nitrogen

Table 5.2: TGA results on weight fraction and maximum degradation temperature of Epikote 828 epoxy resin and MWCNTs/828 composite epoxy resin

Heating Methods	Resin system	Figure	Weight fraction (wt-%)			Maximum degredation temperature(^{0}C)	
			Resin	Residue at 550 °C	Residue at 800 °C	Resin	Carbon residue
Heating method 1	Epikote 828 + DDS	Figure 5.6	77.21	22.79	0.00	428.88	678.34
	MWCNT_short /828	Figure 5.6	72.96	25.63	1.22	429.49	706.65
	MWCNT_long/ 828	Figure 5.6	74.6	24.68	0.71	427.09	729.75
Heating method 2	Epikote 828 + DDS	Figure 5.9	80.03 ± 3.42	18.76 ± 1.74	13.15 ± 1.19	433.37 ± 0.78	-
	MWCNT_short /828	Figure 5.9	81.06 ± 0.49	19.04 ± 0.63	15.67 ± 0.39	426.79 ± 0.121	-
	MWCNT_long/ 828	Figure 5.9	80.93 ± 0.2	19.068 ± 0.20	16.11 ± 0.18	432.92 ± 2.32	-
Heating method 3	Epikote 828 + DDS	Figure 5.4	82.14	17.86	0.62	430.22 ± 0.34	675.41 ± 5.63
	MWCNT_short /828	Figure 5.4	80.89	19.40 ± 0.40	0.77 ± 0.17	423.50 ± 6.50	711.32 ± 3.71
	MWCNT_long/ 828	Figure 5.4	81.35	18.84 ± 0.26	0.96 ± 0.33	428.37 ± 0.83	722.23 ± 2.69

Heating method 1: in air from 20 ^{o}C to 800 ^{o}C

Heating method 2: in nitrogen 20 ^{o}C to 800 ^{o}C

Heating method 3: in nitrogen from 20 ^{o}C to 550 ^{o}C; then being held isothermally for 1 hour at 550 ^{o}C. The purge gas was switched to air after 1 hour to 800 ^{o}C

5.3 TGA analysis for Epikote 828 CFRP laminates

TGA was also used to study the thermal stability of Epikote 828 CFRP composite system. One of the main objectives in this study was to measure the weight percentage of MWCNT in the composite. But, due to the equipment limitation, the variability in the residue at 800C in both air and nitrogen and the small amount of MWCNT added, this could not be determined. Therefore, the TGA was performed at a scan temperature up to 800 °C.

In this study, the TGA was used to measure the weight percentage of carbon fibre in the Epikote 828 CFRP composite. Figure 5.11 shows the thermal degradation behaviour of neat Epikote 828/carbon fibre laminate. The laminate was heated in the TGA using the technique described in Figure 3.15. The laminate was first heated in nitrogen gas atmosphere from 25 °C to 550 °C at 10 °C/min and then was kept at 550 °C for 1 hour and was further heated in air atmosphere to 800 °C at 10 °C/min. Figure 5.11 shows that the laminate started to degrade at 332 °C.

Figure 5.11 can be divided into three different profiles, marked as A, B and C. Stage A shows that the initial weight loss of the moisture content in the laminate was about 0.1 %. Stage B shows the decomposition of the resin and the weight loss gradually increases from 332 °C to 550 °C. The total weight loss of 35.49 wt% was observed in stage B. After keeping the temperature constant at 550 °C for one hour, the purge nitrogen gas was switched to air. The SEM micrograph sample residues in Figure 5.13 (b), which was collected at 550 °C shows that, there was a resin which remains deposited on the carbon fibres. Stage C shows that the resin residue starts to burn at 602 °C and then finishes at 800 °C, with a total weight loss of 24.65 wt%. Derivative weight

curves in Figure 5.12, shows that the maximum degradation temperature of the resin and its residue occurs at 419 °C (point (i)) and 656 °C (point(ii)), respectively. Figure 5.14 (a) and Figure 5.14 (b) show that, the resin was removed from the carbon fibre's surface after the sample was exposed to 800 °C. The TGA curve of the Epikote828/carbon fibre CFRP composite was also compared to the decomposition behaviour of Epikote 828+DDS (as discussed in section 5.1). The TGA curve of Epikote 828+DDS confirms that the resin was heated off at 800 °C. It can be concluded that the material which was remained after 800 °C was in fact the carbon fibre.

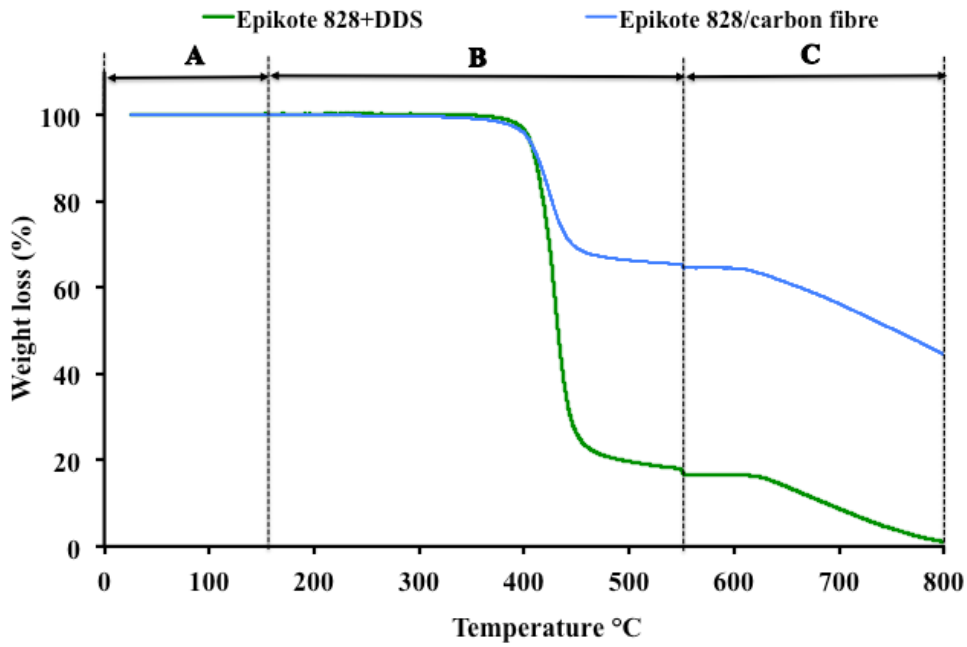

Figure 5.11: Typical TGA results showing the percentage of weight loss versus temperature of Epikote 828+DDS resin and Epikote 828/carbon fibre CFRP

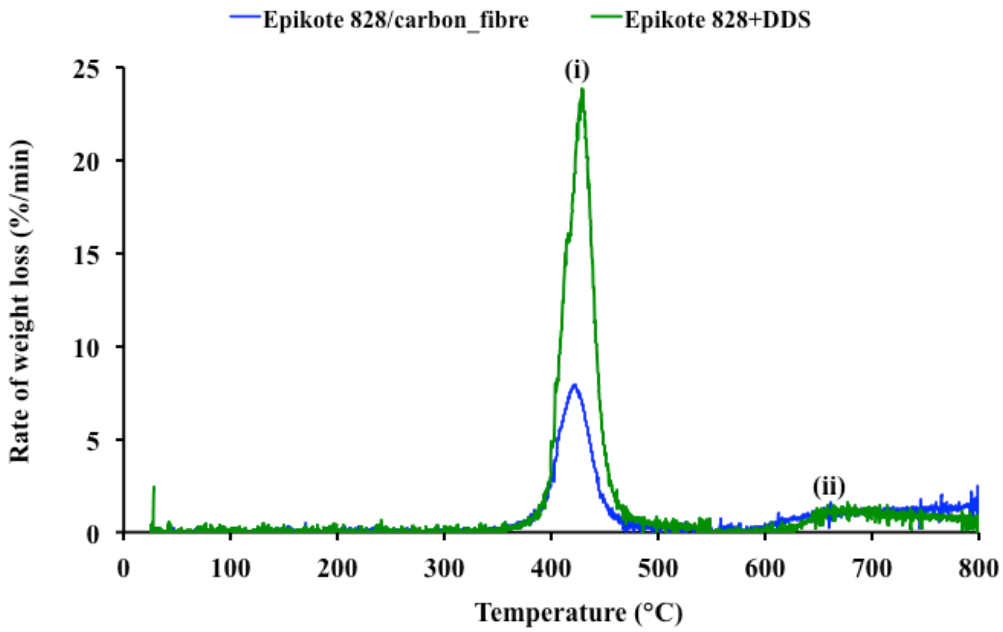

Figure 5.12: Derivative weight curves of neat Epikote 828 resin and Epikote 828/carbon fibre CFRP composites, heated in nitrogen gas from 25 °C to 550 °C then kept at 550 °C for 1 hour and followed by heating in air to 800 °C

The fibre volume fractions in Epikote828/carbon fibre laminate was calculated in accordance to ASTM standard D3171-99 (as discussed in section 3.6.3.2). Two samples were tested. TGA results show that the average weight fraction of carbon fibre and resin were 50.77 wt% and 48.23 wt% respectively. The average of Epikote828/carbon fibre density determined by Accupyc was 1.47 g/cm^3 (summary of result is shown in Table 5.5). The density of plain weave carbon fibre, as given by the manufacturer, was 1.79 g/cm^3 and the density of Epikote 828 polymer is 1.23 g/cm^3 as measured by Accupyc (Table 5.3). The volume fractions of the carbon fibre and the resin in the Epikote828/carbon fibre CFRP laminates were 41.69 vol% and 57.64 vol%,

respectively. The resin volume fraction measured using TGA tecnique was very close to the value measured using Accupyc (Table 5.3).

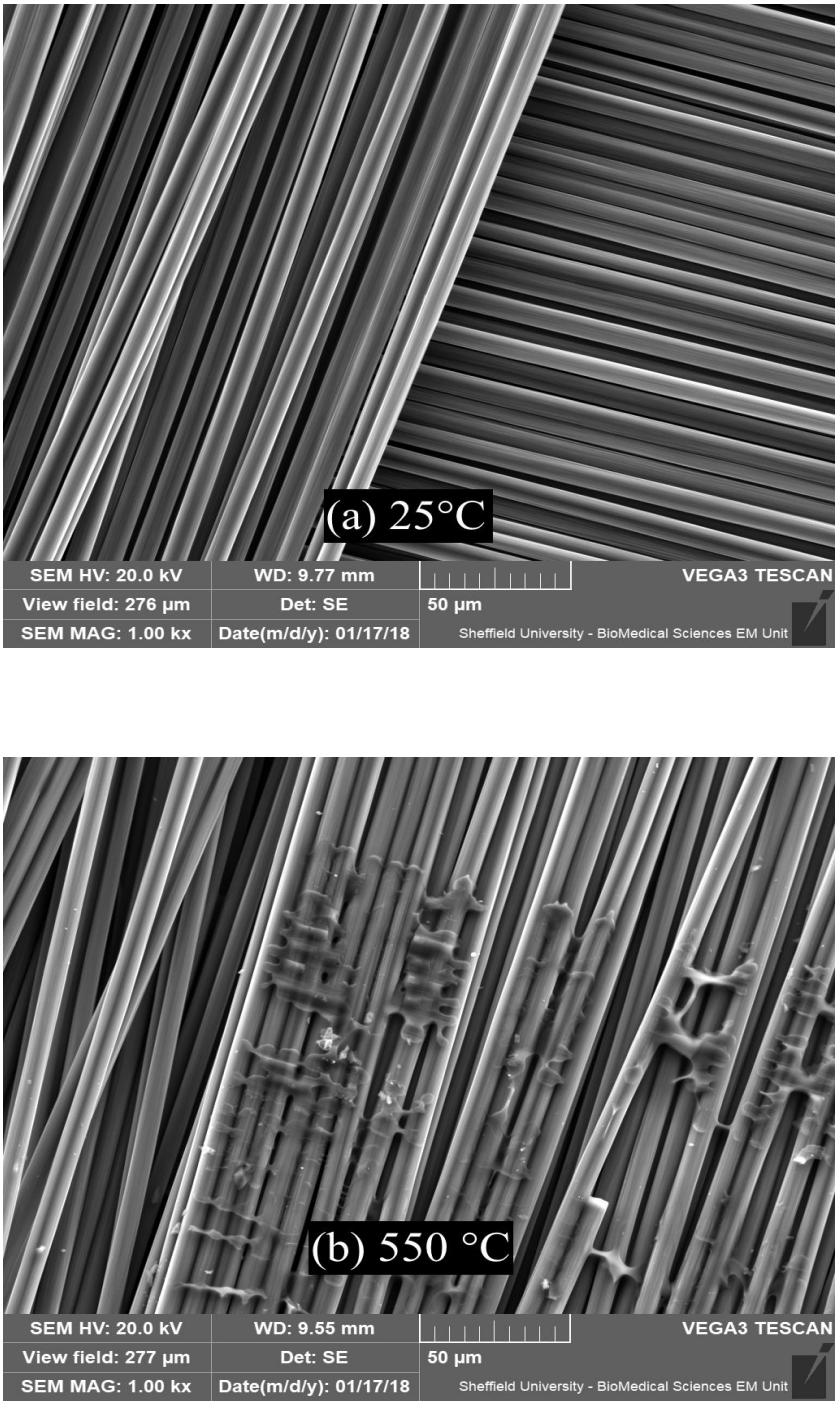

Figure 5.13: SEM micrographs showing the Epikote828/carbon fibre CFRP composites (a) carbon fibre without epoxy and (b) after heating at 550 °C

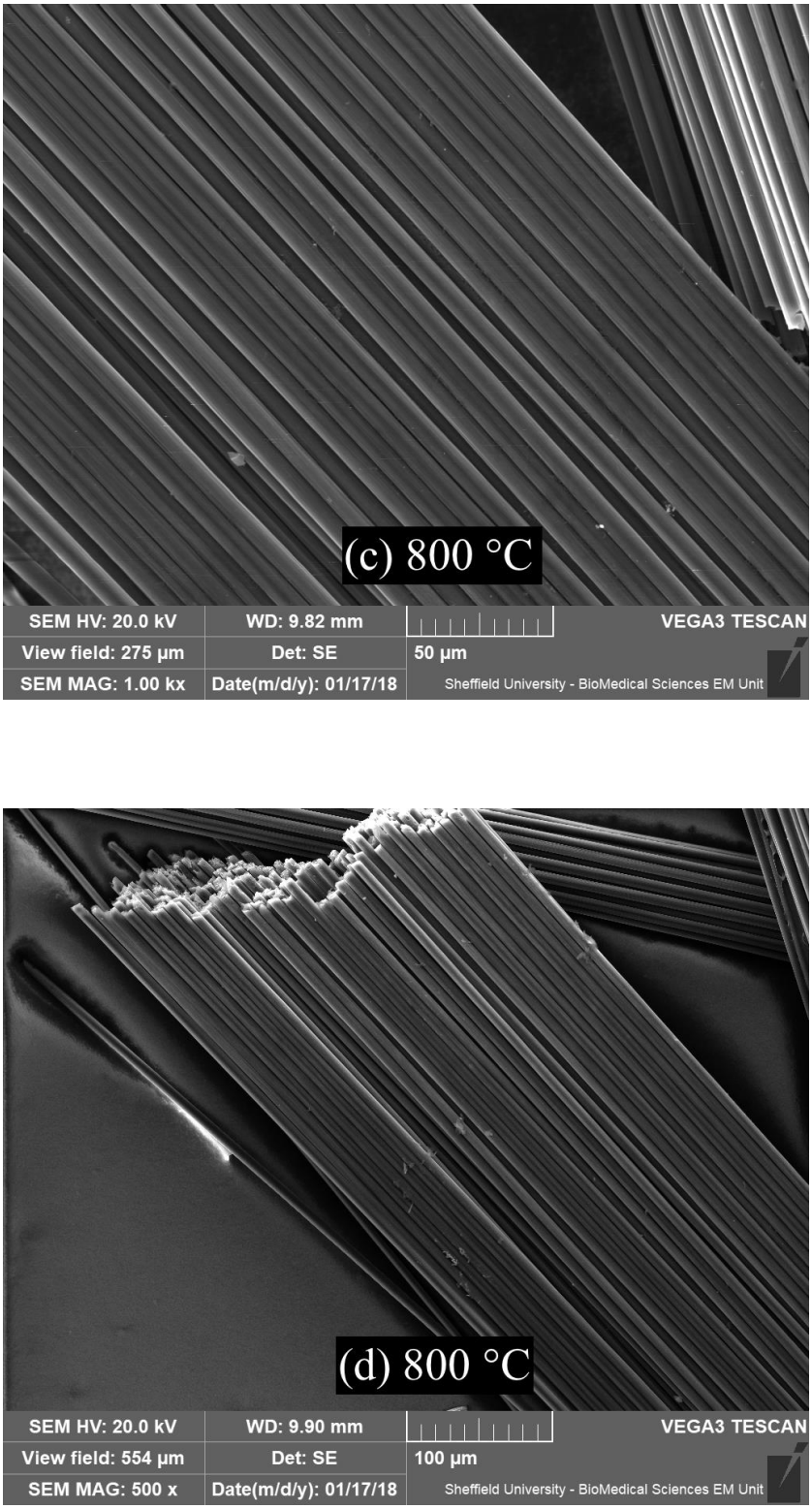

Figure 5.14: SEM micrographs showing the Epikote828/carbon fibre CFRP composites after heating at 800 °C with two different magnification (c) 1000x and (d) 500x

5.4 Density measurement

Table 5.3 and Table 5.4 shows the measurement values of volume and density of Epikote 828+DDS, MWCNT_long/828 and MWCNT_short/828 measured using Accupyc and Geopyc.

Table 5.3: Measurement of volume and density of Epikote 828+DDS, MWCNT_short/828, MWCNT_long/828 using **Accupyc**

Resin system	**Volume (cm^3)**	**Density (g/cm^3)**
Epikote828+DDS	0.59	1.23
MWCNT_short/828	0.59 ± 0.08	1.24 ± 0.002
MWCNT_long/828	0.55	1.24

Table 5.4: Measurement of volume and density of Epikote 828+DDS, MWCNT_short/828, MWCNT_long/828 using **Geopyc**

Resin system	**Volume (cm^3)**	**Density (g/cm^3)**
Epikote 828+DDS	0.86 ± 0.02	1.19 ± 0.016
MWCNT_short/828	0.84	1.24
MWCNT_long/828	0.72 ± 0.22	1.23 ± 0.04

Table 5.5 shows the void calculation of MWCNTs/828/carbon fibre and Epikote828/carbon fibre laminates. MWCNTs/828 nano-modified composite laminate have lower voids compared to that of the neat Epikote828/carbon fibre laminates.

Table 5.5: Void calculation of Epikote828/carbon fibre, MWCNT_short/828/carbon fibre, MWCNT_long/828/carbon fibre using **Accupyc** and **Geopyc** measurement values.

Carbon fibre/resin sytem	**True Density[a] (ρ_A) (g/cm³)**	**Skeleton Density[b] (ρ_G) (g/cm³)**	**Void[c] (%)**
Epikote828/carbon fibre	1.47	1.39 ± 0.007	5 %
MWCNT_short/828/carbon fibre	1.48	1.47 ± 0.12	1 %
MWCNT_long/828/carbon fibre	1.50	1.49 ± 0.003	2 %

a Density measured by using **Accupyc**
b Density measured by using **Geopyc**
c void = $1 - \left(\frac{r_G}{r_A}\right) \times 100$

Figure 5.15 and Figure 5.16 show SEM micrographs cross-section of woven CFRP composite which were made of plain weave carbon fibre, Epikote828/DDS resin and plain weave Epikote828/MWCNT/DDS composite resin respectively. Imperfections in the laminate, such as misalignments of fibre, fibre waviness and microvoids in the matrix could not be completely eliminated during the lay-up process which with these defects can initiate failure. In this study, the strength of the fabricated CFRP specimens was study using short beam shear (SBS) test which will be discussed in section 6.3

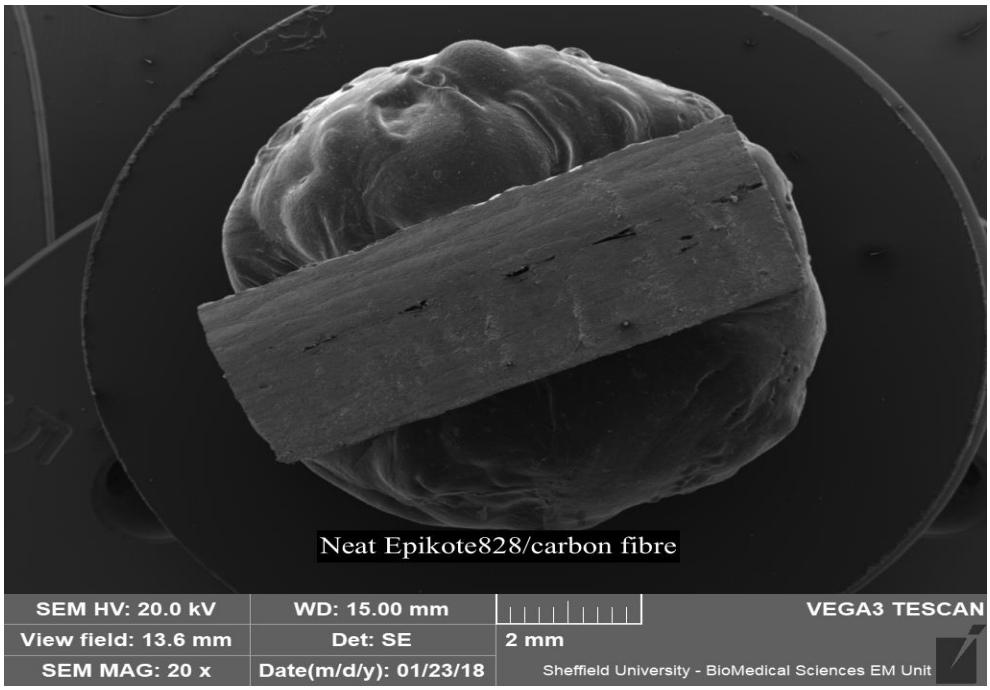

Figure 5.15: SEM micrograph of Epikote828/carbon fibre laminates

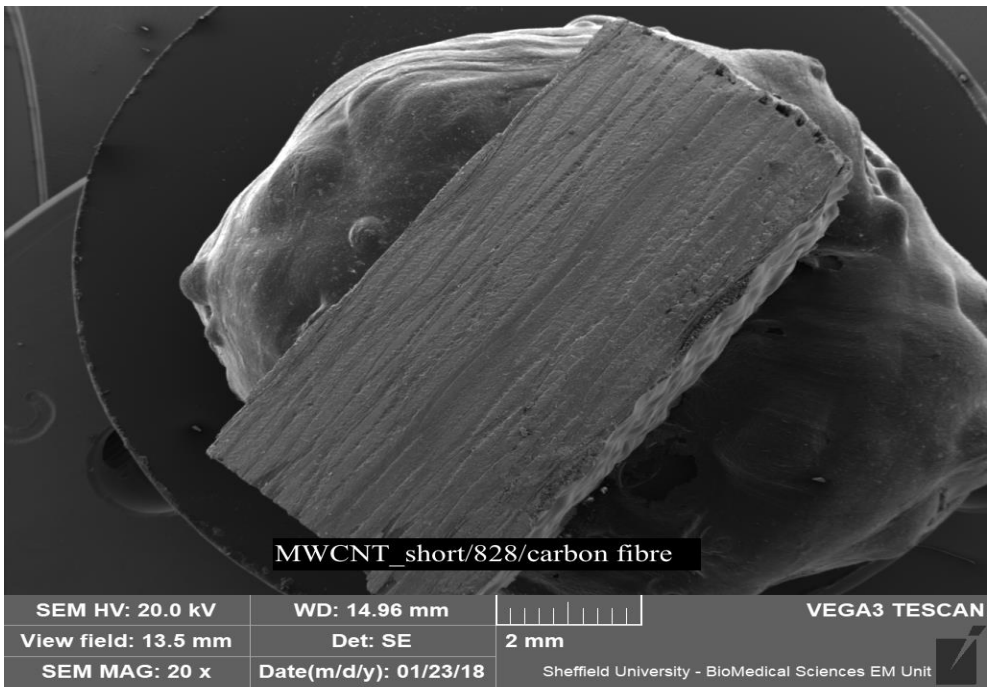

Figure 5.16: SEM micrograph of MWCNT_short/828/carbon fibre laminate

5.5 Dynamic mechanical analysis (DMA) and differential scanning calorimetry (DSC) of Epikote 828 and MWCNT nanomodified resin composite

In this study, DMA was performed to evaluate the effect of MWCNTs addition on the thermal glass transition (T_g) of the nano-modified composites. The test was carried out using three-point bending mode at oscillation frequency of 1 Hz and a scan temperature from room temperature to 250 °C. T_g was determined from the peak of tan delta spectrum at 1 Hz. This temperature represents the onset or the midpoint of the curve. It can also be obtained from the peak temperature of the tan δ, or the peak temperature of the loss modulus curve [110,174,175]. ASTM D 4065-01 suggested that the peak of loss modulus can be documented as T_g [176]. In this study, the T_g was obtained from the peak temperature of tan δ and the peak temperature of the loss modulus curve.

Figure 5.17 and Table 5.6 revealed that the T_g(tan δ), for all the samples were in the range of 200 °C - 201°C. There was no significant difference in the T_g between the Epikote 828 resin system and the MWCNT nano-modified resin system. The same characteristic were shown in Figure 5.18 and Table 5.7. The T_g ranges between 190 °C and 191 °C. There was no significant difference in the T_g between the samples. The value of T_g measured with DMA is slightly larger than DSC and these have been reported by previous researchers and it can vary by up to 25 °C [115,177]. Table 5.7 and Table 5.8 shows that, the T_g (E") values were closer to the T_g (DSC) than the values of T_g(tan δ). The results suggested that the value of T_g obtained from the dynamic test is comparable to the T_g measured using static techniques [178].

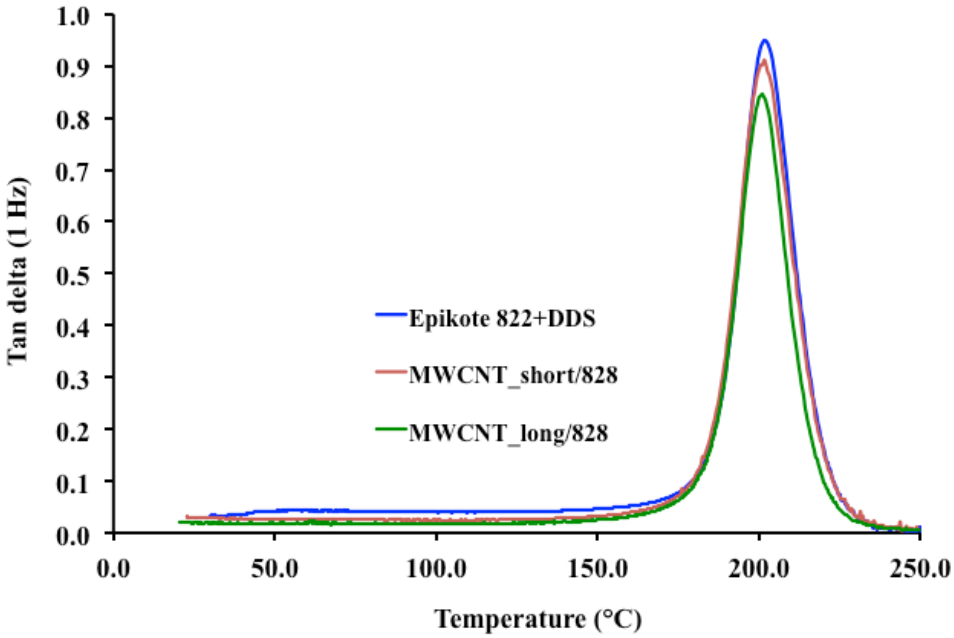

Figure 5.17: Tan δ versus temperatures for Epikote 828+DDS, MWCNT_short/828, MWCNT_long/828 using DMA technique

Table 5.6: Summary of T_g obtained from maximum peak of tan δ at 1 Hz using DMA technique

Type of samples	**T_g (°C) (sample 1)**	**T_g (°C) (sample 2)**	**Average T_g (°C)**
Epikote 828+DDS	201.8	201.8	201.8
MWCNT_short/828	200.1	201.6	200.9
MWCNT_long/828	200.7	201.1	200.9

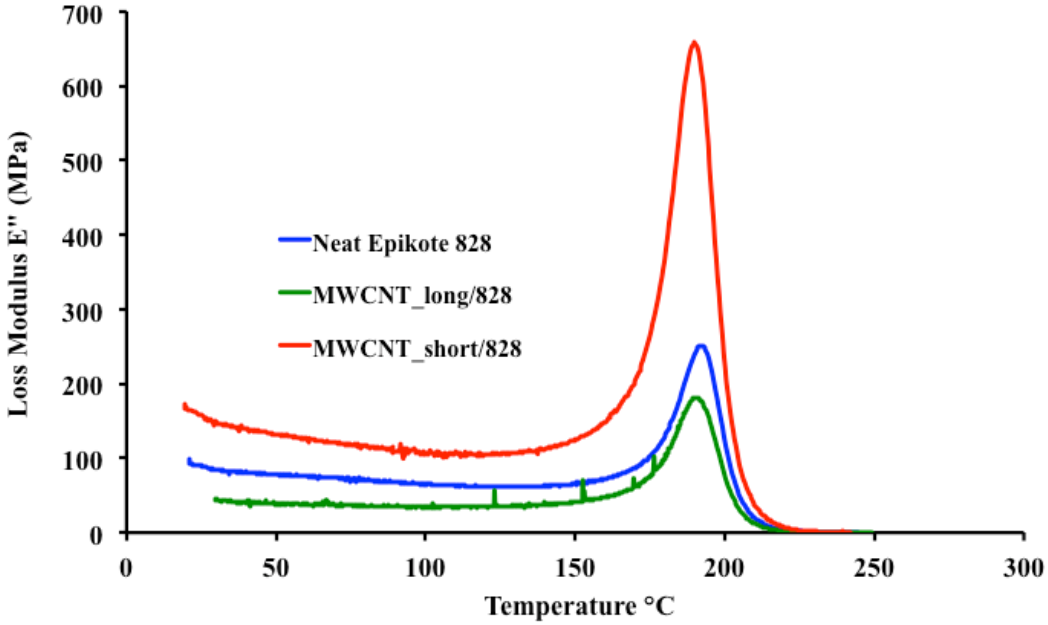

Figure 5.18: Loss modulus (E”) versus temperature for neat Epikote 828, MWCNT_short/828, MWCNT_long/828 using DMA technique

Table 5.7: Summary of T_g obtained from the maximum peak of loss modulus using DMA technique

Type of samples	$T_{g(E'' max)}$ (°C) Sample 1	$T_{g(E'' max)}$ (°C) Sample 2	Average $T_{g(E'' max)}$ (°C)
Epikote 828+DDS	191.9	191.1	191.5
MWCNT_short/828	190.0	190.5	190.3
MWCNT_long/828	190.4	190.4	190.4

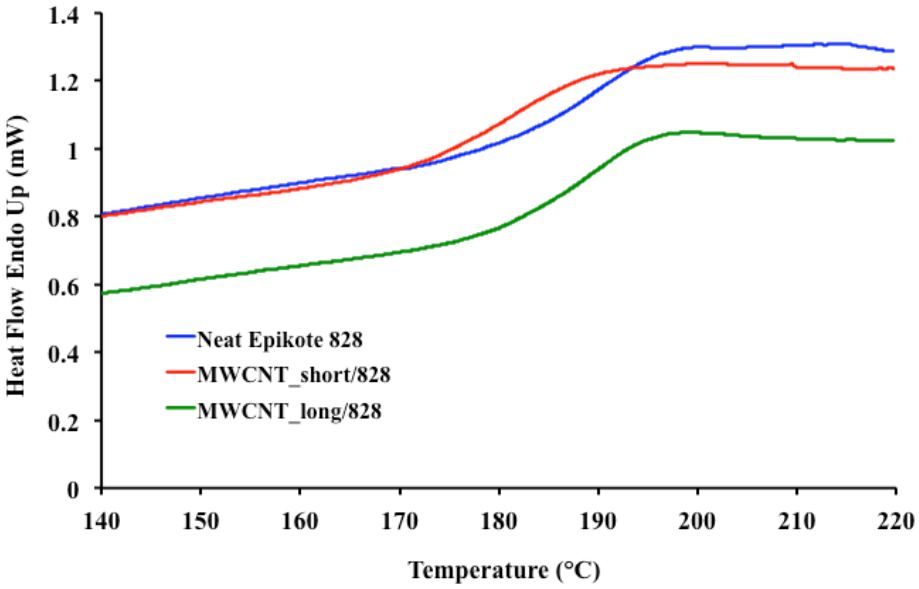

Figure 5.19: DSC results of Epikote 828+DDS, MWCNT_short/828 and MWCNT_long/828 using DSC technique

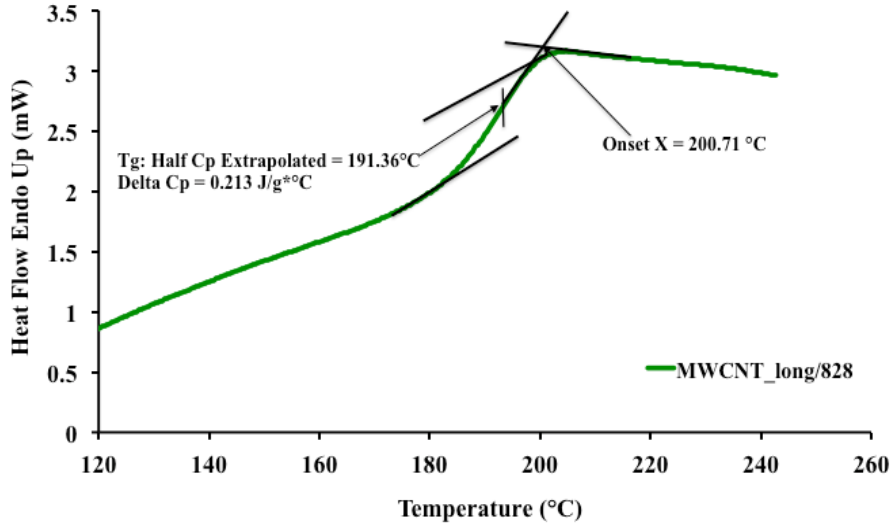

Figure 5.20: T_g obtained from DSC technique is analysed Using Pyris^{TM} Manager software

Table 5.8: Summary of T_g obtained from the DSC technique

Type of samples	$T_{g(DSC)}$ (°C) Sample 1	$T_{g(DSC)}$ (°C) Sample 2	Average $T_{g(DSC)}$ (°C)
Epikote 828+DDS	190.0	191.2	190.6
MWCNT_short/828	184.4	186.1	185.3
MWCNT_long/828	190.3	191.4	190.9

5.6 DMA analysis of Epikote 828 CFRP composite and MWCNT nanomodified CFRP composite

In this study, DMA was also used to measure glass transition temperature (T_g), from the peak position of tan δ vs temperature curves and the peak position of loss modulus, E", vs temperature curves of Epikote828/carbon fibre and MWCNTs_828/carbon fibre CFRP composites. From Figure 5.21 it was observed that T_g from peak of tan δ for the Epikote 828/carbon fibre CFRP composites was lower by about 11 °C than T_g for the MWCNTs_828/carbon fibre CFRP composites. The same pattern was observed for T_g from peak of E" shown in Figure 5.22 which shows that the T_g for Epikote 828/carbon fibre CFRP composites was lower by about 23°C. The results of T_g for neat CFRP composites and CFRP nanocomposites were different in pattern from neat epoxy resin and nanocomposite epoxy resin, where for all the T_g of neat epoxy resin and nanocomposite epoxy resin the average value are the same. Where as for the neat CFRP composites the T_g is significantly lower than the T_g for CFRP nanocomposites.

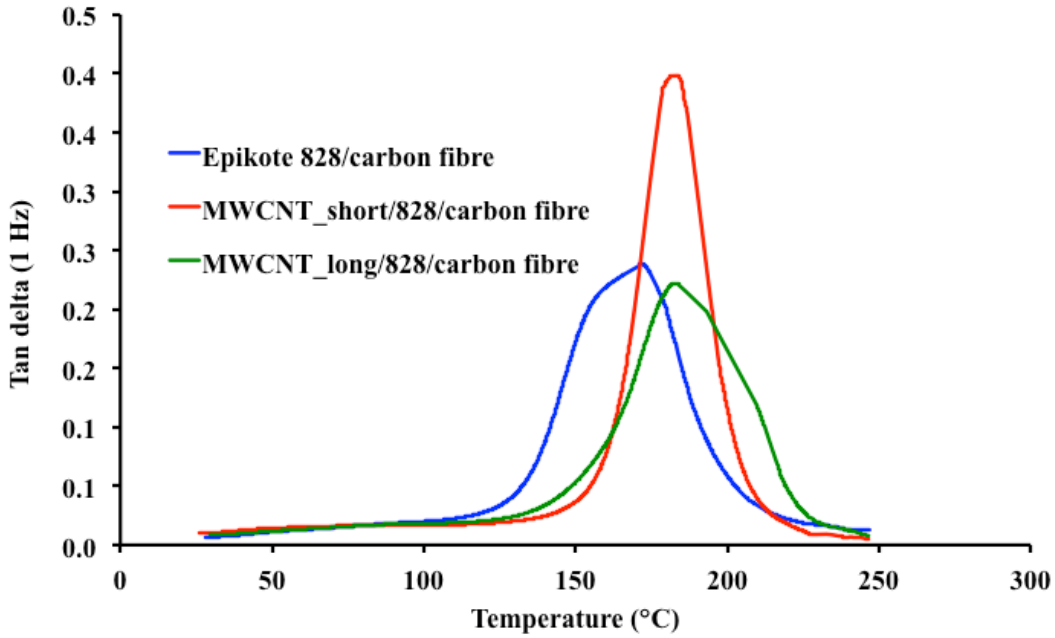

Figure 5.21: Tan δ versus temperature for Epikote 828/carbon fibre, MWCNT_short/828/carbon fibre, MWCNT_long/828/carbon fibre using DMA technique

Table 5.9: Summary of T_g for Epikote 828/carbon fibre, MWCNT_short/828/carbon fibre, MWCNT_long/828/carbon fibre obtained from maximum peak of tan δ at 1 Hz using DMA technique

Type of samples	**$T_{g(\tan \delta)}$ (°C)**
Epikote 828/carbon fibre	171.91
MWCNT_short/828/carbon fibre	183.86
MWCNT_long/828/carbon fibre	182.81

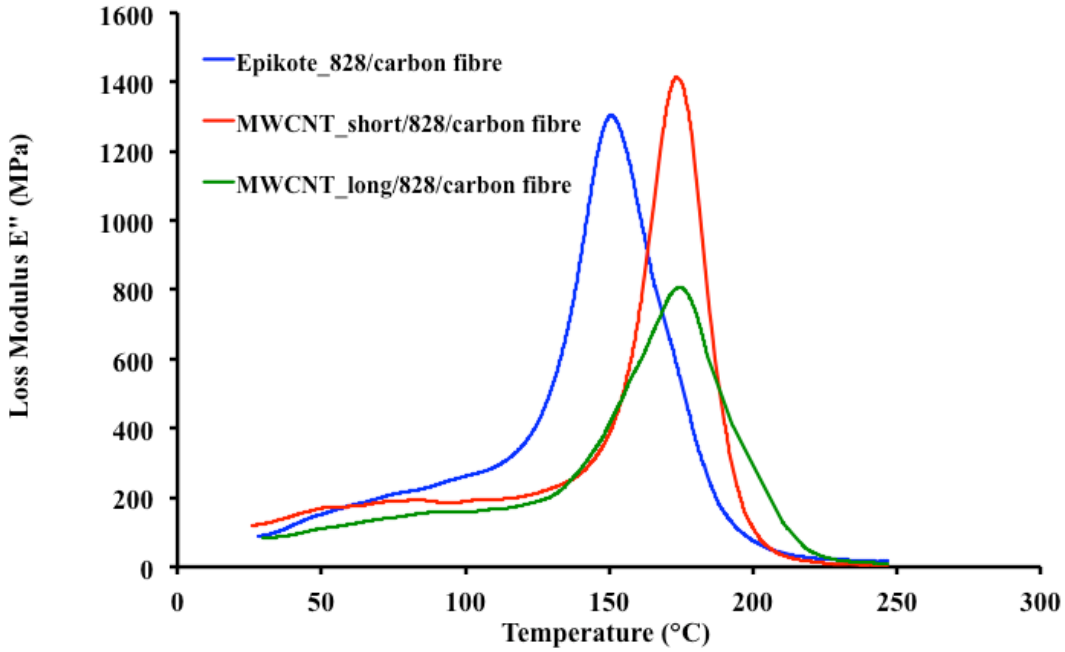

Figure 5.22: Loss modulus (E") versus temperature for Epikote 828/carbon fibre, MWCNT_short/828/carbon fibre, MWCNT_long/828/carbon fibre using DMA

Table 5.10: Summary of T_g for Epikote 828/carbon fibre, MWCNT_short/828/carbon fibre, MWCNT_long/828/carbon fibre obtained from the maximum peak of loss modulusm(E") using DMA technique

Type of samples	**$T_{g(E")}$ (°C)**
Neat Epikote 828/carbon fibre	150.60
MWCNT_short/828/carbon fibre	173.37
MWCNT_long/828/carbon fibre	174.56

The increase in T_g value of MWCNT_long/828/carbon fibre and MWCNT_short/828/carbon fibre as compared to the Epikote 828/carbon fibre show that, the presence of nanoparticles such as MWCNTs may generate a strong interfacial bonds with epoxy resin. This was due to the difficulty of the epoxy to move around the

nanotubes causing mobility reduction thus increasing the corresponding T_g values [141,145,179]. T_g from DSC for CFRP composites for the three different epoxy resin systems cannot be generated as they did not show any distinguish curve in the graph. The prevoius researchers have often found that DSC may not be sensitive enough to measure T_g with high thermosetting resin and high fibre volume fraction as compared to measuring T_g by using DMA [177,180] .

6 Mechanical analysis

6.1 Compression test of epoxy polymer

The static unaxial compression tests of the epoxy resin systems were conducted on cylindrical shape samples. The compressive properties such as elastic modulus, failure at stress and strain, yield strength and strain at yield point, were measured based on BS EN ISO 604:2003 [127] and ASTM standard D695 [125]. Figure 6.1, Figure 6.2, and Figure 6.3 show the typical stress-strain curves of cylindrical samples of neat Epikote 828 epoxy resin, MWCNT_long/828 epoxy resin and MWCNT_short epoxy resin loaded on static uniaxial compression. The compressive modulus of the epoxy was calculated at 2% to 3% compressive strain. Table 6.1 shows the comparison between the compressive properties of neat Epikote 828 epoxy resin, MWCNT_long/828 epoxy resin and MWCNT_short/828 epoxy resin.

The compressive strength or compressive stress at break for both MWCNTs/828 epoxy resin systems were higher than Epikote 828+DDS epoxy resin system. Compressive modulus for Epikote 828+DDS was higher than MWCNT_long but lower than MWCNT_short/828. However, the compressive strain and compressive stress at yield point of the neat Epikote 828 shows the highest value. From the table it can be concluded that the nanocomposite increase in strength as compared to the neat epoxy but became more brittle with the addition of the MWCNTs.

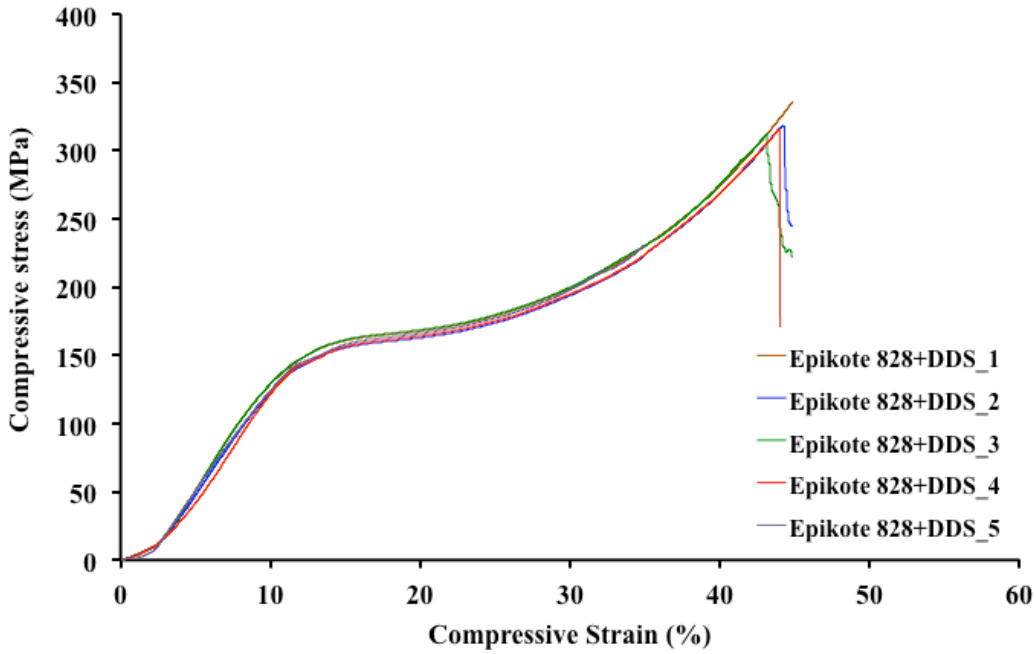

Figure 6.1: Stress – strain curves of cylindrical Epikote 828+DDS epoxy resin system samples loaded in static unaxial compression

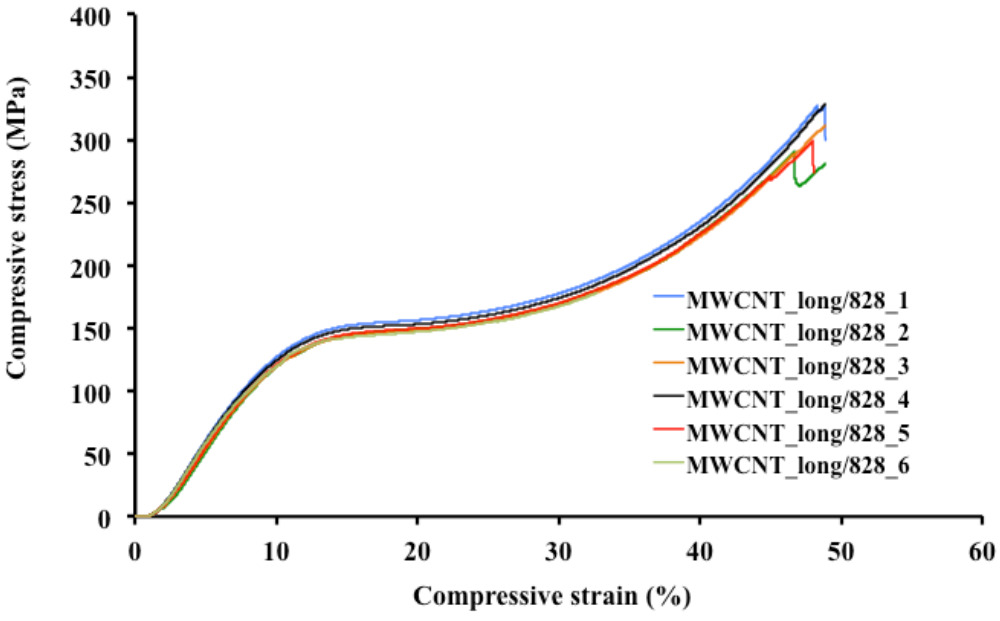

Figure 6.2: Stress – strain curves of cylindrical MWCNT_long/828 epoxy resin system specimens loaded in static unaxial compression

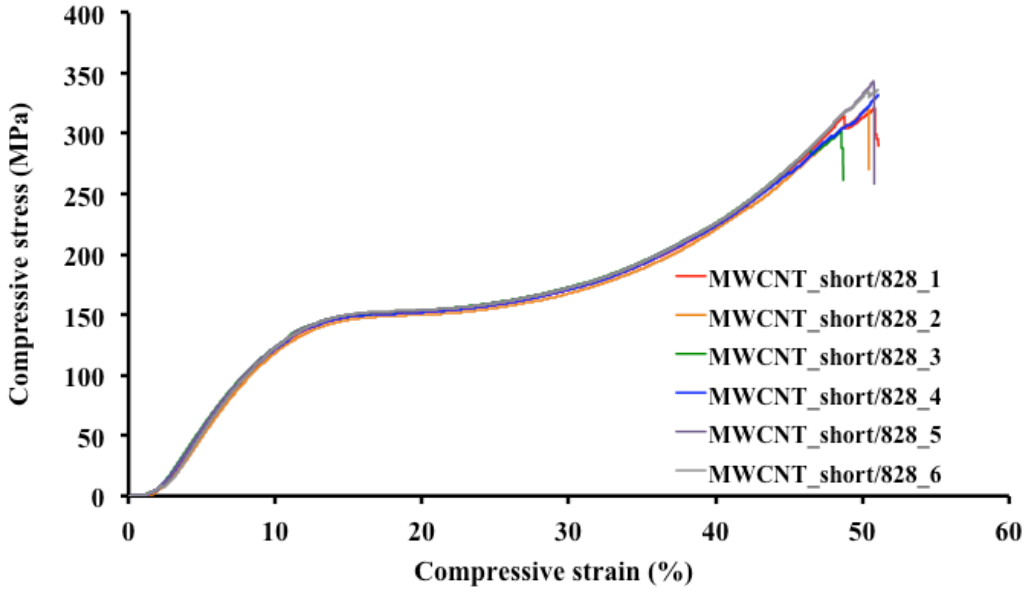

Figure 6.3: Stress – strain curves of cylindrical MWCNT_short/828 epoxy resin system specimens loaded in static unaxial compression

Table 6.1: A summary of compressive properties of Epikote 828+DDS epoxy resin, MWCNT_long/828 epoxy resin and MWCNT_short epoxy resin of cylindrical sample of 10 mm diameter x 10 mm length

Compressive properties	Sample type		
	Epikote 828+DDS	**MWCNT_long/ 828**	**MWCNT_short/ 828**
Compressive modulus, E(GPa)	1.61 ± 0.12	1.56 ± 0.07	1.72 ± 0.08
Compressive stress at yield, σ_y (MPa)	155.34 ± 1.92	140.72 ± 0.27	140.27 ± 0.33
Compressive strain at yield point, ε_y (%)	13.24 ± 0.66	12.56 ± 0.50	12.47 ± 0.58
Compressive stress at break, σ_B (MPa)	315.66 ± 2.90	330.73 ± 5.20	340.86 ± 5.48
Compressive strain at break, ε_B (%)	42.33 ± 0.97	49.12 ± 0.03	51.32 ± 0.78

6.2 Flexural test of epoxy polymer

Figure 6.4, Figure 6.5 and Figure 6.6 show the flexural stress-strain curves of Epikote 828+DDS epoxy resin, MWCNT_long/828 epoxy resin and MWCNT_short epoxy resin. These curves provide useful information on flexural properties such as, flexural strength, failure strain and flexural modulus. These properties were determined using British standard ISO 178:2010. The curves in Figure 6.4, Figure 6.5 and Figure 6.6 obeyed Hooke's law, where the stress initially increases proportionally to the strain, until it reaches the propotional limit at about 4 % flexural strain. Table 6.4 shows that the flexural strength for both nanocomposite epoxy increased by 4.1 % - 4.7 % as compared to the Epikote 822+DDS epoxy resin.

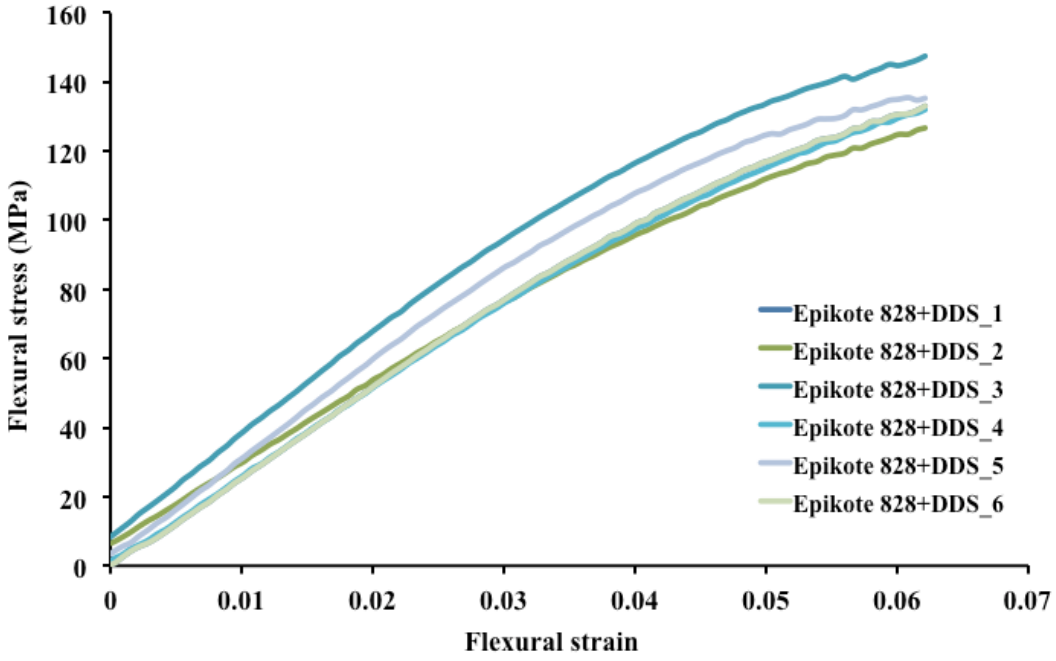

Figure 6.4: Flexural stress-strain response of Epikote 828+DDS samples using a three-point bending fixture

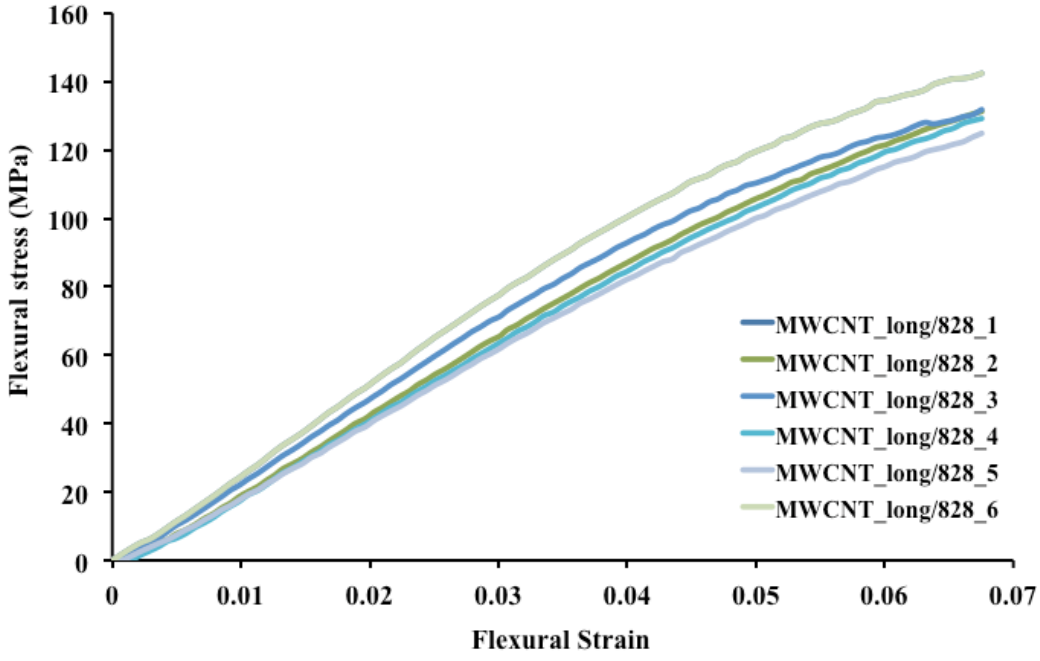

Figure 6.5: Flexural stress-strain response of MWCNT_long/828 epikote samples using a three-point bending fixture

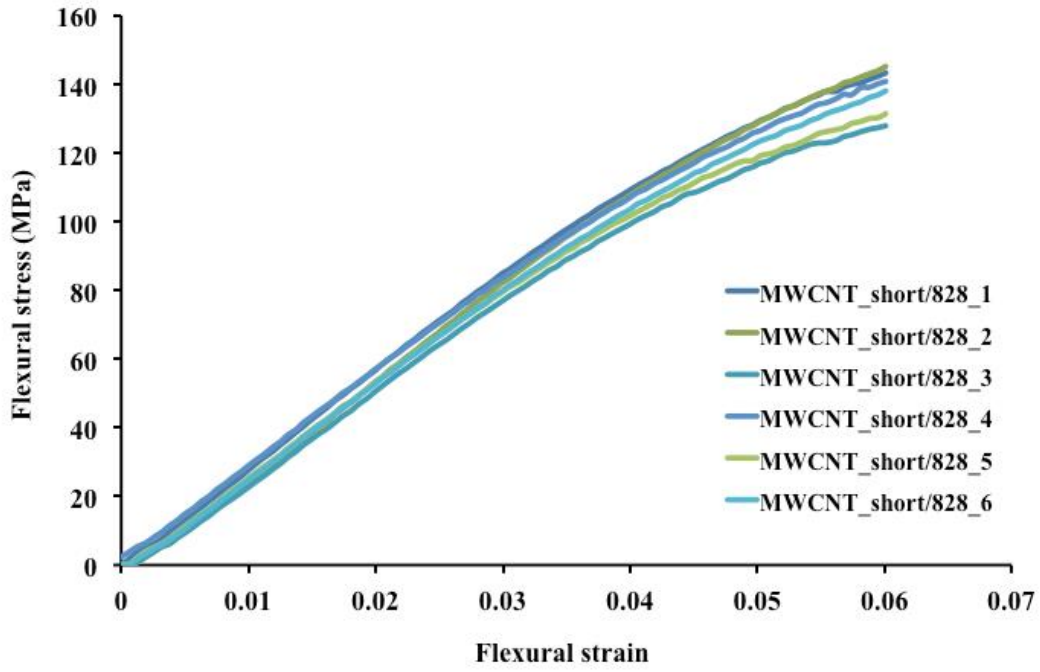

Figure 6.6: Flexural stress-strain response of MWCNT_short/828 epikote samples using a three-point bending fixture

Table 6.2: A summary of flexural properties of Epikote 828+DDS epoxy resin, MWCNT_long/828 epoxy resin and MWCNT_short epoxy resin samples using a three-point bending test fixture

Sample type	Flexural modulus, (GPa)	Flexural strength, (MPa)	Failure strain (%)
Epikote 828+DDS	2.45 ± 0.10	136.19 ± 6.44	6.89 ± 0.53
MWCNT_long/828	2.72 ± 0.09	141.71 ± 5.78	7.11 ± 0.51
MWCNT_short/828	2.88 ± 0.07	142.61 ± 3.09	6.92 ± 0.26

6.3 Short beam shear test for CFRP composites

Interlaminar shear stress (ILSS) of the CFRP composites is determined through short beam shear stress (SBS) test. Based on Bernoulli-Eular beam theory and as recommended by ASTM standard (ASTM D2344) [133], the maximum interlaminar shear stress is calculated using equation that has been discussed in chapter 3.9. The simplicity of SBS test is the main advantage in determining ILSS, where the samples were easy to prepare and required little fixturing.

However, results from the previous studies showed that the samples usually encountered different types of damage before or concurrent with interlaminar shear failure, which causing the samples to also experienced other failures than pure interlaminar shear [14,181–183]. Especially in this study the test was complicated because woven carbon fibre (plain weave carbon fibre) was used as a reinforcement. This material has a non-planar interlaminar regions and relatively tough matrix which can experience different failure modes before it experiences interlaminar shear failure under SBS loading.

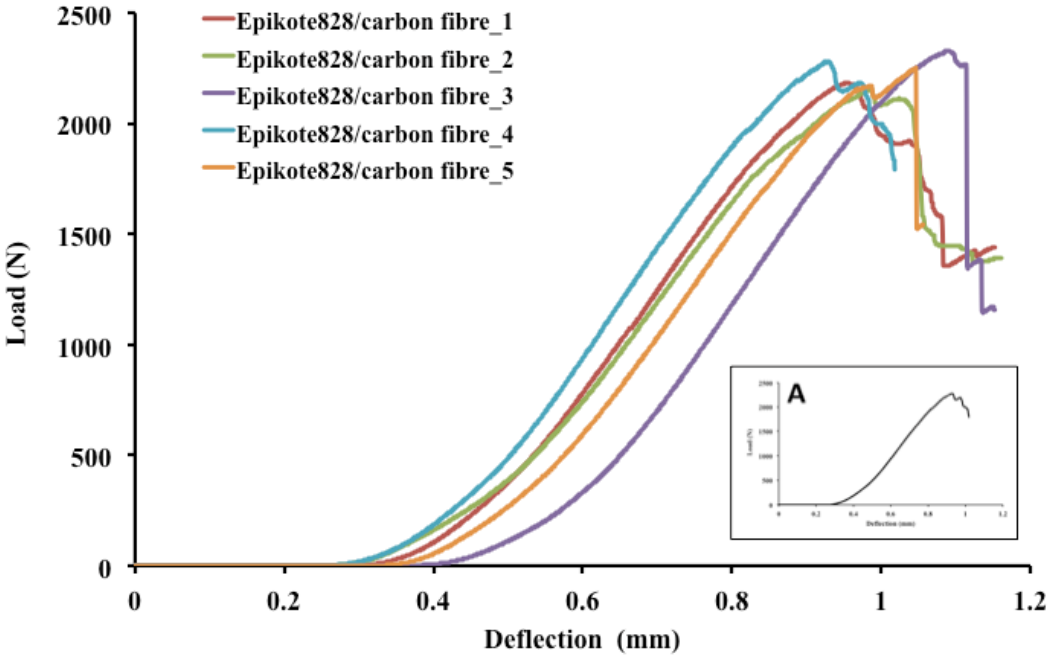

Figure 6.7: Curves of load vs. deflection for a short beam shear for Epikote 828/carbon fibre CFRP composites

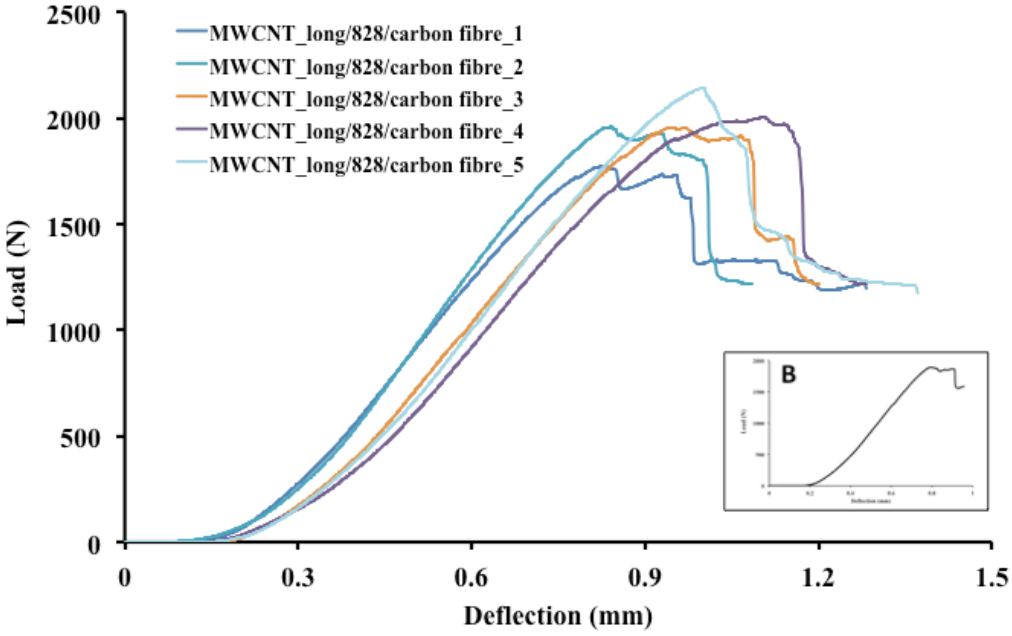

Figure 6.8: Curves of load vs. deflection for a short beam shear for MWCNT_long/ 828/carbon fibre CFRP composites

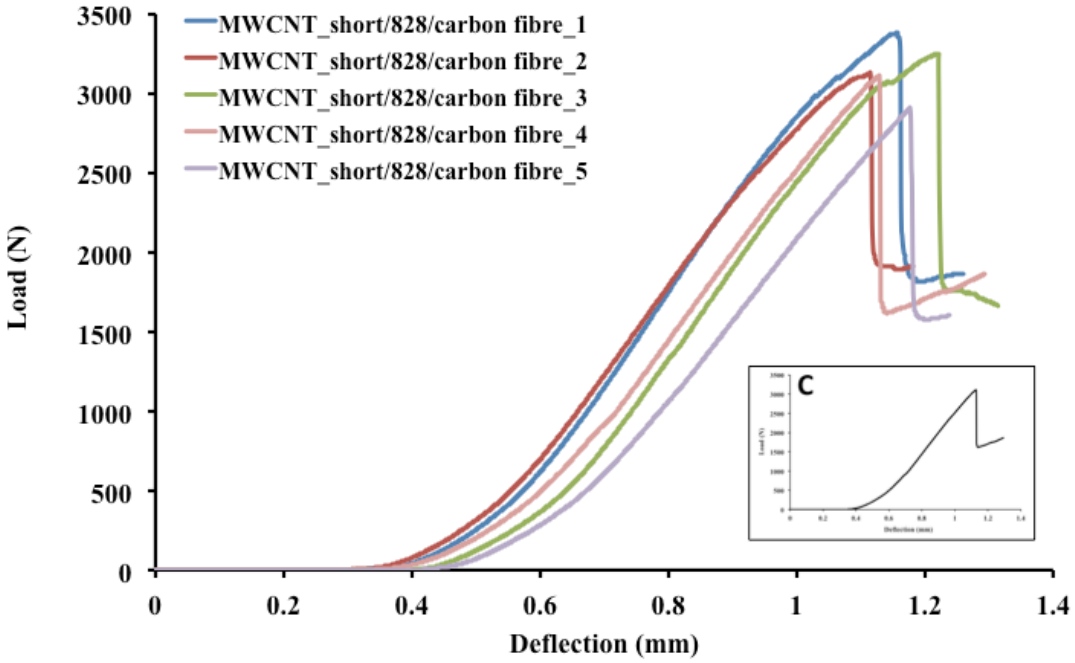

Figure 6.9: Curves of load vs. deflection for a short beam shear for MWCNT_short/ 828/carbon fibre CFRP composites

Results showed two typical SBS strength-deformation behavior when the graphs were plotted. Figure 6.7A and Figure 6.8B which represent Epikote828/carbon fibre and MWCNT_long/828/carbon fibre respectively, exhibit almost the same curve pattern behavior. The two resin systems curves rise, then flattens at some points temporarily before gradually drop after the crack initiation, but this behavior is more significantly experienced by MWCNT_long/828/carbon fibre CFRP composite samples rather than the Epikote828/carbon fibre CFRP composite samples. Meanwhile, MWCNT_short as shown in Figure 6.9 curves rise gradually and increase proportionately with deflection until it reaching the peak and suddenly drops illustrating a distinct failure load developed in the samples. The type of sharp drop of at least more than 30 % after the peak load was reached, was taken as an indication that a pure laminar has occurred in the samples [14,184]. The differences in the behaviour of the epoxy resin systems can be attributed to the different matrix properties in which samples with curve behaviour

such in Figure 6.9C have a brittle structure while samples with the graph curve behaviour similar as shown in Figure 6.8B the epoxy is more ductile [184].

The differences of the curves were also caused by other types of failure besides interlaminar shear failure. Z.Fan *et. al.* [14] analysed the differences of ILSS graph curves and found that, samples generating a curve such as Figure 6.9C is a clear interlaminar shear failure that occurs in the sample. However, micro cracking of the resin inside the fibre tows was observed in the samples that generated curves similar with Figure 6.8B. This was caused by compression and some indentation failures. It was concluded that the samples generating the type of curves shown in Figure 6.8B experienced some other damage modes contributing to the failure.

The average ILSS value of Epikote 828/carbon fibre, MWCNT_long/828/carbon fibre and MWCNT_short/828/carbon fibre CFRP composites as shown in Table 6.3, Table 6.4 and Table 6.5 were 55.19 ± 1.84, 45.29 ± 3.06 and 62.92 ± 3.72, respectively. From the error bar shown in Figure 6.10, it was found that MWCNT_long/828/carbon fibre has lower ILSS as compared to the Epikote828/carbon fibre by 17.93% and MWCNT_short/828/carbon fibre however increased ILSS by 14 %.

Table 6.3: ILSS of of Epikote828/carbon fibre measured using SBS method

Epikote828/carbon fibre samples #	Maximum load (N)	ILSS (MPa)
1	2183.95	54.95
2	2156.38	52.58
3	2329.54	57.66
4	2279.64	55.87
5	2250.55	54.87
Average	2240.01	55.19

Table 6.4: ILSS of MWCNT_long/828/carbon fibre measured using SBS method

MWCNT_long/828/carbon fibre samples #	Maximum load (N)	ILSS (MPa)
1	1775.40	42.00
2	1959.23	45.36
3	1955.93	45.61
4	2006.11	43.40
5	2144.78	50.09
Average	1968.29	45.29

Table 6.5: ILSS of MWCNT_short/828/carbon fibre measured using SBS method

MWCNT_short/828/carbon fibre samples #	Maximum load (N)	ILSS (MPa)
1	3381.32	67.55
2	3127.75	64.55
3	3251.52	64.21
4	3111.19	59.93
5	2908.87	58.36
Average	3156.13	62.92

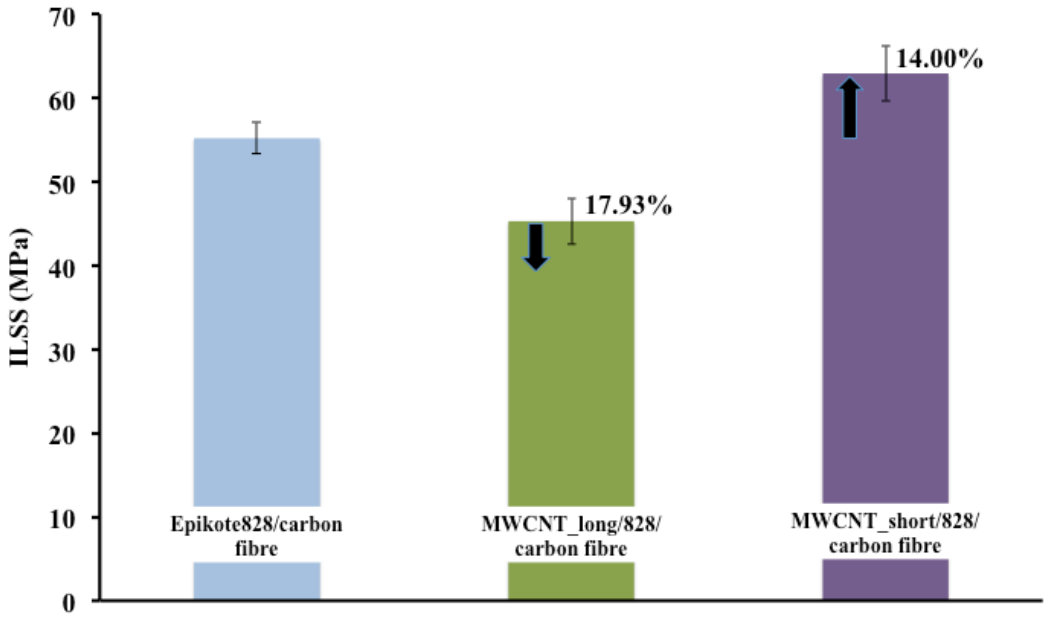

Figure 6.10: ILSS chart of Epikote828/carbon fibre, MWCNT_long/828/carbon fibre and MWCNT_short/828/carbon fibre measured using SBS method

Table 6.6 represent the actual ILSS test data for each group of the resin systems CFRP composites samples as a single p-value derived for this group taken as a whole. The standard deviation of each group of samples or sample coefficient of variation which are represented in percentage were 3.33 % - 6.76 %. The analysis of variance (ANOVA) was used as a tool to statistically analyse the difference between the sample groups [185]. The reason of using ANOVA was, the deviation among the sample groups is not much different from the deviation within each group. SPSS was used to calculate *p*-value. The very small *p*-value, 3×10^{-6} confirms that MWCNTs affects the ILSS of the CFRP composites. It is statistically significant because the *p*-value is less than 0.05, the data from different group is considered statistically distinct.

Table 6.6: Summary of ILSS of Epikote828/carbon fibre, MWCNT_long/828/carbon fibre and MWCNT_short/828/carbon fibre measured using SBS method

Samples number	**ILSS (MPa)**		
	Epikote828/carbon fibre	MWCNT_long/828/ carbon fibre	MWCNT_short/828/carbon fibre
1	54.95	42.00	67.55
2	52.58	45.36	64.55
3	57.66	45.61	64.21
4	55.87	43.40	59.93
5	54.87	50.09	58.36
Average	55.19	45.29	62.92
Standard deviation	1.84	3.06	3.72
Sample coefficient of variation (%)	3.33	6.76	5.91
p-Value	3×10^{-6}		

7 Discussion

7.1 Summary

This chapter discusses the effect of MWCNTs on the properties of epoxy polymers and their contribution to the reinforcement in CFRP composite quality. The influence of MWCNTs on the physical, mechanical and thermal properties of Epikote 828+DDS are discussed based on the results in Chapter 5 and Chapter 6. Based on all the results in section 6.1 MWCNT_short/828 was found to improve in elastic moduli and strengths properties of the Epikote 828+DDS without significant reduction in thermal properties. However, the value of failure at yield point for both strain and stress was lower than Epikote 828. MWCNT_long/828 improved in strength but the value of young moduli and strength at yield point were lower than Epikote 828+DDS. Section 6.2. This shows that both nanomodified systems were found to improve the elastic moduli and strengths of Epikote 828+DDS without any significant reduction in thermal properties and failure strain. Therefore, the investigation was extended to further study the failure properties of nano-modified CFRP composite in order to analysed the interaction between the two resin nano-modified systems with carbon fibre as compared to Epikote 828+DDS epoxy resin. Thus, this chapter is divided into two main sections; (i) the effect of MWCNTs on the properties of Epikote 828 epoxy polymer and (ii) the effect of MWCNTs on the properties of MWCNTs/828/carbon fibre CFRP composites. Conclusion and future study are also discussed in this chapter.

7.2 Effect of MWCNTs on the properties of Epikote 828 epoxy polymer

7.2.1 Degree of MWCNTs distribution

The TEM results (as reported in section 4.1) on the morphology of nano-modified systems showed that MWCNT_long has the best degree of dispersion. MWCNT_short also showed a good dispersion although there were some agglomerations occured, but their size were only ranging from 2 μm to 7 μm. These nano-modified epoxy were succesfully cured with amines curing agent type (DDS). A good system was created based on these materials (MWCNTs, Epikote 828 and (DDS) even at very low weight fraction of 0.38 wt%, it could increase the quality of thermal and mechanical properties of Epikote 828. In addition, the nano-modified composites which were preapred using three mix methods (the high shear mixer ; 10 minutes, ultrasonic probe ; 15 minutes and 3-roll mill) in this study were also successfully done.

7.2.2 Thermal degradation temperature

The effect of MWCNTs on the thermal degradation temperature of Epikote 828 was studied. Two nano-modified epoxy composite systems i) MWCNT_long and ii) MWCNT_short were investegated. The results of both systems showed that nano-modified epoxy composites have higher thermal degradation temperature compared to neat Epikote 828. Figure 7.1 showed the summary of the maximum degradation temperature of resin residue of MWCNTs/828 epoxy composites compared to that of the Epikote 828+DDS epoxy polymers. From Figure 7.1 it can be concluded that nano-modified epoxy composite could increased thermal stability to the Epikote 828+DDS epoxy polymer. The thermal degradation temperature increament suggests that the

interfacial adhesion between nano particle and epoxy matrix is good therefore higher temperature were needed to burn off the epoxy which was glued on the nanoparticles' surface. The increament of thermal degradation of MWCNT_long/828 epoxy composite system was higher than MWCNT_short/828 epoxy composite system probably because of MWCNT_long dispersion was much more spreadable as showed on the TEM micrograph in Figure 4.1 and Figure 4.2.

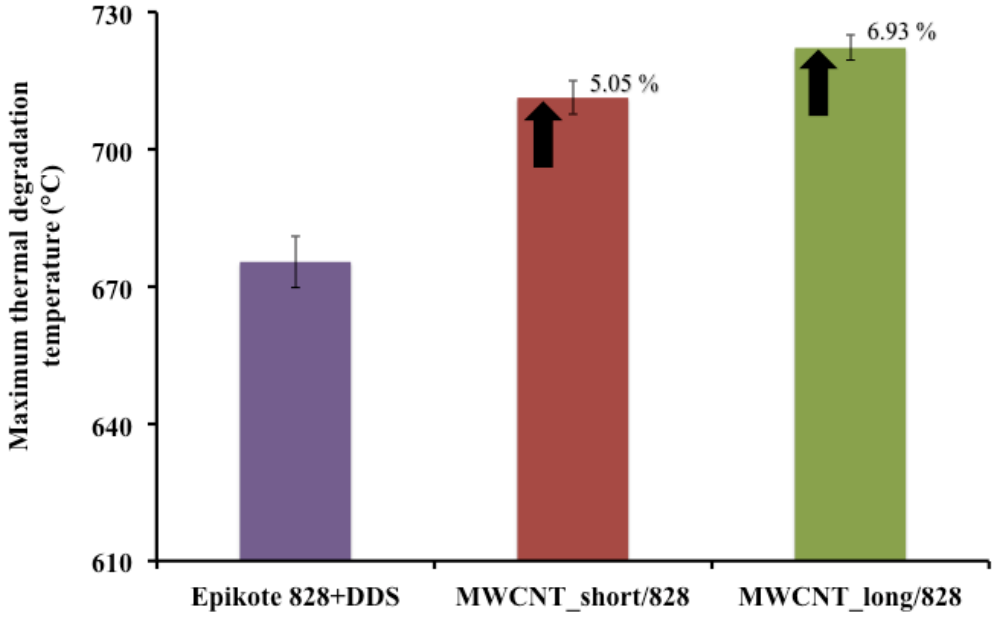

Figure 7.1: Comparison of maximum thermal degradation temperatures of MWCNT_short/828, MWCNT_long/828 with Epikote 828+DDS epoxy

7.2.3 Glass transition temperature

The glass transition temperature (T_g) of a polymer composites is a temperature which changes the state of matrix material either, from glassy to rubbery during heating or from rubbery to glass during cooling. In Figure 7.2, the glass transition is determined

by the peak of Tan δ which was measured using DMA. Both types of nano-modified composite resins showed a slight reduction in T_g compared to Epikote 828+DDS. This concludes that, both types of MWCNTs do not have the best effect on T_g for low molecular weight epoxy, such as Epikote 828. MWCNT_long/828 epoxy composite and MWCNT_short epoxy composite were not significantly different from each other as shown by the error bars.

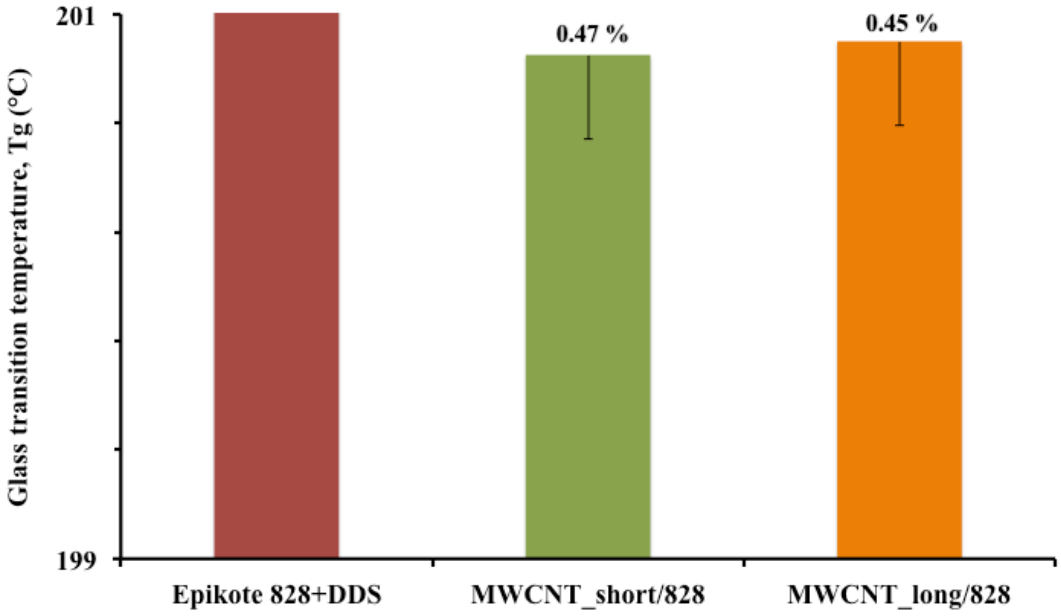

Figure 7.2: Comparison of T_g values of MWCNT_short/828, MWCNT_long/828 with Epikote 828+DDS epoxy

7.3 Elastic modulus

When external forces are applied to a material there will be a resistance to deformation of materials and this resistance is measured as elastic modulus. In this study, the elastic modulus was determined by conducting compression and flexural tests. The results of

elastic modulus were summarised in Figure 7.3. This figure shows that flexural moduli has an increament of 11 % for MWCNT_long/828 epoxy composites and 43 % for MWCNT_short/828 epoxy composites as compared to the Epikote 828+DDS epoxy polymer. Compressive moduli showed no statistically significant value to compare between the epoxy systems, it can be concluded that, MWCNT_short/828 epoxy and MWCNT_long/828 epoxy composites have no effect to Epikote 828. Figure 7.3 also shows that, MWCNT_short/828 epoxy has a higher quality as compared to the MWCNT_long/828 epoxy composites for both compressive and flexural moduli. This may be related to the result in section 4.4 which was discussed on Raman spectroscopy. The intensity ratio (I_D/I_G) of the MWCNT_long was higher than MWCNT_short, with the value of 0.68 and 0.39 respectively. This indicates that MWCNT_long contains large quantity of defects of carbon atoms which were bonded with sp^2 as compared to the MWCNT_short which decreased the quality of the nano-modified resin.

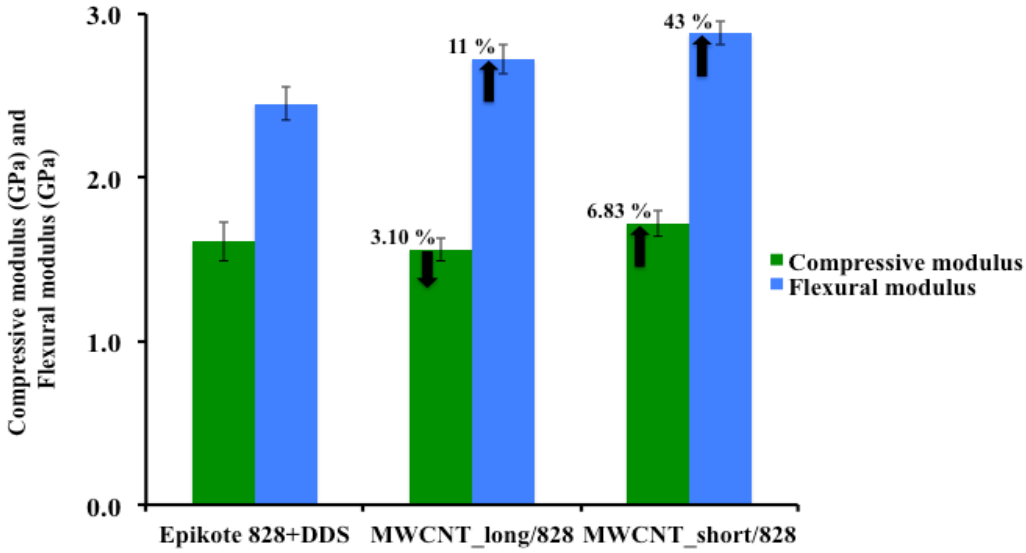

Figure 7.3: Comparison of compressive and flexural moduli of MWCNT_short/828 epoxy and MWCNT_long/828 epoxy composites with Epikote 828+DDS epoxy

7.4 Effect of MWCNTs on the properties of CFRP composites

The previous section has shown that nano-modified epoxy composites with uniformly dispersed MWCNTs, in the average, enhanced compressive and flexural toughness properties with no significant reduction in thermal properties of the Epikote 828. The study was extended to the fabrication of CFRP laminates using 0.38 wt% MWCNTs-modified Epikote 828 with plain weave carbon fibre. There are two types of MWCNTs, which were different in length used in this study. A conventional technique, using hand-layup, resin impregnation and vaccum bagging, were used to fabricate a MWCNTs-modified carbon fibre laminates. Unfortunately the volume contents of MWCNTs cannot be measured because of the device limitation. Density is also one of the important characteristics in composite design. the density of the neat Epikote 828/carbon fibre composite was 1.39 g/cm^3 while the addition of 0.38 wt% of MWCNT_long and MWCNT_short slightly increased the density of the laminate to 1.47 g/cm^3 and 1.49 g/cm^3 respectively. In addition, the TGA results showed an improvement in the thermal stability of the laminate in addition of MWCNTs. From the short beam shear test, it was found that MWCNT_long/828/carbon fibre has lower ILSS as compared to the Epikote828/carbon fibre by 17.93% and MWCNT_short/828/carbon fibre however increased in ILSS by 14 %. Considering the weight fraction of resin in the laminates composites was about 57 %, the MWCNT_long weight fraction in the hybrid composites as whole, was much lower, about 0.38 wt%. This indicates that a small amount of MWCNT can enhanced the ILSS effectively.

8 Conclusion and suggestions for future work

8.1 Conclusion

The interlaminar shear strength of laminated CFRP composites is primarily influenced by the properties of the matrix [14]. Therefore, this study's objective is to enhance the mechanical properties mainly the interlaminar shear strength by introducing MWCNTs into the matrix. In order to achive this, two types of MWCNT-modified resins were evaluated. Based on the thermal and mechanical tests results, some conclusions are made.

1) Stiffer resins were successfully developed using MWCNTs. The elastic modulus of the Epikote 828 epoxy polymer measured in compression and bending was increased with the addition of MWCNTs.

2) MWCNT_short/828 epoxy composite in the average, has the higher elastic modulus compared to the MWCNT_long/828 epoxy composite.

3) MWCNTs were homogeneously dispersed in Epikote 828 polymer.The addition of MWCNTs improved the compressive and flexural toughness and thermal stability of the Epikote 828 epoxy polymer. The major toughening mechanisms involved the formation of micro cracks and plastic yielding as revealed by SEM micrographs.

4) The experimental results showed that MWCNT_short/828 CFRP laminates increased in ILSS in about 14 % by adding only 0.38 wt% of MWCNT.

8.2 Recommendation for future work

In this study, the worked demonstrated the MWCNTs was dispersed in CFRP composite enhanced the interlaminar shear properties. However, other properties must further be studied in order to compete with commercially available systems. The compressive, tensile and fracture toughness of the nano-modified laminates must be further investigated. The CFRP composites are usually characterised by their damage tolerance and resistance. Compression after impact (CAI) and open hole compression (OHC) are the tests to measured these properties. Therefore, these properties are strongly suggest to be investigated for adding MWCNTs into the epoxy.

9 References

[1] Kaufmann, M., Zenkert, D., and Åkermo, M., 2010, "Cost/weight optimization of composite prepreg structures for best draping strategy," Compos. Part A Appl. Sci. Manuf., **41**(4), pp. 464–472.

[2] Ashley, S., 1997, "Carbon composites fly high," Mech. Eng., **119**(9), pp. 66–69.

[3] Balzer, B. B. B., and Mcnabb, J., 2008, "Significant Effect of Microwave Curing on Tensile Strength of Carbon Fiber Composites," J. Ind. Technol., **24**(3).

[4] Shyha, I., Soo, S. L., Aspinwall, D., and Bradley, S., 2010, "Effect of laminate configuration and feed rate on cutting performance when drilling holes in carbon fibre reinforced plastic composites," J. Mater. Process. Technol., **210**(8), pp. 1023–1034.

[5] Kwak, M., Wise, R., Robinson, P., and Bismarck, a., 2015, "Microwave Curing of Carbon-Epoxy Composites: Penetration Depth and Material Characterisation," Compos. Part A Appl. Sci. Manuf.

[6] Marsh, G., 2007, "Airbus takes on Boeing with reinforced plastic A350 XWB," Reinf. Plast., **51**(11), pp. 23–26.

[7] Soutis, C., 2005, "Fibre reinforced composites in aircraft construction," Prog. Aerosp. Sci., **41**(2), pp. 143–151.

[8] Jumahat, A., Soutis, C., Jones, F. R., and Hodzic, A., 2009, "Fracture mechanisms and failure analysis of carbon fibre/toughened epoxy composites subjected to compressive loading," Compos. Struct., **92**, pp. 295–305.

[9] C.Soutis, 1993, "Compressive Failure of Notched Carbon Fibre Composites," Mathematical and physical sciences, The Royal Society, pp. 241–256.

[10] P.E.Irving, and C.Soutis, eds., 2015, Polymer composites in the aerospace

industry, Elsevier and Book Aid International, Cambridge UK.

[11] Johnson, W., Masters, J., Fleck, N., Jelf, P., and Curtis, P., 1995, "Compressive Failure of Laminated and Woven Composites," J. Compos. Technol. Res., **17**, p. 212.

[12] Jia, X., Zhu, J., Li, W., Chen, X., and Yang, X., 2015, "Compressive and tensile response of CFRP cylinders induced by multi-walled carbon nanotubes," Compos. Sci. Technol., **110**, pp. 35–44.

[13] Ha, S. K., and Jeong, J. Y., 2005, "Effects of winding angles on through-thickness properties and residual strains of thick filament wound composite rings," Compos. Sci. Technol., **65**(1), pp. 27–35.

[14] Fan, Z., Santare, M. H., and Advani, S. G., 2008, "Interlaminar shear strength of glass fiber reinforced epoxy composites enhanced with multi-walled carbon nanotubes," Compos. Part A Appl. Sci. Manuf., **39**(3), pp. 540–554.

[15] Rosselli, F., and Santare, M. H., 1997, "Comparison of the short beam shear (SBS) and interlaminar shear device (ISD) tests," Compos. Part A Appl. Sci. Manuf., **28**(6), pp. 587–594.

[16] Byrd, L. W., and Birman, V., 2006, "Effectiveness of z-pins in preventing delamination of co-cured composite joints on the example of a double cantilever test," Compos. Part B Eng., **37**(4–5), pp. 365–378.

[17] Lalit K. Jain, and Mai, Y.-W., 1993, "ON THE EFFECT OF STITCHING ON MODE I DELAMINATION TOUGHNESS OF LAMINATED COMPOSITES," Compos. Scince Technol., **51**(1994), pp. 331–345.

[18] Partridge, I. K., and Cartié, D. D. R., 2005, "Delamination resistant laminates by Z-Fiber (R) pinning: Part I manufacture and fracture performance," Compos.

Part A Appl. Sci. Manuf., **36**(1), pp. 55–64.

[19] Sharma, S., and Sankar, B., 1997, "Effects of stitching on impact and interlaminar properties of graphite/epoxy laminates," J. Thermoplast. Compos. Mater., **10**(3), pp. 241–253.

[20] Shivakumar, K., Pora, A., and Abali, F., "Interlaminar Shear Test for Laminated Textile Fabric Composites."

[21] Gojny, F., Wichmann, M., Fiedler, B., and Schulte, K., 2005, "Influence of different carbon nanotubes on the mechanical properties of epoxy matrix composites – A comparative study," Compos. Sci. Technol., **65**(15–16), pp. 2300–2313.

[22] Seyhan, a. T., Tanoğlu, M., and Schulte, K., 2009, "Tensile mechanical behavior and fracture toughness of MWCNT and DWCNT modified vinyl-ester/polyester hybrid nanocomposites produced by 3-roll milling," Mater. Sci. Eng. A, **523**, pp. 85–92.

[23] Ma, P.-C., Siddiqui, N. a., Marom, G., and Kim, J.-K., 2010, "Dispersion and functionalization of carbon nanotubes for polymer-based nanocomposites: A review," Compos. Part A Appl. Sci. Manuf., **41**(10), pp. 1345–1367.

[24] Gojny, F. H., Wichmann, M. H. G., Köpke, U., Fiedler, B., and Schulte, K., 2004, "Carbon nanotube-reinforced epoxy-composites: enhanced stiffness and fracture toughness at low nanotube content," Compos. Sci. Technol., **64**(15), pp. 2363–2371.

[25] Knoll, J. B., Riecken, B. T., Kosmann, N., Chandrasekaran, S., Schulte, K., and Fiedler, B., 2014, "Composites : Part A The effect of carbon nanoparticles on the fatigue performance of carbon fibre reinforced epoxy," Compos. PART A, **67**,

pp. 233–240.

[26] Cadek, M., Coleman, J. N., Ryan, K. P., Nicolosi, V., Bister, G., Fonseca, A., Nagy, J. B., Szostak, K., Béguin, F., and Blau, W. J., 2004, "Reinforcement of Polymers with Carbon Nanotubes: The Role of Nanotube Surface Area," Nano Lett., **4**(2), pp. 353–356.

[27] Rahmanian, S., Thean, K. S., Suraya, a. R., Shazed, M. a., Mohd Salleh, M. a., and Yusoff, H. M., 2013, "Carbon and glass hierarchical fibers: Influence of carbon nanotubes on tensile, flexural and impact properties of short fiber reinforced composites," Mater. Des., **43**, pp. 10–16.

[28] Yu, H., Lu, J., Song, Q., Li, K., Li, H., Fu, Q., and Zhang, L., 2014, "Compressive properties of carbon/carbon composites reinforced by carbon nanotubes with different orientations and lengths," Vacuum, **99**, pp. 76–79.

[29] Rodriguez, F., Cohen, C., K.Ober, C., and A.Archer, L., 2015, Principles of Polymer System, CRC Press Taylor & Francis Group, Boca Raton, London, New York.

[30] Kumar, A., and Gupta, R. K. ., 2003, Fundamentals of Polymer Engineering Second Edition Revised and Expanded, Marcel Dekker, Inc, New York.

[31] Debdatta, R., 2009, Handbook of Thermoset Resins, iSmithers.

[32] S.Bauer, R., 1979, "Epoxy Resin Chemistry," ACS Symposium Series No.114, American Chemical Society, DC,USA.

[33] Odian, G., 2004, "PRINCIPLES OF POLYMERIZATION," Wiley-Interscince,A JOHN WILEY & SONS, INC., PUBLICATION, New York.

[34] Gong, X., Kang, H., Liu, Y., and Wu, S., 2015, "Decomposition mechanisms and kinetics of amine/anhydride-cured DGEBA epoxy resin in near-critical

water," RSC Adv., **5**(50), pp. 40269–40282.

[35] Li, Y., Li, N., and Gao, J., 2014, "Tooling design and microwave curing technologies for the manufacturing of fiber-reinforced polymer composites in aerospace applications," Int. J. Adv. Manuf. Technol., **70**(1–4), pp. 591–606.

[36] Li, N., Li, Y., Hang, X., and Gao, J., 2014, "Analysis and optimization of temperature distribution in carbon fiber reinforced composite materials during microwave curing process," J. Mater. Process. Technol., **214**(3), pp. 544–550.

[37] Berbinau, P., Soutis, C., Goutas, P., and Curtis, P. T., 1999, "Effect of off-axis ply orientation on 0??-fibre microbuckling," Compos. Part A Appl. Sci. Manuf., **30**(10), pp. 1197–1207.

[38] Budiansky, B., and Fleck, N. a., 1994, "Compressive Kinking of Fiber Composites: A Topical Review," Appl. Mech. Rev., **47**(6S), p. S246.

[39] Jumahat, A., Soutis, C., Mahmud, J., and Ahmad, N., 2012, "Compressive properties of nanoclay / epoxy nanocomposites," **41**(IRIS), pp. 1607–1613.

[40] Soutis, C., 2005, "Carbon fiber reinforced plastics in aircraft construction," Mater. Sci. Eng. A, **412**(1–2), pp. 171–176.

[41] Mallikarachchi, H., and Pellegrino, S., 2012, "Failure criterion for two-ply plain-weave CFRP laminates," J. Compos. Mater.

[42] Yokozeki, T., Aoki, T., Arai, A., Ishibashi, M., and Yanagisawa, T., 2009, "Fabrication of CNT-Dispersed CFRP Using Length-Controlled CNTs: Measurement of CNT Length and Characterization of Mechanical Properties," Tsinghua Sci. Technol., **14**(SUPPL. 2), pp. 100–104.

[43] Hong, S. K., Kim, D., Lee, S., Kim, B. W., Theilmann, P., and Park, S. H., 2015, "Enhanced thermal and mechanical properties of carbon nanotube composites through the use of functionalized CNT-reactive polymer linkages and three-roll

milling," Compos. Part A Appl. Sci. Manuf., **77**, pp. 142–146.

[44] Visco, A., Calabrese, L., and Milone, C., 2009, "Cure Rate and Mechanical Properties of a DGEBF Epoxy Resin Modified with Carbon Nanotubes," J. Reinf. Plast. Compos.

[45] Pumera, M., Merkoçi, A., and Alegret, S., 2006, "Carbon nanotube-epoxy composites for electrochemical sensing," Sensors Actuators, B Chem., **113**(2), pp. 617–622.

[46] Li, X., Gao, H., Scrivens, W. a, Fei, D., Xu, X., Sutton, M. a, Reynolds, A. P., and Myrick, M. L., 2004, "Nanomechanical characterization of single-walled carbon nanotube reinforced epoxy composites," Nanotechnology, **15**(11), pp. 1416–1423.

[47] Hsiao, K., Alms, J., and Advani, S. G., 2003, "Use of epoxy / multiwalled carbon nanotubes as adhesives to join graphite," Nanotechnology, **14**, pp. 791–793.

[48] Behabtu, N., Ma, A. W. K., Bengio, E. A., Waarbeek, R. F., Jong, J. J. De, Hoogerwerf, R. E., Fairchild, S. B., Ferguson, J. B., Maruyama, B., Kono, J., Talmon, Y., Cohen, Y., Otto, M. J., and Pasquali, M., 2013, "Strong, Light, Multifunctional Fibres of Carbon Nanotubes with Ultrahigh Conductivity," Science (80-.)., **339**(11), pp. 182–186.

[49] Inam, F., Vo, T., Jones, J. P., and Lee, X., 2012, "Effect of carbon nanotube lengths on the mechanical properties of epoxy resin: An experimental study," J. Compos. Mater., **47**(19), pp. 2321–2330.

[50] Higginbotham, A. L., Moloney, P. G., Waid, M. C., Duque, J. G., Kittrell, C., Schmidt, H. K., Stephenson, J. J., Arepalli, S., Yowell, L. L., and Tour, J. M., 2008, "Carbon nanotube composite curing through absorption of microwave

radiation," Compos. Sci. Technol., **68**(15–16), pp. 3087–3092.

[51] Spitalsky, Z., Tasis, D., Papagelis, K., and Galiotis, C., 2010, "Carbon nanotube – polymer composites : Chemistry , processing , mechanical and electrical properties," Prog. Polym. Sci., **35**(3), pp. 357–401.

[52] Rana, S., Alagirusamy, R., and Joshi, M., 2009, "A Review on Carbon Epoxy Nanocomposites," J. Reinf. Plast. Compos., **28**(4), p. 461.

[53] Ijima, S., Ichihashi, T., 1993, "Single-Shell Carbon Nanotubes of 1-nm Diameter," Nature, **363**, pp. 603–605.

[54] Tasis, D., Tagmatarchis, N., Bianco, A., and Prato, M., 2006, "Chemistry of Carbon Nanotubes," Chem. Rev., **106**(3), pp. 1105–1136.

[55] Grobert, N., 2007, "Carbon nanotubes - becoming clean," Mater. Today, **10**(1–2), pp. 28–35.

[56] Popov, V. N., 2004, "Carbon nanotubes: Properties and application," Mater. Sci. Eng. R Reports, **43**(3), pp. 61–102.

[57] Thostenson, E. T., Ren, Z., and Chou, T.-W., 2001, "Advances in the science and technology of carbon nanotubes and their composites: a review," Compos. Sci. Technol., **61**(13), pp. 1899–1912.

[58] Trojanowicz, M., 2006, "Analytical applications of carbon nanotubes: a review," TrAC Trends Anal. Chem., **25**(5), pp. 480–489.

[59] Rogers, B., Pennathur, S., and Adams, J., 2008, Nanotechnology: Understanding Small Systems, CRC Press, Taylor and Francis Group, Boca Raton, London, New York.

[60] Barman, S. N., Lemieux, M. C., Baek, J., Rivera, R., and Bao, Z., 2010, "Effects of dispersion conditions of single-walled carbon nanotubes on the electrical characteristics of thin film network transistors," ACS Appl. Mater. Interfaces,

2(9), pp. 2672–2678.

[61] Yuan, W., and Chan-Park, M. B., 2012, "Covalent cum noncovalent functionalizations of carbon nanotubes for effective reinforcement of a solution cast composite film.," ACS Appl. Mater. Interfaces, **4**(4), pp. 2065–73.

[62] Hamon, B. M. A., Chen, J., Hu, H., and Chen, Y., 1999, "Dissolution of Single-Walled Carbon Nanotubes **," **55**(10), pp. 834–840.

[63] Niyogi, S., Hamon, M. a., Perea, D. E., Kang, C. B., Zhao, B., Pal, S. K., Wyant, a. E., Itkis, M. E., and Haddon, R. C., 2003, "Ultrasonic Dispersions of Single-Walled Carbon Nanotubes," J. Phys. Chem. B, **107**(34), pp. 8799–8804.

[64] Ijima, S., 1991, "Helical Microtubules of Graphitic Carbon," Nature, **354**, pp. 56–58.

[65] Coleman, J. N., Khan, U., Blau, W. J., and Gun'ko, Y. K., 2006, "Small but strong: A review of the mechanical properties of carbon nanotube–polymer composites," Carbon N. Y., **44**(9), pp. 1624–1652.

[66] Naik, R. B., Jagtap, S. B., Naik, R. S., Malvankar, N. G., and Ratna, D., 2014, "Effect of non-ionic surfactants on thermomechanical properties of epoxy/multiwall carbon nanotubes composites," Prog. Org. Coatings.

[67] Paradise, M., and Goswami, T., 2007, "Carbon nanotubes - Production and industrial applications," Mater. Des., **28**(5), pp. 1477–1489.

[68] Andrews, R., and Weisenberger, M. ., 2004, "Carbon nanotube polymer composites," Curr. Opin. Solid State Mater. Sci., **8**(1), pp. 31–37.

[69] Guo, P., Chen, X., Gao, X., Song, H., and Shen, H., 2007, "Fabrication and mechanical properties of well-dispersed multiwalled carbon nanotubes/epoxy composites," Compos. Sci. Technol., **67**(15–16), pp. 3331–3337.

[70] Wagner, H. D., Lourie, O., Feldman, Y., and Tenne, R., 1998, "Stress-induced

fragmentation of multiwall carbon nanotubes in a polymer matrix," Appl. Phys. Lett., **72**(2), pp. 188–190.

[71] Martin-Gallego, M., Yuste-Sanchez, V., Sanchez-Hidalgo, R., Verdejo, R., and Lopez-Manchado, M. A., 2018, "Epoxy Nanocomposites filled with Carbon Nanoparticles," Chem. Rec., pp. 1–13.

[72] Zakaria, M. R., Abdul Kudus, M. H., Md. Akil, H., and Mohd Thirmizir, M. Z., 2017, "Comparative study of graphene nanoparticle and multiwall carbon nanotube filled epoxy nanocomposites based on mechanical, thermal and dielectric properties," Compos. Part B Eng., **119**, pp. 57–66.

[73] Bisht, A., Dasgupta, K., and Lahiri, D., 2018, "Effect of graphene and CNT reinforcement on mechanical and thermomechanical behavior of epoxy—A comparative study," J. Appl. Polym. Sci., **135**(14), pp. 1–11.

[74] Schadler, L. S., Giannaris, S. C., and Ajayan, P. M., 1998, "Load transfer in carbon nanotube epoxy composites," Appl. Phys. Lett., **73**(26), pp. 3842–3844.

[75] Cooper, C. A., Cohen, S. R., Barber, A. H., and Wagner, H. D., 2002, "Detachment of nanotubes from a polymer matrix," Appl. Phys. Lett., **81**(20), pp. 3873–3875.

[76] Ghaleb, Z., Mariatti, M., and Ariff, Z., 2017, "Synergy effects of graphene and multiwalled carbon nanotubes hybrid system on properties of epoxy nanocomposites," J. Reinf. Plast. Compos., **36**(9), pp. 685–695.

[77] Bilalis, P., Katsigiannopoulos, D., Avgeropoulos, A., and Sakellariou, G., 2014, "Non-covalent functionalization of carbon nanotubes with polymers," RSC Adv., **4**(6), p. 2911.

[78] Rana, S., Alagirusamy, R., and Joshi, M., 2008, "A Review on Carbon Epoxy

Nanocomposites," J. Reinf. Plast. Compos., **28**(4), pp. 461–487.

[79] Song, Y. S., and Youn, J. R., 2005, "Influence of dispersion states of carbon nanotubes on physical properties of epoxy nanocomposites," Carbon N. Y., **43**(7), pp. 1378–1385.

[80] Polo-Luque, M. L., Simonet, B. M., and Valcárcel, M., 2013, "Functionalization and dispersion of carbon nanotubes in ionic liquids," TrAC Trends Anal. Chem., **47**, pp. 99–110.

[81] Ajayan, P. M., and Zhou, O. Z., 2001, "Applications of Carbon Nanotubes," Most, **425**, pp. 391–425.

[82] S.G., A., and Z., F., 2007, "Dispersion, Bonding and Orientation of Carbon Nanotubes in Polymer Matrices," Processing and Properties of Nanocomposites, World Scientific Publishing Co., NJ, USA.

[83] Bal, S., and Samal, S. S., 2007, "Carbon nanotube reinforced polymer composites—A state of the art," Bull. Mater. Sci., **30**, pp. 379–386.

[84] Chang, J., Liang, G., Gu, A., Cai, S., and Yuan, L., 2011, "The production of carbon nanotube /epoxy composites with a very high dielectric constant and low dielectric loss by microwave curing," Carbon N. Y., **50**, pp. 689–698.

[85] Sanchez, S. R., Bachilo, S. M., Zheng, Y., Streit, J. K., and Weisman, R. B., 2017, "Variance Spectroscopy Monitors the Sonication-Induced Cutting and Debundling of Single-Walled Carbon Nanotubes," Meet. Abstr. , **MA2017-01**(9), p. 697.

[86] Fu, S. Y., Chen, Z. K., Hong, S., and Han, C. C., 2009, "The reduction of carbon nanotube (CNT) length during the manufacture of CNT/polymer composites and a method to simultaneously determine the resulting CNT and interfacial

strengths," Carbon N. Y., **47**(14), pp. 3192–3200.

[87] Russ, M., Rahatekar, S. S., Koziol, K., Farmer, B., and Peng, H. X., 2013, "Length-dependent electrical and thermal properties of carbon nanotube-loaded epoxy nanocomposites," Compos. Sci. Technol., **81**, pp. 42–47.

[88] Huang, Y. Y., and Terentjev, E. M., 2012, "Dispersion of carbon nanotubes: Mixing, sonication, stabilization, and composite properties," Polymers (Basel)., **4**(1), pp. 275–295.

[89] Thostenson, E. T., and Chou, T. W., 2006, "Processing-structure-multi-functional property relationship in carbon nanotube/epoxy composites," Carbon N. Y., **44**(14), pp. 3022–3029.

[90] Le, V. T., Ngo, C. L., Le, Q. T., Ngo, T. T., Nguyen, D. N., and Vu, M. T., 2013, "Surface modification and functionalization of carbon nanotube with some organic compounds," Adv. Nat. Sci. Nanosci. Nanotechnol., **4**(3), p. 35017.

[91] Sahoo, N. G., Rana, S., Cho, J. W., Li, L., and Chan, S. H., 2010, "Polymer nanocomposites based on functionalized carbon nanotubes," Prog. Polym. Sci., **35**(7), pp. 837–867.

[92] Tunckol, M., Fantini, S., Malbosc, F., Durand, J., and Serp, P., 2013, "Effect of the synthetic strategy on the non-covalent functionalization of multi-walled carbon nanotubes with polymerized ionic liquids," Carbon N. Y., **57**, pp. 209–216.

[93] Wang, Z., Colorad, H. a., Guo, Z.-H., Kim, H., Park, C.-L., Hahn, H. T., Lee, S.-G., Lee, K.-H., and Shang, Y.-Q., 2012, "Effective functionalization of carbon nanotubes for bisphenol F epoxy matrix composites," Mater. Res., **15**(4), pp. 510–516.

[94] Hirsch, A., and Vostrowsky, O., 2005, "Functionalization of carbon nanotubes,"

Funct. Mol. nanostructures, pp. 193–237.

[95] Blake, R., Gun'ko, Y. K., Coleman, J., Cadek, M., Fonseca, A., Nagy, J. B., and Blau, W. J., 2004, "A generic organometallic approach toward ultra-strong carbon nanotube polymer composites.," J. Am. Chem. Soc., **126**(33), pp. 10226–7.

[96] Chun, Y. S., Shin, J. Y., Song, C. E., and Lee, S., 2008, "Palladium nanoparticles supported onto ionic carbon nanotubes as robust recyclable catalysts in an ionic liquid.," Chem. Commun. (Camb)., **7345**(8), pp. 942–4.

[97] Park, M., Lee, J., Lee, B., and Lee, Y., 2006, "Covalent modification of multiwalled carbon nanotubes with imidazolium-based ionic liquids: effect of anions on solubility," Chem. Mater…, **18**(6), pp. 1546–1551.

[98] Holzinger, M., Abraham, J., Whelan, P., Graupner, R., Ley, L., Hennrich, F., Kappes, M., Hirsch, A., Physik, T., Chemie, P., and V, T. U., 2003, "Functionalization of Single-Walled Carbon Nanotubes with," (5), pp. 8566–8580.

[99] Kasperski, a., Weibel, a., Estournès, C., Laurent, C., and Peigney, a., 2014, "Multi-walled carbon nanotube–Al2O3 composites: Covalent or non-covalent functionalization for mechanical reinforcement," Scr. Mater., **75**, pp. 46–49.

[100] Banerjee, S., Hemraj-Benny, T., and Wong, S. S., 2005, "Covalent Surface Chemistry of Single-Walled Carbon Nanotubes," Adv. Mater., **17**(1), pp. 17–29.

[101] Kang, I., Heung, Y., Kim, J., and Lee, J., 2006, "Introduction to carbon nanotube and nanofiber smart materials," Elsevier Compos. Part B Eng., pp. 382–394.

[102] Movva, S. S., 2010, "Effects of carbon Nanoparticles on Properties of

Thermoset Polymer Systems," The Ohio State University.

[103] "http://www.nanoamor.com/inc/pdetail?v=1&pid=1365."

[104] Wang, Y., Wu, J., and Wei, F., 2003, "A treatment method to give separated multi-walled carbon nanotubes with high purity, high crystallization and a large aspect ratio," Carbon N. Y., **41**(15), pp. 2939–2948.

[105] Silverson, 2018, "http://www.silverson.com/us/products/laboratory-mixers/how-it-works."

[106] Bałdyga, J., Orciuch, W., Makowski, Ł., Malski-Brodzicki, M., and Malik, K., 2007, "Break up of nano-particle clusters in high-shear devices," Chem. Eng. Process. Process Intensif., **46**(9 SPEC. ISS.), pp. 851–861.

[107] Korayem, A. H., Barati, M. R., Chen, S. J., Simon, G. P., Zhao, X. L., and Duan, W. H., 2015, "Optimizing the degree of carbon nanotube dispersion in a solvent for producing reinforced epoxy matrices," Powder Technol., **284**, pp. 541–550.

[108] Exakt, 2018, "Exakt 80E 'https://exaktusa.com/pharmacy-equipment/products/exakt-80e/,'" Exakt Technol. Inc. [Online]. Available: https://exaktusa.com/pharmacy-equipment/products/exakt-80e/.

[109] Wu, T., Lo, T., and Kuo, W., 2010, "Effect of Dispersion on Graphite Nanosheet Composites," Polym. Compos., pp. 292–298.

[110] Khan, L. A., Kausar, A., Hussain, S. T., Iqbal, Z., Day, R. J., Syed, A. S., and Khan, Z. M., 2014, "Cure characterization of Cycom 977-2A carbon/epoxy composites for quickstep processing," Polym. Eng. Sci., **54**(4), pp. 887–898.

[111] Menczel, J. D., and Prime, R. B., 2008, Thermal Analysis Of Polymers: Fundamentals And Applications, Wiley, Canada.

[112] ASTM, 2004, ASTM E473-03 "Standard Terminology Relating to Thermal

Analysis."

[113] ISO 11357-2: 2013 "Plastics — Differential scanning temperature and glass transition step height."

[114] PerkinElmer, "PYRIS Diamond DSC," http://www-omcs.materials.ox.ac.uk/uploads/diamond%20dsc%20tech%20sheet.pdf.

[115] P.Menard, K., 2008, Dynamic Mechanical Analysis: A practical Introduction, CRC Press, Taylor and Francis Group, Boca Raton, London, New York.

[116] Gyaneshwar Tandon, University of Dayton,OH, U., ed., Composite, Hybrid, and Multifunctional Materials, Volume 4, Springer, New York.

[117] Wasik, T., 2005, "Effect of fiber volume fraction on fracture mechanics in continuously reinforced fiber composite materials," University of South Florida.

[118] Zhou, Y., Pervin, F., Lewis, L., and Jeelani, S., 2007, "Experimental study on the thermal and mechanical properties of multi-walled carbon nanotube-reinforced epoxy," Mater. Sci. Eng. A, **452**–**453**, pp. 657–664.

[119] Mikhalchan, A., Gspann, T., and Windle, A., 2016, "Aligned carbon nanotube epoxy composites: the effect of nanotube organization on strength, stiffness, and toughness," J. Mater. Sci., **51**(22), pp. 10005–10025.

[120] Sydlik, S. a., Lee, J.-H., Walish, J. J., Thomas, E. L., and Swager, T. M., 2013, "Epoxy functionalized multi-walled carbon nanotubes for improved adhesives," Carbon N. Y., **59**, pp. 109–120.

[121] Zhou, Y., Pervin, F., Lewis, L., and Jeelani, S., 2008, "Fabrication and characterization of carbon/epoxy composites mixed with multi-walled carbon nanotubes," Mater. Sci. Eng. A, **475**(1–2), pp. 157–165.

[122] PerkinElmer, 2000, Thermogravimetric Analysis (TGA) "A Beginner ' s

Guide."

[123] ASTM, 1998, Standard Test Method for Compositional Analysis by Thermogravimetry.

[124] ASTM Standard D3171-11, 2011, Standard Test Methods for Constituent Content of Composite Materials 1.

[125] ASTM, 2002, ASTM D695 - 02a "Standard Test Method for Compressive Properties of Rigid Plastics."

[126] Behzadi, S., and Jones, F. R., 2008, "The effect of temperature on stress transfer between a broken fibre and the adjacent fibres in unidirectional fibre composites," Compos. Sci. Technol., **68**(13), pp. 2690–2696.

[127] 2003, British Standard BS EN ISO 604:2003 "Plastics — Determination of compressive properties."

[128] Kalidindi, S. R., Abusafieh, a., and El-Danaf, E., 1997, "Accurate characterization of machine compliance for simple compression testing," Exp. Mech., **37**(2), pp. 210–215.

[129] International Organisation for Standardisation, 2012, "BSI Standards Publication Plastics — Determination of tensile properties Part 1 : General principles," Management.

[130] International Organisation for Standardisation, 2012, "BSI Standards Publication Plastics — Determination of tensile properties Part 2 : Test conditions for moulding and extrusion plastics."

[131] British Standards Institutions, 2010, "BS EN ISO 178:2010 'Plastics-Determination of flexural properties.'"

[132] Schneider, K., and Lauke, B., 2001, "Compression Shear Test (CST) – A Convenient Apparatus for the Estimation of Apparent Shear Strength of

Composite Materials," Appl. Compos. Mater., **8**, pp. 43–62.

[133] ASTM D 2344/D 2344M, 2000, Standard Test Method for Short-Beam Strength of Polymer Matrix Composite Materials and Their Laminates.

[134] Li, Z. F., Luo, G. H., Zhou, W. P., Wei, F., Xiang, R., and Liu, Y. P., 2006, "The quantitative characterization of the concentration and dispersion of multi-walled carbon nanotubes in suspension by spectrophotometry," Nanotechnology, **17**(15), pp. 3692–3698.

[135] Huang, Y. Y., Knowles, T. P. J., and Terentjev, E. M., 2009, "Strength of nanotubes, filaments, and nanowires from sonication-onduced scission," Adv. Mater., **21**(38–39), pp. 3945–3948.

[136] Chandrasekaran, S., Sato, N., Tölle, F., Mülhaupt, R., Fiedler, B., and Schulte, K., 2014, "Fracture toughness and failure mechanism of graphene based epoxy composites," Compos. Sci. Technol., **97**, pp. 90–99.

[137] Hilding, J., Grulke, E. A., Zhang, Z. G., and Lockwood, F., 2003, "Dispersion of carbon nanotubes in liquids," J. Dispers. Sci. Technol., **24**(1), pp. 1–41.

[138] Min-Feng, Oleg Lourie, Mark J.Dyer, Katerina Moloni, Thomas F.Kelly, R. S. R., 2013, "Strenght and Breaking Mechanism of Multiwalled Carbon Nanotubes Under Tensile Load," **287**(January), pp. 1–4.

[139] Yu Files, Bradley S, Arepalli, Sivaram, Ruoff, Rodney S, M.-F., 2000, "Tensile loading of ropes of single wall carbon nanotubes and their mechanical properties," Phys. Rev. Lett., **84**(24), p. 5552.

[140] Xie, S., Li, W., Pan, Z., Chang, B., and Sun, L., 2000, "Mechanical and physical properties on carbon nanotube.," J. Phys. Chem. Solids, **61**, pp. 1153–1158.

[141] Hosur, M., Barua, R., Zainuddin, S., Kumar, A., Trovillion, J., and Jeelani, S., 2013, "Effect of processing techniques on the performance of Epoxy/MWCNT

nanocomposites," J. Appl. Polym. Sci., **127**(6), pp. 4211–4224.

[142] Singh, S., Srivastava, V. K., and Prakash, R., 2013, "Characterisation of multi-walled carbon nanotube reinforced epoxy resin composites," Mater. Sci. Technol., **29**(9), pp. 1130–1134.

[143] Nwigboji, I. H., Ejembi, J. I., Wang, Z., Bagayoko, D., and Zhao, G. L., 2015, "Microwave absorption properties of multi-walled carbon nanotube (outer diameter 20-30 nm)-epoxy composites from 1 to 26.5 GHz," Diam. Relat. Mater., **52**(April), pp. 66–71.

[144] Zhou, Z., Bouwman, W. G., Schut, H., and Pappas, C., 2014, "Interpretation of X-ray diffraction patterns of (nuclear) graphite," Carbon N. Y., **69**.

[145] Kumar, A., Kumar, K., Ghosh, P. K., and Yadav, K. L., 2017, "MWCNT / TiO 2 hybrid nano filler toward high- performance epoxy composite," Ultrason. - Sonochemistry, **41**(September), pp. 37–46.

[146] Wang, Z., and Zhao, G., 2013, "Microwave Absorption Properties of Carbon Nanotubes-Epoxy Composites in a Frequency Range of 2 - 20 GHz," Open J. Compos. Mater., **3**(April), pp. 17–23.

[147] Ferrari, A. C., and Robertson, J., 2000, "Interpretation of Raman spectra of disordrred and amorphous carbon," Phys. Rev. B, **61**(20), p. 14 295.

[148] Kiefer, W., Mazzolini, A. P., and Stoddart, P. R., 2007, "Recent Advances in linear and nonlinear Raman spectroscopy I," J. Raman Spectrosc., **38**(April), pp. 1538–1553.

[149] Saito, R., Hofmann, M., Dresselhaus, G., Jorio, A., and Dresselhaus, M. S., 2011, "Raman spectroscopy of graphene and carbon nanotubes," Adv. Phys., **60**(3), pp. 413–550.

[150] Dresselhaus, M. S., Dresselhaus, G., Saito, R., and Jorio, a., 2005, "Raman

spectroscopy of carbon nanotubes," Phys. Rep., **409**(2), pp. 47–99.

[151] Liu, W., Chai, S., Rahman, A., and Hashim, U., 2014, "Journal of Industrial and Engineering Chemistry Synthesis and characterization of graphene and carbon nanotubes : A review on the past and recent developments," J. Ind. Eng. Chem., **20**(4), pp. 1171–1185.

[152] Tuinstra, F., and Koenig, J. L., 1970, "Raman Spectrum of Graphite," J. Chem. Phys., **53**(3), pp. 1126–1130.

[153] Osswald, S., Havel, M., and Gogotsi, Y., 2007, "Monitoring oxidation of multiwalled carbon nanotubes by Raman spectroscopy," J. Raman Spectrosc., **38**(April), pp. 728–736.

[154] Inam, F., Reece, M. J., and Peijs, T., 2012, "Shortened carbon nanotubes and their influence on the electrical properties of polymer nanocomposites," J. Compos. Mater., **46**(11), pp. 1313–1322.

[155] Straughan, B. P. and Walker, S., 1976, Spectroscopy, John Wiley and Sons.

[156] Loos, M. R., Coelho, L. A. F., Pezzin, S. H., and Amico, S. C., 2008, "Effect of carbon nanotubes addition on the mechanical and thermal properties of epoxy matrices," Mater. Res., **11**(3), pp. 347–352.

[157] Lau, K. T., Lu, M., Lam, C. K., Cheung, H. Y., Sheng, F. L., and Li, H. L., 2005, "Thermal and mechanical properties of single-walled carbon nanotube bundle-reinforced epoxy nanocomposites: The role of solvent for nanotube dispersion," Compos. Sci. Technol., **65**(5 SPEC. ISS.), pp. 719–725.

[158] Pizzutto, C. E., Suave, J., Bertholdi, J., Pezzin, S. H., Coelho, L. A. F., and Amico, S. C., 2011, "Study of epoxy/CNT nanocomposites prepared via dispersion in the hardener," Mater. Res., **14**(2), pp. 256–263.

[159] Hong, S., and Wu, C., 1998, "DSC and FTIR analysis of the curing behaviors

of epoxy / DICY / solvent open systems," Thermochim. Acta, **316**, pp. 167–175.

[160] Romão, B. M. V, Diniz, M. F., Margarete, F. P., Lourenço, V. L., Pardini, L. C., and Dutra, R. C. L., 2006, "Characterization of the Curing Agents Used in Epoxy Resins with TG / FT-IR Technique," Polímeros Ciência e Tecnol., **16**, pp. 94–98.

[161] González-González, M., Cabanelas, J. C., and Baselga, J., 2012, "Applications of FTIR on Epoxy Resins - Identification, Monitoring the Curing Process, Phase Separation and Water Uptake," Univ. Carlos III Madrid, **2**, pp. 261–284.

[162] Jagtap, S. B., and Ratna, D., 2013, "Preparation and characterization of rubbery epoxy/multiwall carbon nanotubes composites using amino acid salt assisted dispersion technique," Express Polym. Lett., **7**(4), pp. 329–339.

[163] Jumahat, A., Zamani, N. R., Soutis, C., and Roseley, N. R. N., 2014, "Thermogravimetry analysis of nanosilica-filled epoxy polymer," Mater. Res. Innov., **18**(sup6), pp. S6-274-S6-279.

[164] Moosa, A. A., A, A. R. S., Abdul, F., Kubba, K., and Raad, M., 2017, "Synergetic Effects of Graphene and Nonfunctionalized Carbon Nanotubes Hybrid Reinforced Epoxy Matrix on Mechanical , Thermal and Wettability Properties of Nanocomposites," **7**(1), pp. 1–11.

[165] Kim, P. ; Shi, L. ; Majumdar, A. ; McEuen, P. ., 2001, "Thermal transport measurements of individual multiwalled nanotubes," Phys. Rev. Lett., **Vol.87(21)**, p. pp.215502-1-215502-4.

[166] Chung, S. L., and Lin, J. S., 2016, "Thermal conductivity of epoxy resin composites filled with combustion synthesized h-BN particles," Molecules, **21**(5), pp. 1–11.

[167] Garrett, K. W., and Rosenberg, H. M., 1974, "The thermal conductivity of

epoxy-resin/powder composite materials," J. Phys. D. Appl. Phys., **7**(9), pp. 1247–1258.

[168] Min, C., and Yu, D., 2012, "A graphite nanoplatelet / epoxy composite with high dielectric constant and high thermal conductivity," Carbon N. Y., **55**, pp. 116–125.

[169] Paszkiewicz, S., 2014, "Polymer Hybrid Nanocomposites Containing Carbon Nanoparticles . in Situ Synthesis and Physical Properties," WEST POMERANIAN UNIVERSITY OF TECHNOLOGY IN SZCZECIN.

[170] Boyd, R., Feldman, M. W., Transmission, C., Laland, K. N., Richerson, P. J., Aoki, K., Kumm, J., Nakanishi, D., Valone, T. J., Templeton, J. J., Eriksson, K., Ghirlanda, S., Laland, K., Wagner, R. H., Huck, S., Oechssler, J., Rendell, L., Osborne, R. W., Nehaniv, C. L., Mcelreath, R., Pike, T. W., Hamilton, W. D., Xanthopoulos, A., Valimaki, J., Fischer, P., and Tsitsiklis, J. N., 2010, "Two-Dimensional Phonon Transport," **328**(April), pp. 213–216.

[171] Kim, S., Kim, J. T., Kim, H., Rhee, K., and Kathi, J., 2012, "Thermal and Mechanical Properties of Epoxy / Carbon Fiber Composites Reinforced with Multi- walled Carbon Nanotubes," J. Macromol. Scince, Part BPhysiscs, **2348**.

[172] Zhou, Z., Liu, K., Lai, C., Zhang, L., Li, J., Hou, H., Reneker, D. H., and Fong, H., 2010, "Graphitic carbon nano fi bers developed from bundles of aligned electrospun polyacrylonitrile nano fi bers containing phosphoric acid," Polymer (Guildf)., **51**, pp. 2360–2367.

[173] Kaur, N., Kumar, V., and Dhakate, S. R., 2016, "Synthesis and characterization of multiwalled CNT–PAN based composite carbon nanofibers via electrospinning," Springerplus, **5**(1).

[174] HDBK-17-1F, 2002, "Department of defense handbook :'Composite Materials

Handbook Volume 1 . Polymer Matrix Composites Guidelines for Characterization,'" Dep. Defense, United States Am., **1**(June).

[175] Sims, G. D., and Gnaniah, S. J. P., 2009, "Improved procedures for the determination of Tg by DMA," ICCM, Edinburgh, Scotland, pp. 0–9.

[176] ASTM D4065-01, 2011, "Standard Practice for Plastics : Dynamic Mechanical Properties : Determination and Report of Procedures," Annu. B. ASTM Stand., pp. 1–7.

[177] Goertzen, W. K., and Kessler, M. R., 2007, "Dynamic mechanical analysis of carbon/epoxy composites for structural pipeline repair," Compos. Part B Eng., **38**(1), pp. 1–9.

[178] Seyler, R. J., 1994, Assignment of the Glass Transition, ASTM International.

[179] Seyhan, A. T., Gojny, F. H., Tanoğlu, M., and Schulte, K., 2007, "Critical aspects related to processing of carbon nanotube/unsaturated thermoset polyester nanocomposites," Eur. Polym. J., **43**(2), pp. 374–379.

[180] Jean_Pierre Pascault, Henry Sautereau, Jacques Verdu, and Roberto J.J. Williams, 2002, Thermosetting Polymers, Marcel Dekker, Inc, New York.

[181] Abali, F., Pora, A., and Shivakumar, K., 2003, "Modified short beam shear test for measuring interlaminar shear strength of composites," J. Compos. Mater., **37**(5), pp. 453–464.

[182] Shindo, Y., Wang, R., and Horiguchi, K., 2001, "Analytical and Experimental Studies of Short-Beam Interlaminar Shear Strength of G-10CR Glass-Cloth/Epoxy Laminates at Cryogenic Temperatures," J. Eng. Mater. Technol., **123**(1), p. 112.

[183] Cui, W. C., and Wisnom, M. R., 1992, "Contact finite element analysis of three- and four-point short- beam bending of unidirectional composites," Compos. Sci.

Technol., **45**(4), pp. 323–334.

[184] Gürkan, I., and Cebeci, H., 2016, "An approach to identify complex CNT reinforcement effect on the interlaminar shear strength of prepreg composites by Taguchi method," Compos. Struct., **141**, pp. 172–178.

[185] Andrew Rutherford, 2001, Introducing ANOVA and ANCOVA: a GLM approach (introducing statistical methods series), Sage Publications Ltd, London, Thousand Oaks, New Delhi.